THE UNIVERSITY OF CHICAGO

REDUCED DENSITY MATRICES AND TENSOR FACTORIZATIONS FOR LOW COST QUANTUM CHEMISTRY

A DISSERTATION SUBMITTED TO
THE FACULTY OF THE DIVISION OF THE PHYSICAL SCIENCES
IN CANDIDACY FOR THE DEGREE OF
DOCTOR OF PHILOSOPHY

DEPARTMENT OF CHEMISTRY

BY
ERIK P. HOY

CHICAGO, ILLINOIS
DECEMBER 2015

To Alice

TABLE OF CONTENTS

LIST OF FIGURES

LIST OF TABLES

ABSTRACT

Conventional low cost computational methods in quantum chemistry such as Hartree-Fock and density functional theory often fail to properly describe electron correlation. Of the two types of electron correlation, dynamic and static, or multi-reference, correlation is particularly difficult to obtain using low cost methods. This type of electron correlation results when multiple Hartree-Fock reference states are needed to describe a system. One class of methods which are able to describe both types effectively are 2-electron reduced density matrix (2-RDM) methods. These methods use the 2-electron density matrix as the primary variable in the electronic Schrödinger equation in place of the wavefunction. By circumventing the wavefunction, one replaces an exponentially scaling problem with a polynomially scaling one, and unlike density functional theory, the energy is a linear functional of the 2-RDM. The lowest cost 2-RDM method currently available is known as the parametric 2-electron reduced density matrix method (p2-RDM). The method has equivalent scaling to configuration interaction with single and double excitations (CISD) and is able to treat both dynamic and static correlation. This work examines both the correlation recovery abilities of the p2-RDM method and potential scaling improvements to the method using tensor factorization. We first investigated several molecular systems including the conversion of hydroxylamine to ammonia oxide, the hydridotrioxygen atmospheric radical, and the benzene and cyclobutadiene diradicals. The purpose of these studies was to further clarify the ability of the parametric method to capture various mixes of both types of correlation. We then investigated using two different tensor factorizations, low rank spectral expansion and tensor hypercontraction, to reduce the scaling of the p2-RDM toward that of Hartree-Fock and density functional theory. Based on these results, we developed a new tensor factorization to address the shortcomings of previous methods and provide a promising, new technique to generate a fourth order p2-RDM method capable of capturing both dynamic and static correlation.

ACKNOWLEDGMENTS

My time at the University of Chicago has been a unique experience with many unexpected highs and lows. It has been one of the best and most challenging experiences of my life so far. I am deeply grateful to all the people who helped me to make it to this point.

First, I want to acknowledge the role that my family have played in helping me make it to the University of Chicago. Both my mother and father have been very supportive of me throughout my life, and I can always count on them when I need help the most. Their willingness to sacrifice their time, energy, and effort on my behalf has deeply touched me, and I can only hope to follow their lead in the future. I also want to thank my sister Lauren, although we don't always see eye to eye, for reminding me to always keep others (animals included) in mind. A life isn't just the story of one person.

I want to thank my friends and mentors from my hometown of Cookeville who inspired me to reach for a doctorate in chemistry. First, I want to thank an amazing pair of English teachers, Ms. Rosie Andrews and Professor Connie Hood, who both showed me how learning can be fun and inspired me to pursue a life of love and learning. I also can't forget my chemistry professors and mentors, Dr. Ed Lisic and Dr. Robert Glinski, for giving me my first taste of scientific research in chemistry and inspiring me to explore the wonderful world of physical chemistry. I also want to thank the friends that I met along the way including but very much not limited to Clinton, Scott, Quinton, Avery, Kristen, Ian, Dylan, Kayla, Chase, Joe, Jon, Luc, Molly, Jordan, and Kathleen. All of them have made my life so much more meaningful and enjoyable, and I miss every one of them so much.

One does not go though graduate school without making new friends. I want to thank my fellow Mazziotti group members: Jay, Srikant, Chad, Nick, Andrew, Christine, Alison, Valentine, Lexie, Romit, Ali, Erica, Luke, Charles, Anthony, Manas, Kade, and Claire for being my comrades over the past five years. I particularly want to thank Christine Schwerdtfeger for helping me get started as a graduate student and Andrew Sand who was both my favourite office buddy for all five years and my best chess opponent. I also can't forget

Alison McManus who is one of the best undergraduates that I have ever taught or worked with. I'm grateful for all the new friends that I made during my time here including but again not limited to Dmitriy, John, James, Patrick (O. and F.), Nicky, and Zack. Many of them really helped me make it through the hard times of graduate school, and for that I am forever grateful. I also want to thank Robin and the PSD LAN party organizers for some of the most fun social times that I had in graduate school.

Just as one can't complete a Ph.D. without making new friends, one can't complete a Ph.D. without his advisor. I am especially grateful to have Professor David Mazziotti as my advisor. He has been both a mentor and a friend to me and has always known just how to make theoretical research exciting. Working for him has made me both a better researcher and a scientist. If I had to start my Ph.D. over again, I would gladly choose to work for him all over again.

Last but certainly not least, I want to thank a very special person who unexpectedly came into my life just one and a half years ago. Alice Pang has been one of the best partners that one can ask for. She always brightens up my day and never fails to remind me to always consider the brighter side of life no manner how hard things seem to be. Just meeting her has by itself made my time in graduate school worth it as I would have never met her if I had not come to the University of Chicago.

CHAPTER 1

INTRODUCTION

One of the key problems for modern chemical theory is how to treat large molecular systems at a reasonable computational cost, particularly those of organic or biological origin such as small proteins and organic semiconductors. While many theories, in principle, provide exact or near exact solutions to chemical problems, the computational cost required is often intractable for current computational systems. This is particularly true for electronic structure methods where the cost of the most accurate available method scales exponentially with the system size. While various computationally cheaper, approximate methods exist, the accuracy losses caused by these approximations can result in calculated values that are significantly different from the experimental results. To better understand why these problems exist, we need to examine the basic concepts behind electronic structure methods.

1.1 Hartree-Fock

Traditional *ab initio* electronic structure methods generally attempt to solve the time independent electronic Schrödinger equation to obtain an N-electron wavefunction [1],

$$\hat{H}\Psi = E\Psi, \tag{1.1}$$

where $\hat{H}$ is the electronic Hamiltonian used to describe the motion of N electrons in a field of M nuclear point charges,

$$\hat{H} = (-\frac{1}{2}\sum_{i=1}^{N}\nabla_i^2 - \sum_{i=1}^{N}\sum_{K=1}^{M}\frac{Z_K}{r_{iK}}) + \sum_{i=1}^{N}\sum_{j>i}^{N}\frac{1}{r_{ij}}. \tag{1.2}$$

Solving this equation directly is not possible for systems with more than 1 electron and several layers of approximations are required for even the smallest of molecules. The first, the Born-Oppenheimer approximation, has already been applied to the Hamilitonian given in

Equation 1.2 above. In the Born-Oppenheimer approximation, the wavefunction is separated into electronic and nuclear parts as the electrons move much faster than the nuclei which can be considered effectively stationary in comparison. The next approximation is one in which each electron is assigned its own separate spin orbital so that the wavefunction can be expressed as a product of X orthonormal, one-electron molecular spin orbitals,

$$\Psi = \theta(1) * \theta(2)....\theta(N). \tag{1.3}$$

This formulation does not account for the anti-symmetry principle/Pauli Exclusion Principle which states that a wavefunction must be antisymmetric with respect to the interchange of any two electrons,

$$\theta_i(1) * \theta_j(2)....\theta_x(N) = -\theta_i(2) * \theta_j(1)....\theta_x(N). \tag{1.4}$$

The preceding problem can be solved by using a normalized linear combination of product wavefunctions. This is often expressed as a determinant referred to as a Slater determinant,

$$\Psi(1,2,3,...,N) = (N!)^{-1/2} \begin{vmatrix} \theta_i(1) & \theta_j(1) & \dots & \theta_x(1) \\ \theta_i(2) & \theta_j(2) & \dots & \theta_x(2) \\ \vdots & \vdots & \vdots & \vdots \\ \theta_i(N) & \theta_j(N) & \dots & \theta_x(N) \end{vmatrix}. \tag{1.5}$$

We can represent this determinant in a shorthand form which shows only the diagonal elements and implicitly includes the normalization constant,

$$\Psi(1,2,3,...,N) = |\theta_i(1)\theta_j(2)....\theta_x(N)\rangle = |\theta_i\theta_j....\theta_x\rangle. \tag{1.6}$$

If the wavefunction is approximated using only a single Slater determinant and a Hartree-Fock formulation (see Ref. [2] for details) is used for the ground state Schrödinger equation

the resulting method is known as the Hartree-Fock method. Due to these approximations, the Hartree-Fock method allows for only one configuration of electrons and replaces the direct interactions between electrons with interactions between an electron and the average electric fields of the other electrons. It has excellent computational scaling of approximately $o(r^3)$ to $o(r^4)$ with r being the number of molecular orbitals, but due to the approximations discussed, the method is often not quantitatively accurate due to a lack of electron correlation energy [1].

1.2 Electron Correlation

Correlation energy is defined to be the energy difference between the Hartree-Fock and full configuration interaction (FCI) electronic energies for a system[2]. Full configuration interaction addresses the lack of correlation in the Hartree-Fock method by including all possible spin orbital configurations (or all possible Slater determinants) in its wavefunction,

$$|\Psi_{FCI}\rangle = C_0|\Theta_0\rangle + \sum_{ia} C_i^a|\Theta_i^a\rangle + \frac{1}{4}\sum_{ijab} C_{ij}^{ab}|\Theta_{ij}^{ab}\rangle + \frac{1}{36}\sum_{ijkabc} C_{ijk}^{abc}|\Theta_{ijk}^{abc}\rangle + \dots. \quad (1.7)$$

Here Θ_0 is the Hartree-Fock wavefunction. Θ_i^a, Θ_{ij}^{ab}, and Θ_{ijk}^{abc} are singly excited, doubly excited, and triply excited wavefunctions respectively. For each excitation, an electron is removed from an occupied Hartree-Fock orbital i,j, or k and placed in an unoccupied (virtual) orbital a,b, or c. The C values are the weighting coefficients for each configuration.

The correlation recovered by full configuration interaction can be divided into two types: static and dynamic correlation. Dynamic or single reference correlation results from the direct electrostatic interaction of electrons which Hartree-Fock theory replaces with the interaction between electron clouds. Static or multi-reference correlation occurs when more than one Slater determinant is needed to represent a molecular system which the Hartree-Fock method can not account for, as it has only one Slater determinant (single-reference). Neglecting correlation energy can lead to large errors in the potential energy surface with the

calculated barriers being several kcal/mol different from experimental results [3]. The full configuration interaction method is usually considered to be the most accurate time independent *ab initio* approach possible as, by definition, it recovers all possible correlation energy. Unfortunately its computational cost scales exponentially with the number of electrons, as each electron added requires adding a new and larger set of summations. This limits the method to only very small molecular systems of 14 or less orbitals. To deal with limitation, various correlated approximate methods have been developed such as truncated configuration interaction (CI), coupled cluster (CC), multi-configurational self-consistent field theory (MCSCF), and perturbation theory (PT).

1.3 2-Electron Reduced Density Matrix

While these correlated methods are less expensive than full configuration interaction, most of them have notable drawbacks in terms of computational scaling, convergence in large systems, or the ability to simultaneously capture both dynamic and static correlation energy. Individual methods often come with their own unique flaws. Two well known families of methods are the truncated configuration interaction methods which predict energies that do not scale linearly with the size of the system .i.e. are not *size extensive* and the perturbation theory methods which have problems with potential energy surface divergences. For most known methods, recovering static correlation is particularly difficult and is usually accomplished by performing a full configuration interaction calculation on a subset, i.e. active space, of the total number of orbitals. Ideally, we would prefer a method that is able to handle both types of correlation energy simultaneously without having to perform a cost prohibitive configuration interaction computation. Additionally, the method should be size extensive and free of divergence problems or similar errors. One class of methods that have these properties are the 2-electron reduced density matrix (2-RDM) family of methods.

Since the Hamiltonian of an N-electron system contains at most pairwise interactions, the N-electron wavefunction can be mapped onto the two-electron reduced density matrix

(2-RDM), without the loss of its energetic and 1-/2-electron properties [4–6]. This allows for the energy to be expressed as a functional of the 2-RDM and the reduced Hamiltonian, ${}^2K$, without needing prior knowledge of the wavefunction of a system,

$$E = \mathrm{Tr}({}^2K\,{}^2D), \tag{1.8}$$

where ${}^2K$ is the Hamiltonian matrix corresponding to the following reduced Hamiltonian operator,

$${}^2\hat{K} = N\left(-\frac{1}{2}\nabla_1^2 - \sum_k \frac{Z_k}{r_{1k}}\right) + \frac{N(N-1)}{2}\frac{1}{r_{12}}, \tag{1.9}$$

and ${}^2D$ is the 2-electron reduced density matrix whose elements are given by,

$${}^2D^{pq}_{st} = \langle\Psi|\, a_p^\dagger\, a_q^\dagger\, a_t\, a_s|\Psi\rangle. \tag{1.10}$$

In this notation the a operators are annihilation operators which remove an electron from an orbital of the wavefunction on the right side of Equation 1.10. The $a^\dagger$ operators are creation operators which add an electron to an orbital of the wavefunction on the right side of the equation. The reverse is true if the operators act on the ajoint wavefunction on the left side. The compact notation for ${}^2D$ is shown on the left side of equation 1.10. In this notation, the superscript indices represent the orbitals to which electrons added and the subscripts are the indices of the orbitals from which the electrons are removed.

With the proper constraints, one can solve for the electronic energy considering only a polynomial scaling number of variables compared to the exponential scaling number of variables in CI wavefunction methods. The least expensive 2-RDM method, the parametric 2-electron reduced density matrix method, scales equivalently to configuration interaction with single and double excitations (CISD) at a computational cost on the order of $o(r^6)$ with r being the number of molecular orbitals.

1.4 Computational Cost Reduction in Chemistry

For many problems in chemistry however, even sixth order scaling is insufficient. For problems involving large organic and inorganic molecules such as proteins and organic semiconductors, correlated *ab initio* electronic structure methods beyond perturbation theory are too computationally costly to use. As a result, many scientists employ density functional theory based methods to study these kinds of systems which generally have a computational scaling on the order of $o(r^3)$ to $o(r^4)$. Density functional theory, like the 2-RDM methods, rewrites the energy to be a functional of a density matrix, in this case the 1-RDM. Density functional methods, however, have many well known drawbacks compared to traditional *ab initio* methods particularly their general inability to capture static correlation. No widely accepted electronic structure method currently exists which can reliably capture both dynamic and static correlation at a cost of $o(r^4)$ or less. As will be demonstrated in Chapters 3, 4, and 5 of this work, being able to capture both correlation types is very important to ensuring accurate results even in systems where only one type of correlation is expected to be of importance.

Producing a less than $o(r^4)$ method that is size extensive, free of potential energy divergence errors, and which can capture both types of electron correlation is not a trivial problem. As noted before, the cheapest 2-RDM method, the p2-RDM method, which processes those three characteristics has 2 orders of magnitude higher computational scaling than density functional theory at $o(r^6)$. It is possible however to reduce the cost of p2-RDM and similar double excitation *ab initio* methods such as coupled cluster and configuration interaction with single and double excitations and to understand how we need to examine the 2 primary driving causes, tensor summation and storage costs, of the scaling of this class of methods. The first primary determination factor for the computational scaling is the summations of pairs of fourth-order tensors (higher order matrices) summations such as

the p2-RDM expression for the energy of the occupied orbitals,

$$E_{occ} = \frac{1}{2} \sum_{i<j,k<l} {}^2V_{ij}^{kl} \sum_{ab} {}^2T_{ij}^{ab} \, {}^2T_{kl}^{ab}. \tag{1.11}$$

where ${}^2T_{ij}^{ab}$ is the double excitation tensor and ${}^2V_{ij}^{kl}$ is the 2-electron integral tensor,

$${}^2V_{ij}^{kl} = \frac{1}{2} \int \theta_k^*(1)\theta_l^*(2)(\frac{1}{r_{12}})\theta_i(1)\theta_j(2) \, d1 \, d2. \tag{1.12}$$

In this summation, there are are total of 6 non-matching indices resulting in computational cost of $o(r^6)$ in order to compute this summation. In addition to the summation cost, the amount of computer storage space needed for the for these summation is often prohibitive. For a 1000 orbital molecular system, storing the full 2-electron integrals without consideration of any integral or point group symmetries would require 8000 Gigabytes of storage space while a comparable 2-index tensor would only require a few Gigabytes. In order to reduce these costs and make such systems accessible to *ab initio* methods, the tensors and their summations need to be replaced. One way to accomplish this is to break up the fourth order tensors, ${}^2T$ and ${}^2V$, and represent them using summations of the products of lower order tensors, which is known as tensor factorization.

1.5 Tensor Factorization

Tensor factorizations are a well studied approach in numerical linear algebra for treating large, sparse matrices and tensors. They are particularly useful for applications such as signal processing, data analysis, and computational cost reduction [7]. The last application has been of particular interest since the tensor factorization was first applied to quantum chemistry in the 1970s and has received increased interest in recent years for reducing both storage costs and computational time [8–12]. Many different factorizations have been adopted and further developed for chemistry since then, such as the spectral expansion and tensor hyper-

contraction factorizations [13–15]. As an example, one of the simplest factorizations used in chemistry is the CANDECOMP/PARAFAC factorization [7, 14],

$$^{2}\,V_{ij}^{kl} = \sum_{a} E_{a}^{l} F_{a}^{k} G_{a}^{i} H_{a}^{j}. \tag{1.13}$$

This factorization breaks an n^{th} order tensor into n second order tensors (matrices). Each of the n types of second order tensors has a molecular index (i, k, j, and l) and a factorization index (a). The factorization tensors and indices can be thought of as forming a new basis set for the factorization which is not necessarily related to the original molecular basis set. The quality of the new basis and similarly the accuracy of the factorization depend heavily on both the factorization chosen and the size of the factorization basis. Using this new factorization basis, we can rewrite the higher order summations, such as that shown in Equation 1.11, into multiple lower order partial summations such as:

$$\sum_{i} G_{i}^{c2}\, T_{ij}^{ab} = \; B_{cj}^{ab} \sim \; o(r^{5}). \tag{1.14}$$

The actual computational cost reduction achieved depends on the size of the factorization basis, order of the factorization tensors, and how many of the higher order tensors are factorized. Consideration of both the accuracy and likely computational cost motivated the work in Chapters 6 and 7. The overall goal of this portion of the work presented in these chapters was to find the factorization best suited to treating the particular tensors and summations found in double excitation methods such as the parametric 2-RDM.

1.6 Chapter Overview

In the following chapters, we will explore both the ability of the parametric 2-RDM method to serve as a low cost method for treating molecular systems containing both dynamic and static correlation as well as the effectiveness of tensor factorization methods. In Chapter 2,

we review the theory behind the parametric 2-RDM method. We examine its effectiveness for treating systems of small to moderate amounts of static correlation in Chapters 3 and 4. In Chapter 3, we compare the parametric 2-RDM treatment of hydroxylamine to a previous study of oxywater to determine how the method behaves at varied but moderate levels of static correlation. We follow this in Chapter 4 with an examination of another moderately correlated system, the HO_3 radical. We then examine the ability of the parametric method to treat multi-reference correlation in diradical systems by examining the benzene and cyclobutadiene diradicals in Chapter 5. In Chapter 6, we examine both the accuracy and potential cost reduction capabilities of two different tensor factorizations, low-rank spectral expansion and tensor hypercontraction, as applied to the parametric 2-RDM method. In this study, we obtain a clearer picture of the strengths and weaknesses of each factorization as well as a better understanding of what type of factorization is needed to improve *ab initio* methods. Based on the results of this study, we introduce a new family of tensor factorizations known as the positive semi-definite factorizations in Chapter 7 which improves on existing factorizations for reducing the scaling of double excitation methods like parametric 2-RDM.

1.7 References

[1] I. N. Levine, *Quantum Chemistry* (Pearson Prentice Hall, New Jersey, 2006), 6th ed.

[2] A. Szabo and M. Ostlund, *Modern Quantum Chemistry* (Dover, Mineola, 1989).

[3] T. Bally and W. T. Borden, *Calculations on Open-Shell Molecules: A Beginner's Guide* (John Wiley and Sons Inc, New York, 2007), pp. 1–97.

[4] D. A. Mazziotti, ed., *Two-Electron Reduced-Density-Matrix Mechanics*, vol. 134 of *Advances in Chemical Physics* (Wiley, New York, 2007).

[5] A. J. Coleman and V. I. Yukalov, *Reduced Density Matrices: Coulson's Challenge* (Springer, New York, 2000).

[6] J. Cioslowski, ed., *Many-Electron Densities and Reduced Density Matrices*, Mathematical and Computational Chemistry (Kluwer Academic/Plenum Publishers, New York, 2000).

[7] A. Cichocki, R. Zdunek, A. H. Phan, and S. Amari, *Nonnegative Matrix and Tensor Factorization* (Wiley, West Sussex, 2009).

[8] N. H. F. Beebe and J. Linderberg, Int. J. Quantum Chem. **12**, 683 (1977).

[9] F. Bell, D. S. Lambrecht, and M. Head-Gordon, Molecular Physics **108**, 2759 (2010).

[10] A. E. DePrince and C. D. Sherrill, J. Comp. Theo. Chem. **9**, 2687 (2013).

[11] E. Epifanovsky, D. Zuev, X. Feng, K. Khistyaev, Y. Shao, and A. I. Krylov, J. Chem. Phys. **139**, 134105 (2013).

[12] K. Brandhorst and M. Head-Gordon, J. Comp. Theo. Chem. **7**, 351 (2011).

[13] E. P. Hoy, N. Shenvi, and D. A. Mazziotti, J. Phys. Chem. **139**, 034105 (2013).

[14] E. G. Hohenstein, R. M. Parrish, and T. J. Martinez, J. Chem. Phys. **137**, 044103 (2012).

[15] E. G. Hohenstein, R. M. Parrish, C. D. Sherrill, and T. J. Martinez, J. Chem. Phys. **138**, 12411 (2013).

CHAPTER 2

THEORY: PARAMETRIC 2-ELECTRON REDUCED DENSITY METHOD (P2-RDM)

2.1 Introduction and Overview

Since Coulson first issued his challenge to develop a viable two-electron reduced density matrix (2-RDM) method in 1959, 2-RDM methods have gathered much attention as possible replacements for traditional wavefunction- based approaches. Since the Hamiltonian of an N-electron system contains at most pairwise interactions, the N-electron wavefunction can be mapped onto the two-electron reduced density matrix (2-RDM) without loss of its energetic and 1- and 2-electron properties [1–3]. One can then calculate the ground state energy as a functional of the 2-RDM. A direct variational calculation of the energy, however, yields energy results that are well below the results predicted by the full configuration interaction (FCI) method, violating the variational principle [4]. This is due to the fact that the set of possible 2-RDMs is larger than the set of those derivable from N-electron wavefunctions. In order to insure that the 2-RDM can be mapped from an N-electron wavefunction, a set of constraints known as the N-representability conditions must be imposed [4–7]. Using N-representability conditions to directly minimize the 2-RDM is known as the variational 2-RDM method.

While direct 2-RDM minimization significantly reduces computational cost compared to wavefunction methods of similar accuracy, it is possible to lower computational costs still further. Truncated configuration interaction methods reduce the cost of an energy minimization compared to the full configuration interaction method by redefining the wavefunction in terms of only a limited number of expansion coefficients. For example, a normalized, truncated configuration interaction wavefunction which depends only on the double excitations

coefficients, C_{ij}^{ab}, can be written as follows

$$|\Psi_{CID}\rangle = |\Psi_0\rangle + \frac{1}{4}\sum_{ijab}{}^{2}\, C_{ij}^{ab}|\Psi_{ij}^{ab}\rangle. \tag{2.1}$$

In a similar manner, the computational cost of the 2-RDM energy minimization can be reduced by redefining our 2-RDM in terms of a limited number of parameters. This was first demonstrated by Kollmar in 2006 [8–15]. In 2008, Mazziotti developed an alternative parametrization of the 2-RDM elements which exceeds the accuracy of the coupled cluster with single and double excitations method (CCSD)[13, 14]. The resulting M parametrization scales linearly with system size (this is called *size extensive*) is approximately N-representable, and returns more correlation energy than coupled cluster with single and double excitations (CCSD). The p2-RDM method has a computational cost similar to that of configuration interaction with single and double excitations (CISD), which is lower than CCSD by an integer pre-factor [13–15]. The resulting parametric 2-RDM method with the M functional, or p2-RDM, has been used to study a variety of closed- and open-shell molecules. Most importantly, it is capable of describing moderate amounts of both types of correlation [13–17]. The following chapter contains an overview of the theory behind the parametric 2-RDM method. It is based on the 2010 *Physical Review* paper by David Mazziotti which gives a comprehensive overview of parametric theory [14].

2.2 Parametric 2-RDM

As was discussed in the previous chapter, the energy of an N-electron system can be calculated without approximation using the two-electron reduced density matrix (2-RDM),

$$E = \mathrm{Tr}(\,{}^{2}K\,{}^{2}D), \tag{2.2}$$

where ${}^2K$ is the Hamiltonian matrix corresponding to the following reduced Hamiltonian operator,

$$ {}^2\hat{K} = \frac{1}{N-1}\left(-\frac{1}{2}\nabla_1^2 - \sum_k \frac{Z_k}{r_{1k}}\right) + \frac{1}{2}\frac{1}{r_{12}}, \tag{2.3} $$

and ${}^2\,D$ is the 2-electron reduced density matrix whose elements are given by,

$$ {}^2\,D^{pq}_{st} = \langle\Psi|\, a_p^\dagger\, a_q^\dagger\, a_t\, a_s|\Psi\rangle. \tag{2.4} $$

In this notation, the molecular orbitals indices are specified by p, q, s, and t, which represent an arbitrary set of orbitals. Occupied orbitals in this chapter will be specified using the letters i through o, and unoccupied orbitals will be specified using the letters a through h.

To parametrize the 2-RDM, we express it as a wedge product of 1-RDMs. The wedge product is anti-symmetric operator and is used in place of a Slater determinant. The 1-RDM alone does not contain enough information to fully describe the 2-RDM and the missing information is added to the expansion in the form of a term known as the cumulant, ${}^2\Delta$, [18–20]

$$ {}^2D^{pq}_{st} = 2\,{}^1D^p_s \wedge {}^1D^q_s + {}^2\Delta^{pq}_{st}, \tag{2.5} $$

$$ {}^2D^{pq}_{st} = {}^1D^p_s\,{}^1D^q_t - {}^1D^p_t\,{}^1D^q_s + {}^2\Delta^{pq}_{st}. \tag{2.6} $$

The 1-RDM can be written in a similar manner although it is not a cumulant expansion,

$$ {}^1D^p_q = ({}^1\,D_0)^p_q + {}^1\Delta^p_q. \tag{2.7} $$

The cumulant 2- and 1-RDMs represent the correlated (or connected) parts of the RDM which are not contained in the lower order RDMs and which vanish in the absence of electron correlation[14].

For the parametric method, we want to re-express the cumulant terms ${}^1\Delta$ and ${}^2\Delta$ in terms of their lowest order components. If a parameter λ is defined such that $\lambda = 0$

corresponds to the Hartree-Fock solution for the quantum system and $\lambda = 1$ corresponds to the fully correlated quantum system, we can express our 2-RDM as an expansion in terms of λ and the excitation coefficient ${}^2T$,

$$ {}^2D = {}^2D_0 + {}^2\Delta, \tag{2.8}$$

$$ {}^2D = {}^2D_0 + \lambda\, {}^2T + O(\lambda^2). \tag{2.9}$$

These cumulant 2-RDM and 1-RDM can be written as the sum of their first and second order Hermitian parts or ${}^2T$ and ${}^1T$ respectively and a higher order remainder, R,

$$ {}^2\Delta = {}^2T + {}^2R(\lambda^2), \tag{2.10}$$

$$ {}^1\Delta = {}^1T + {}^1R(\lambda^3). \tag{2.11}$$

where the only non-zero part of the first order 2-RDM cumulant is

$$ {}^2\Delta^{ab}_{ij} \approx {}^2T^{ab}_{ij}. \tag{2.12}$$

In order to simplify the remaining discussions and equations in this chapter, we assume that the single excitations vanish until the third order (${}^1T$ vanishes). This can be accomplished by performing a second-order rotation of the Hartree-Fock orbitals to Brueckner-like orbitals [21]. Adding in explicit single excitations will be discussed in the last paragraph of this chapter.

In a similar manner to expressing RDMs as products of lower order RDMs, an RDM can also be expressed as a sum of higher order RDMs. In a finite orbital basis, an RDM of order p-1 can be represented by a sum (contraction) of p-RDMs over a single index,

$$ {}^{p-1}D^{q,r,\ldots,t}_{v,x,\ldots,z} = \sum_u {}^pD^{q,r,\ldots,t,u}_{v,x,\ldots,z,u}. \tag{2.13}$$

As the higher order RDMs contain all the information needed to reconstruct the lower order ones, no cumulant expansion is needed.

Contracting the 3- and 4-RDMs over 1 electron and equating the connected parts gives the following approximate relations since the correlated part of ${}^1\Delta$ vanishes until the third order in λ,

$$n_s^p \, {}^1\Delta_s^p = \sum_q {}^2\Delta_{sq}^{pq} + O(\lambda^4) \tag{2.14}$$

$$n_{tu}^{pq} \, {}^2\Delta_{tu}^{pq} = \sum_s {}^3\Delta_{tus}^{pqs} + O(\lambda^3), \tag{2.15}$$

$$n_{uyv}^{pqs} \, {}^3\Delta_{uvy}^{pqs} = -\sum_t \hat{A}({}^2\Delta_{uv}^{pt} * {}^2\Delta_{qs}^{ty}) + O(\lambda^3), \tag{2.16}$$

$${}^2\Delta_{ia}^{jb} = -\sum_s {}^3\Delta_{iak}^{jbk} + O(\lambda^3). \tag{2.17}$$

where $\hat{A}$ is an anti-symmetric permutation operator and

$$n_s^p = n_p + n_s - 1, \tag{2.18}$$

$$n_{tu}^{pq} = n_p + n_q + n_t + n_u - 2, \tag{2.19}$$

$$n_{uyv}^{pqs} = n_p + n_q + n_s + n_u + n_y + n_v - 3. \tag{2.20}$$

Here n_p is either 0 or 1 depending on whether the Hartree-Fock orbital is unoccupied or occupied. By combining these relations with equations 2.10 and 2.11, we obtain the following 1- and 2-cumulant relations.

$${}^2\Delta_{ij}^{kl} = \sum_{a<b} {}^2T_{kl}^{ab} \, {}^2T_{ij}^{ab} + O(\lambda^4), \tag{2.21}$$

$$ {}^2\Delta_{ia}^{jb} = -\sum_{kc} {}^2T_{jk}^{ac}\,{}^2T_{ik}^{bc} + O(\lambda^4), \tag{2.22} $$

$$ {}^2\Delta_{ab}^{cd} = \sum_{i<j} {}^2T_{ij}^{cd}\,{}^2T_{ij}^{ab} + O(\lambda^4), \tag{2.23} $$

$$ {}^1\Delta_{i}^{j} = -\sum_{k} {}^2\Delta_{ik}^{jk} + O(\lambda^4), \tag{2.24} $$

$$ {}^1\Delta_{a}^{b} = \sum_{c} {}^2\Delta_{ac}^{bc} + O(\lambda^4). \tag{2.25} $$

The 1-RDM elements can now also be represented in terms of ${}^2\,T$,

$$ {}^1\Delta_{i}^{j} = -\sum_{k,a<b} {}^2T_{jk}^{ab}\,{}^2T_{ik}^{ab} + O(\lambda^4), \tag{2.26} $$

$$ {}^1\Delta_{a}^{b} = \sum_{c,i<j} {}^2T_{ij}^{ac}\,{}^2T_{ij}^{bc} + O(\lambda^4). \tag{2.27} $$

Using these contraction relations, we can re-express our 2-RDM cumulant elements from Equation 2.10 as four new equations,

$$ {}^2\,D_{ij}^{kl} = 4\,{}^2\,I_{ij}^{kl} + 4({}^1\,\Delta_{k}^{i} \wedge {}^1\,I_{j}^{l}) + {}^2\,\Delta_{ij}^{kl} + O(\lambda^4), \tag{2.28} $$

$$ {}^2\,D_{ia}^{jb} = {}^1\,I_{j}^{i}\,{}^1\,\Delta_{k}^{i} + {}^2\,\Delta_{ia}^{jb} + O(\lambda^4), \tag{2.29} $$

$$ {}^2\,D_{ab}^{cd} = {}^2\,\Delta_{cd}^{cd} + O(\lambda^4), \tag{2.30} $$

$$ {}^2\,D_{ij}^{ab} = {}^2\,\Delta_{ij}^{ab} + O(\lambda^3), \tag{2.31} $$

where ${}^2\,I$ is the 2-electron identity matrix,

$$ {}^2\,I_{st}^{pq} = {}^1\,I_{s}^{p} \wedge {}^1\,I_{t}^{q}. \tag{2.32} $$

Likewise the 1-RDM elements are now

$$^1 D_i^j = {}^1 \ I_s^p \, {}^1\Delta_i^j + O(\lambda^4), \tag{2.33}$$

$$^1 D_a^b = {}^1\Delta_a^b + O(\lambda^4). \tag{2.34}$$

This allows us to write the 2-RDM as a function of only its first order part,

$$^2 \Delta_{ij}^{ab} = {}^2T_{ij}^{ab}. \tag{2.35}$$

This parametrization of the 2-RDM is equivalent to the method known as CEPA. It is size extensive but not N-representable [8, 13]. The lack of N-representability leads to large correlation energy errors and makes the method almost unusable. We need to consider an alternative parameterizamation

2.2.1 The M Parametrization

To construct a parametrization that is N-representable, consider the following parametrization for $^2 \Delta_{ij}^{ab}$,

$$^2\Delta_{ij}^{ab} = {}^2T_{ij}^{ab} \sqrt{1 - \frac{1}{4} \sum_{klcd} |\, {}^2T_{kl}^{cd}|^2}. \tag{2.36}$$

This is the parametrization of $^2\Delta_{ij}^{ab}$ that arises if one constructs the 2-RDM using a configuration interaction with double excitations wavefunction,

$$|\Psi_{CID}\rangle = |\Psi_0\rangle + \sum_{ia} {}^1 T_i^a |\Psi_i^a\rangle + \sum_{ijab} {}^2 T_{ij}^{ab} |\Psi_{ij}^{ab}\rangle. \tag{2.37}$$

All other cumulant terms of the CID parametrization are identical to the ones given above for the CEPA-like parameterization. A CID-like parametrization is N-representable as its corresponding 2-RDM is directly derived from an N-electron wavefunction, but it is no longer size extensive, a well-known problem with truncated CI methods.

To make the parametrization that is both approximately N-representable and size extensive, consider a subset of the N-representability conditions known as the 2-positivity conditions,

$$^2D \succeq 0, \tag{2.38}$$

$$^2Q \succeq 0, \tag{2.39}$$

$$^2G \succeq 0. \tag{2.40}$$

These conditions ensure that the probabilities of finding 2-particles, 2-holes, and 1-particle, 1-hole are non negative and that the corresponding density matrices have non-negative eigenvalues. These two-positivity conditions imply another set of N-representablity conditions known as the Cauchy-Schwarz inequalities. The inequalities for the 2-particle and 2-hole density matrices are

$$(\,^2D^{ij}_{ab})^2 \leq {}^2D^{ij}_{ij}\,{}^2D^{ab}_{ab} \tag{2.41}$$

$$(\,^2Q^{ij}_{ab})^2 \leq {}^2Q^{ij}_{ij}\,{}^2Q^{ab}_{ab}. \tag{2.42}$$

Similar inequalities can be defined for the 1-particle, 1-hole matrix. Averaging these two inequalities and equating the connected parts then applying it to Equation 2.36 yields a new definition of the $^2\Delta^{ab}_{ij}$ term known as the M functional or p2-RDM [13–15]. We can rewrite Equation 2.36 in a more general form to include this functional form as well as the CID and CEPA functionals,

$$^2\Delta^{ab}_{ij} = {}^2T^{ab}_{ij}\sqrt{1 - \frac{1}{4}\sum_{klcd} f^{abcd}_{ijkl}|\,{}^2T^{cd}_{kl}|^2}. \tag{2.43}$$

The valve of topological factor, f, given in Table 2.1 depends on the number of indices shared between $^2T^{ab}_{ij}$ and $^2T^{cd}_{kl}$. Using different averages of the Cauchy-Schwarz inequalities

Table 2.1: The table below contains the topological factors for equation [12]. The factor in the table $f_{n_v}^{n_o}$, represents the factor f_{ijkl}^{abcd} from above where n_0 is the number of occupied spin orbitals shared by i,j and k,l, and n_v is the number of virtual orbitals shared by a,b and c,d. This gives a total of nine possible combinations for the topological factor, as shown this table. The D and Q factors given below represent the parametrizations that result from applying the D and Q Cauchy-Schwarz inequalities to the 2-RDM elements [13, 14].

	Topological factor, $f_{n_v}^{n_o}$								
Method	0/0	1/0	2/0	0/1	0/2	1/1	2/1	1/2	2/2
CEPA	0	0	0	0	0	0	0	0	0
CID	1	1	1	1	1	1	1	1	1
D	0	1	1	0	0	1	1	1	1
Q	0	0	0	1	1	1	1	1	1
M	0	0	1	0	1	1	1	1	1

given in Equation 2.41 gives a family of 2-RDM parametrizations. The removal of the unconnected 0/0 terms ensures linear scaling with the system size of the parametrization, and the averaging of the D and Q factors maintains the approximate N-representablity.

While the previous equation only implicitly includes single excitations, it is possible to add them explicitly to the M parametrization as demonstrated by Mazziotti in 2010 [14]. This version of the M parametrization is used for the computations in the following chapter. An extension of the method to open-shell systems which allows for orbitals to be occupied by only 1 electron instead of requiring double occupation, as is the case with closed-shell methods, has also been developed and was used for all computations in the remaining chapters of this work [16].

2.3 References

[1] D. A. Mazziotti, ed., *Two-Electron Reduced-Density-Matrix Mechanics*, vol. 134 of *Advances in Chemical Physics* (Wiley, New York, 2007).

[2] A. J. Coleman and V. I. Yukalov, *Reduced Density Matrices: Coulson's Challenge* (Springer, New York, 2000).

[3] J. Cioslowski, ed., *Many-Electron Densities and Reduced Density Matrices*, Mathematical and Computational Chemistry (Kluwer Academic/Plenum Publishers, New York, 2000).

[4] A. J. Coleman, Rev. Mod. Phys. **35**, 668 (1963).

[5] C. Garrod and J. Percus, J. Math. Phys. **5**, 1756 (1964).

[6] J. E. Harriman, Phys. Rev. A **17**, 1257 (1978).

[7] R. M. Erdahl, Int. J. Quantum Chem. **13**, 697 (1978).

[8] C. Kollmar, J. Chem. Phys. **125**, 084108 (2006).

[9] A. E. DePrince III and D. A. Mazziotti, Phys. Rev. A **76**, 042501 (2007).

[10] A. E. DePrince III and D. A. Mazziotti, J. Chem. Phys. B **112**, 16158 (2008).

[11] A. E. DePrince III, E. Kamarchik, and D. A. Mazziotti, J. Chem. Phys. **128**, 234103 (2008).

[12] A. E. DePrince III and D. A. Mazziotti, J. Chem. Phys. **130**, 164109 (2009).

[13] D. A. Mazziotti, Phys. Rev. Lett. **101**, 253002 (2008).

[14] D. A. Mazziotti, Phys. Rev. A **81**, 062515 (2010).

[15] C. A. Schwerdtfeger, A. E. DePrince III, and D. A. Mazziotti, J. Chem. Phys. **134**, 174102 (2011).

[16] C. A. Schwerdtfeger and D. A. Mazziotti, J. Phys. Chem. A **115**, 12011 (2011).

[17] D. A. Mazziotti, Chem. Rev. **112**, 244 (2012).

[18] J. Harriman, Phys. Rev. A **65**, 052507 (2002).

[19] D. A. Mazziotti, Chem. Phys. Letters **289**, 419 (1998).

[20] D. A. Mazziotti, Int. J. Quantum Chem. **70**, 557 (1998).

[21] R. K. Nesbet, Phys. Rev. **109**, 1632 (1958).

CHAPTER 3

ISOELECTRONIC ANALOGUE OF OXYWATER: A PARAMETRIC 2-ELECTRON REDUCED-DENSITY-MATRIX STUDY OF AMMONIA OXIDE

This chapter contains parts of an article that was originally published in *Molecular Physics*. Reprinted with permission from [E. P. Hoy, C. A. Schwerdtfeger, and D. A. Mazziotti, *Mol. Phys.*, **110**, 765 (2012)].

3.1 Introduction

Parametrization of the 2-RDM can be used to calculate electronic ground-state energies directly without using the N-electron wavefunction [1–5]. This density-matrix parametrization is derived using a subset of the *N-representability conditions* on the 2-RDM that approximately preserve its relationship to an N-electron wavefunction [6–9]. In 2006 Kollmar employed Cauchy-Schwarz inequalities, based on 2-positivity conditions, to parametrize the 2-RDM; in 2008 Mazziotti introduced a general family of parametrizations including Kollmar's (K) parametrization [10–14] as well as the M parametrization [1, 2, 15–17]. The 2-RDMs computed with the M parametrization are nearly N-representable with *size extensive* energies. The results from the M parametric 2-RDM method improve on the results from coupled cluster with single and double excitations (CCSD) at a computational cost equivalent to configuration interaction with single and double excitations (CISD) [1, 2, 15].

The M parametric 2-RDM method was recently applied to study oxywater by Schwerdtfeger, DePrince and Mazziotti [15]. The water oxide molecule or "oxywater" is connected to its isomer, hydrogen peroxide, by an intramolecular hydrogen transfer. Although oxywater has never been observed experimentally, its stability has been investigated in multiple theoretical studies [15, 18–22]. While coupled cluster methods predict a barrier from oxywater to the transition state between 4 to 6 kcal/mol, multi-reference perturbation theory methods

(CASPT2) predict a small energy barrier of 0.2 kcal/mol or show no barrier at all [15, 23, 24]. The parametric 2-RDM method predicted a barrier between these two results, a small 2.1 kcal/mol barrier at the extrapolated basis set limit.

In this work, we study a system whose molecular states are isoelectronic to hydrogen peroxide and oxywater, hydroxylamine's conversion to ammonia oxide. Similar to oxywater, ammonia oxide is believed to form from hydroxylamine through an intramolecular hydrogen transfer reaction. Unlike oxywater, whose existence is not currently experimentally supported, experimental evidence for the existence of ammonia oxide has recently emerged [19, 25, 26]. Kirby *et al.* found ammonia oxide molecules in crystalline $(NH_2OH)_2HCl$ using X-ray crystallography and suggested that ammonia oxide might comprise up to 18 percent of 1 M hydroxylamine solutions at 25 °C [25, 26].

Several studies employing electronic structure methods have been performed on the hydroxylamine/oxywater system [18, 27–34, 34–37]. It has been shown using coupled cluster methods and perturbation theory that ammonia oxide is stable relative to the transition state by 24-27 kcal/mol. In contrast to the oxywater system, a method that can capture multi-reference correlation has not yet been applied to this reaction pathway. The disagreement between single and multi-reference methods for the oxywater system transition barriers, suggests that it is worthwhile to examine the ammonia oxide system using the parametric 2-RDM method.

3.2 Applications

In the first section we describe the computational methods employed to study the isomerization reaction between hydroxylamine and ammonia oxide. In Section 3.2.2 we present and the results and compare them to those from the oxywater calculations.

3.2.1 Computational Methods

We studied three molecules in the ammonia oxide system, hydroxylamine, ammonia oxide, and their transition state, using the parametric 2-RDM(M) method as well as three coupled cluster methods, coupled cluster with single and double excitations (CCSD) [38, 39], completely renormalized coupled cluster [CR-CC(T)] [39–41], and coupled cluster with perturbative triple excitations [CCSD(T)] [38, 39]. The computations were preformed in three basis sets, augmented correlation-consistent polarized double-zeta (aug-cc-pVDZ), triple-zeta (aug-cc-pVTZ), and quadruple-zeta (aug-cc-pVQZ) basis-sets [38, 42] with the results being extrapolated to the basis-set limit. The aug-cc-pVQZ is the largest basis set yet employed to study the hydroxylamine to ammonia oxide isomerization. Coupled cluster and Hartree-Fock calculations were carried out using the electronic structure package GAMESS [43], and the parametric 2-RDM calculations were performed using the implementation in Ref. [15]. We optimized the geometries of all three molecules using the aug-cc-pVDZ and aug-cc-pVTZ basis sets, freezing two core orbitals, and we calculated single-point energies for each molecule in the aug-cc-pVQZ basis set at the aug-cc-pVTZ optimized geometries. These results were extrapolated to the basis set limit (EBSL) using a two part scheme. The Hartree-Fock energies [44–46] were fitted to an exponential function, $a + b\exp(-cx)$, and the correlation energies [47, 48] were fitted to a polynomial function, $a + b/x^3 + c/x^5$, where x equals 2, 3, and 4. The variables a, b, and c were fit using the aug-cc-pVDZ, aug-cc-pVTZ, and aug-cc-pVQZ energies with a representing the extrapolated energy.

3.2.2 Results

Optimized Hartree-Fock energies and the electronic correlation energies for ammonia oxide, hydroxylamine, and their transition state are contained in Table 3.1. For each molecule the 2-RDM(M) method recovers more correlation energy than CCSD but less than CCSD(T). For hydroxylamine the parametric method recovers 84.1% of the energy improvement of CR-CC(T) over CCSD at the extrapolated basis-set limit. At the transition state agreement

Table 3.1: Correlation energies for hydroxylamine(HA), ammonia oxide(AO), and their transition state(TS) were calculated using the parametric 2-RDM(M) method as well as several coupled cluster methods in aug-cc-pVDZ, aug-cc-pVTZ, and aug-cc-pVQZ basis sets with extrapolation to the basis-set limit (EBSL).

		Energy (H)	Correlation energy (H)			
Molecule	Basis Set	HF	CCSD	2-RDM(M)	CR-CC(T)	CCSD(T)
HA	aug-cc-pVDZ	-131.0152	-0.4115	-0.4218	-0.4223	-0.4241
	aug-cc-pVTZ	-131.0472	-0.4887	-0.5024	-0.5044	-0.5083
	aug-cc-pVQZ	-131.0559	-0.5136	-0.5281	-0.5305	-0.5346
	EBSL	-131.0591	-0.5341	-0.5492	-0.5519	-0.5560
TS	aug-cc-pVDZ	-130.9157	-0.4237	-0.4383	-0.4366	-0.4404
	aug-cc-pVTZ	-130.9477	-0.5008	-0.5180	-0.5188	-0.5248
	aug-cc-pVQZ	-130.9555	-0.5257	-0.5438	-0.5449	-0.5501
	EBSL	-130.9586	-0.5461	-0.5651	-0.5663	-0.5715
AO	aug-cc-pVDZ	-130.9627	-0.4097	-0.4191	-0.4201	-0.4227
	aug-cc-pVTZ	-131.0076	-0.4875	-0.5000	-0.5030	-0.5067
	aug-cc-pVQZ	-131.0160	-0.5126	-0.5257	-0.5293	-0.5333
	EBSL	-131.0180	-0.5333	-0.5468	-0.5509	-0.5549

between the CR-CC(T) and the 2-RDM(M) results further improves with the parametric method recovering 96.7% of the energy change from CCSD to CR-CC(T). This recovery of CR-CC(T)'s correlation energy is consistent with the earlier results for the conversion of oxywater to hydrogen peroxide where the 2-RDM(M) method captured 96.7% of the change in correlation energy from CCSD to CR-CC(T) at the oxywater transition state [15]. The 2-RDM(M)'s improvement in energy relative to CCSD is consistent with the derivation of the M parametrization [1], which parameterizes the 2-RDM to approach the boundary of its N-representable set as closely as possible upon minimization of the energy. The proximity of the optimized 2-RDM to its boundary enables the treatment of correlation effects in the 2-RDM(M) method that typically require wavefunction methods with triple excitations and/or a multi-configuration reference.

Table 3.2 gives the natural-orbital occupation numbers (eigenvalues of the 1-RDM) for the ammonia oxide and oxywater reactions [49]. Deviation of these numbers from the Hartree-Fock case where the highest occupied orbital occupation number is 1 and the lowest un-

occupied orbital occupation number is 0 implies a more correlated (multi-reference) state. Comparing all six molecules, we can see that *the molecules in the ammonia-oxide reactions are less correlated than their oxywater counterparts* according to both the CCSD and 2-RDM(M) results. For both the ammonia oxide and oxywater systems, the transition state is the most correlated state followed by the lowest state (hydroxylamine and hydrogen peroxide respectively) and then the oxide state. We also note that for all states the 2-RDM occupation numbers predict more multi-reference character than CCSD. The differences between the CCSD and 2-RDM(M) occupation numbers are notably larger for the molecules of oxywater reactions than for the molecules of the ammonia-oxide reaction, especially at the oxywater transition state which is the most multi-referenced molecule of the six studied.

The lowest eigenvalues of the positive semidefinite metric matrices ${}^2D$, ${}^2Q$, and ${}^2G$ provide a measure for the N-representability of the 2-RDM. These eigenvalues are reported for oxywater, hydrogen peroxide, and its transition state in Ref. [15]. While negative, the absolute values of these eigenvalues are approximately three orders of magnitude smaller than the largest positive eigenvalues, which are on the order of unity, except for ${}^2G$ where the largest eigenvalue is on the order of N. Similar results (not shown) are found for ammonia oxide, hydroxylamine, and its transition state. Hence, the parametric 2-RDM(M) method produces 2-RDMs that are nearly N-representable.

The results from geometry optimization in the aug-cc-pVTZ basis set are presented in Table 3.3. Overall the hydrogen-bond lengths and angles predicted by the parametric 2-RDM method show good agreement with those from the CR-CC(T) and CCSD(T) methods for all molecules. The most noticeable difference between the parametric 2-RDM and the coupled cluster results is the nitrogen-oxygen bond length of the ammonia-oxide transition state. The parametric 2-RDM(M) method predicts a bond length that is 0.0235 Å longer than the bond length predicted by CR-CC(T) and 0.0165 Å longer than the one predicted by CCSD(T). In contrast to the transition-state results, the nitrogen-oxygen bond lengths predicted by the parametric 2-RDM method for hydroxylamine and ammonia oxide, 1.3797

Table 3.2: The occupation numbers of the highest occupied natural orbital (HONO) and the lowest unoccupied natural orbital (LUNO) for all six molecules are presented in the aug-cc-pVTZ basis set from the CCSD and 2-RDM(M) methods.

	Natural orbital occupation numbers			
	HONO		LUNO	
Molecule	CCSD	2-RDM(M)	CCSD	2-RDM(M)
Ammonia Oxide	0.9727	0.9687	0.0218	0.0255
Transition State	0.9655	0.9530	0.0300	0.0431
Hydroxylamine	0.9711	0.9649	0.0239	0.0299
Oxywater	0.9683	0.9594	0.0316	0.0462
Transition State	0.9607	0.9446	0.0394	0.0639
Hydrogen Peroxide	0.9635	0.9504	0.0333	0.0468

Table 3.3: Optimized geometries for hydroxylamine, ammonia oxide, and their transition state are presented from the parametric 2-RDM(M) method and the coupled cluster methods in the aug-cc-pVTZ basis set. The molecular point groups employed were C_s for hydroxylamine and the transition state and C_{3v} for ammonia oxide.

		Bond lengths (Å) and angles (°)				
Molecule	Parameter	HF	CCSD	2-RDM(M)	CR-CC(T)	CCSD(T)
Hydroxylamine	r_{no}	1.3969	1.4364	1.4502	1.4459	1.4499
	r_{hn}	0.9989	1.0147	1.0167	1.0173	1.0177
	r_{oh}	0.9393	0.9588	0.9610	0.9613	0.9621
	a_{hon}	104.85	102.48	102.00	102.07	101.91
	a_{hno}	105.66	103.92	103.39	103.55	103.39
	d_{h2no}	113.48	110.41	109.70	109.95	109.76
	d_{hnoh}	123.23	124.79	125.15	125.02	125.12
Transition State	r_{no}	1.4912	1.5206	1.5553	1.5318	1.5388
	r_{nho}	1.1029	1.1075	1.1086	1.1078	1.1084
	r_{nh}	0.9939	1.0084	1.0103	1.0101	1.0109
	a_{hno}	54.31	56.19	55.68	56.39	56.39
	a_{nho}	110.18	109.61	108.64	109.39	109.23
	d_{hnoh}	116.25	116.89	117.36	117.02	117.10
	d_{h2no}	127.51	126.22	125.28	125.97	125.79
Ammonia Oxide	r_{no}	1.3621	1.3735	1.3797	1.3776	1.3796
	r_{hn}	1.0074	1.0238	1.0265	1.0259	1.0268
	a_{hno}	111.48	111.82	111.82	111.86	111.87
	d_{h2no}	120.00	120.00	120.00	120.00	120.00

and 1.4502 Å respectively, are within 0.0003 Å of those from CCSD(T). A similar lengthening of the oxygen-oxygen bond was observed for all three molecules in the oxywater study [15]. The parametric 2-RDM method predicted an oxygen-oxygen bond length of 1.6841 Å in the transition state, which is 0.02 Å longer than that predicted by CCSD(T) method and 0.05 Å longer than that from CCSD. The oxywater study also found smaller deviations, 0.03 to 0.04 Å, from CCSD for the hydrogen peroxide and oxywater molecules. All of these molecules are more correlated than the ammonia-oxide transition state. Multi-reference character is known to be statistically correlated with bond lengthening, and the oxygen-oxygen bond is more likely to have multi-reference character than the nitrogen-oxygen bond due to the greater energy-level degeneracy of a homogenous bond.

A comparison of the energy differences for the ammonia-oxide and oxywater reactions at the extrapolated basis-set limit are presented in Table 3.4. CCSD predicts the highest barriers of the correlation methods. For the ammonia oxide CCSD predicts a 54.63 kcal/mol barrier for the hydroxylamine-to-ammonia-oxide transition and a 29.90 kcal/mol barrier for the ammonia-oxide-to-hydroxylamine transition. For oxywater CCSD predicts a hydrogen-peroxide-to-oxywater barrier of 52.69 kcal/mol and a 6.43 kcal/mol barrier for the oxywater-to hydrogen-peroxide transition. The CR-CC(T) method, which predicts correlation energies between CCSD and CCSD(T), lowers the barriers predicted by CCSD by 1-2 kcal/mol for both oxywater and ammonia oxide. The CCSD(T) method further lowers the CCSD barriers by 2-3 kcal/mol for both systems. Adding additional correlation energy lowers the barriers for both the oxywater and ammonia oxide systems.

Comparing the parametric 2-RDM(M) results for the ammonia oxide and oxywater systems to the coupled cluster results reveals differences in the degree of multi-reference correlation in these isoelectronic reactions. For ammonia oxide the parametric 2-RDM method predicts reaction and barrier energies within 1 kcal/mol of those from the CCSD(T) and CR-CC(T) methods. Furthermore, the energy barrier for the transition from hydroxylamine to ammonia oxide is similar for both the parametric method and CCSD(T) (52.32 and 52.15

Table 3.4: Energy differences of the ammonia-oxide reaction are compared with those of the oxywater reaction. All energy differences were computed from energies at the extrapolated basis-set limit. The oxywater energies are vibrationally corrected by a harmonic zero-point correlation [15], but the ammonia-oxide results are not since such corrections are small relative to the reaction and barrier energies. The chemical formulas (or abbreviations) used for the molecules are NH_2OH (hydroxylamine), NH_3O (ammonia oxide), HOOH (hydrogen peroxide), H_2OO (oxywater), and TS (transition state).

		$\Delta E_{\text{X-Y}}$			
Molecule Set	X-Y	CCSD	2-RDM(M)	CR-CC(T)	CCSD(T)
Ammonia Oxide	TS-NH_2OH	54.63	52.36	52.87	52.15
	NH_3O-NH_2OH	24.73	24.83	24.55	24.46
	TS-NH_3O	29.90	27.53	28.33	27.69
Oxywater	TS-HOOH	52.69	48.35	51.21	50.39
	H_2OO-HOOH	46.26	46.25	46.08	46.19
	TS-H_2OO	6.43	2.12	5.13	4.21

kcal/mol), and the reaction energy from hydroxylamine to ammonia oxide shows only a slight lowering (0.16 kcal/mol) to 27.53 kcal/mol when compared to the CCSD(T) result. In contrast, for the oxywater reaction the parametric 2-RDM(M) method predicts energy barriers that are over 2 kcal/mol lower than those from CCSD(T); specifically, it lowers the barrier from hydrogen peroxide to oxywater down from 50.39 to 48.35 kcal/mol and the barrier from oxywater to hydrogen peroxide from 4.21 kcal/mol to 2.12 kcal/mol. Therefore, in agreement with the occupation numbers, the parametric 2-RDM(M) method predicts greater multi-reference correlation in the oxywater reaction than in its isoelectronic analogue—the ammonia-oxide reaction.

Complementing Table 3.4, Figure 3.1 compares the 2-RDM(M) energies of the ammonia-oxide and oxywater reactions at the extrapolated basis-set limit. The similarity in the size of the forward barriers is readily apparent as is the difference in the reverse barriers. We observe that the barrier from oxywater to hydrogen peroxide is much smaller than the barrier from ammonia oxide to hydroxylamine. The transition state of the oxywater reaction is much closer in both energy and geometry to oxywater than the transition state of the ammonia oxide reaction is close to ammonia oxide.

Table 3.5: Trends in barrier heights across basis sets are compared for the ammonia-oxide-to-hydroxylamine and the oxywater-to-hydrogen-peroxide reactions. Coupled cluster methods are represented by the highest level method CCSD(T), but the trends are the same for both CCSD and CR-CC(T).

		$\Delta E_{\text{X-Y}}$	
X-Y	Basis Set	2-RDM(M)	CCSD(T)
TS-NH_3O	aug-cc-pVDZ	26.78	27.03
	aug-cc-pVTZ	26.74	26.95
	aug-cc-pVQZ	27.17	27.32
	EBSL	27.53	27.69
TS-H_2OO	aug-cc-pVDZ	2.96	3.60
	aug-cc-pVTZ	2.96	3.59
	aug-cc-pVQZ	2.58	4.01
	EBSL	2.12	4.21

A comparison of the trends in barrier heights across basis sets of the ammonia-oxide-to-hydroxylamine and oxywater-to-hydrogen-peroxide reactions can be found in Table 3.5. From ammonia oxide to hydroxylamine the barrier height increases from aug-cc-pVDZ to the basis-set limit with a small dip at aug-cc-pVTZ for both the 2-RDM(M) and CCSD(T) methods. The parametric 2-RDM(M) method raises the predicted barrier from 26.78 kcal/mol to 27.53 kcal/mol while CCSD(T) raises its predicted barrier from 27.03 to 27.69 kcal/mol. These small changes in barrier heights are notable compared to the larger changes in barrier eights observed in the oxywater system. For the oxywater-to-hydrogen-peroxide transition the 2-RDM(M) barrier decreases by 0.84 kcal/mol as the basis set increases from aug-cc-pVDZ to the basis-set limit while it increases for the coupled cluster methods by 0.61 kcal/mol. In contrast to coupled cluster, the parametric 2-RDM(M) method lowers the transition-state energy relative to oxywater as the size of the basis set increases.

3.3 Discussion and Conclusions

Using the parametric 2-RDM method, we studied the conversion of ammonia oxide to hydroxylamine and compared the results to the isoelectronic conversion of oxywater [15] to hydrogen

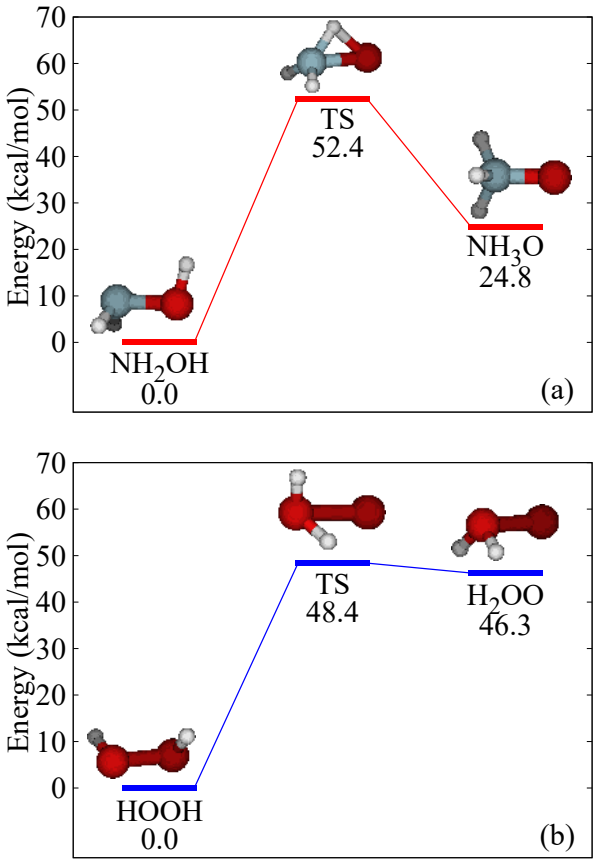

Figure 3.1: Isomerization reactions from the parametric 2-RDM(M), (a) the conversion of hydroxylamine to ammonia oxide and (b) the conversion of hydrogen peroxide to oxywater, are compared at the extrapolated basis set limit. The oxywater energies include a harmonic zero-point correction.

peroxide. The parametric 2-RDM(M) method and the computationally more expensive CR-CC(T) method recovers a similar amount of correlation energy, which is consistent with the previous study of the oxywater reaction. The correlation energies and the natural-orbital occupation numbers show that the most correlated molecule for both systems is the transition state and that the oxywater set of molecules is slightly more correlated than the ammonia oxide set of molecules. The addition of electron correlation stabilizes the transition state and hence, lowers the energy barrier within the reaction. Correlation also affects the ammonia oxide and oxywater geometries with notable bond lengthening of the O-O bonds in hydrogen peroxide, oxywater, and their transition state and the N-O bond in the transition state of the ammonia-oxide reaction.

For the relative energy differences between hydroxylamine, ammonia oxide, and their transition state, we found that the 2-RDM(M) results for the hydroxylamine-to-ammonia-oxide barrier and the ammonia-oxide-to-hydroxylamine barrier are comparable to the coupled cluster methods across all three basis sets and at the extrapolated basis-set limit. The differences between the parametric 2-RDM(M) and coupled cluster methods noted in this paper are not likely to be thermodynamically significant as they involve differences of at most 2 kcal/mol when the reverse barrier has been shown to be 27-29 kcal/mol. The size of the reverse barrier compared to the forward barrier supports the stability of ammonia oxide as seen in previous theoretical studies [18, 34–36]. The increase in barrier height with increasing basis-set size, observed for both the parametric and coupled cluster methods, suggests increased stability for ammonia oxide relative to its transition state in the basis-set limit.

In contrast to the results for ammonia oxide, because the barrier from oxywater to hydrogen peroxide is small, differences in electron correlation between methods can have a significant effect on reaction probabilities. The parametric 2-RDM(M) method predicts a small oxywater-to hydrogen-peroxide isomerization barrier of only 2.12 kcal/mol at the extrapolated basis-set limit while CCSD(T), the closest of the tested methods to the parametric

2-RDM method in terms of the barrier heights, gave a reverse barrier of 4.21 kcal/mol at the basis-set limit. Notably, this is a larger difference in both relative and absolute terms than was found for the ammonia-oxide isomerization where the ammonia oxide to hydroxylamine barrier calculated by CCSD(T) was only 0.34 kcal/mol higher than the parametric method. In addition, we find that the relative stabilization with increasing basis set size of the oxywater transition state with respect to oxywater is unique among the methods and states tested. In considering the role of multi-reference correlation in causing these differences, we note that for oxywater the energy barrier from the parametric 2-RDM(M) lies between those predicted by the coupled-cluster methods and the multi-reference methods [23, 24].

In this study we employed the parametric 2-RDM method with the M functional and several coupled cluster methods to compare the conversion of ammonia oxide to hydroxylamine to the conversion of oxywater to hydrogen peroxide. We used multiple basis sets including the largest basis set aug-cc-pVQZ that has yet to be applied to ammonia oxide. We found that the parametric 2-RDM(M) method gives similar results to coupled cluster methods and previous studies in contrast to the results for its isoelectronic cousin oxywater, where the parametric 2-RDM(M) method significantly lowers the barrier predicted by coupled cluster methods. The parametric 2-RDM method agrees with dynamic correlation methods such as coupled cluster when the multi-reference character of the system is minimal but incorporates additional multi-reference correlation, usually requiring specially designed multi-reference methods, as the amount of multi-reference correlation increases. This demonstrates the ability of the parametric method combined with the M functional to describe both dynamic and multi-reference correlation simultaneously to provide chemically accurate results at a low computational cost.

The M parametric 2-RDM method has been recently applied to studying the kinetic stability of oxywater [15], the relative populations of carbonic acid at 210 K [16], and the barrier to rotation separating the *cis* and *trans* isomers of diazene [17]. These results in conjunction with the present results for the conversion of ammonia oxide to hydroxylamine

demonstrate the ability of the parametric 2-RDM method to treat a broad range of chemical problems. Importantly, the parametric 2-RDM method with the M functional generally yields energies that approach the accuracy of coupled cluster theory with full triple excitations. Calculations of diradical transition states and bond stretches also indicate the M parametric 2-RDM method correctly treats some multi-reference correlation effects that are typically inaccessible to tradition single-reference wavefunction methods. With a computational cost like CISD the parametric 2-RDM method is more cost efficient than CCSD. A comparison of computational timings for oxywater is presented elsewhere [15]. Because the M parametrization of 2-RDM is derived from general relations from N-representability, the method with its combination of accuracy and efficiency has wide application to studying electron correlation in chemistry and physics.

3.4 References

[1] D. A. Mazziotti, Phys. Rev. Lett. **101**, 253002 (2008).

[2] D. A. Mazziotti, Phys. Rev. A **81**, 062515 (2010).

[3] D. A. Mazziotti, ed., *Two-Electron Reduced-Density-Matrix Mechanics*, vol. 134 of *Advances in Chemical Physics* (Wiley, New York, 2007).

[4] A. J. Coleman and V. I. Yukalov, *Reduced Density Matrices: Coulson's Challenge* (Springer, New York, 2000).

[5] J. Cioslowski, ed., *Many-Electron Densities and Reduced Density Matrices*, Mathematical and Computational Chemistry (Kluwer Academic/Plenum Publishers, New York, 2000).

[6] A. J. Coleman, Rev. Mod. Phys. **35**, 668 (1963).

[7] C. Garrod and J. Percus, J. Math. Phys. **5**, 1756 (1964).

[8] J. E. Harriman, Phys. Rev. A **17**, 1257 (1978).

[9] R. M. Erdahl, Int. J. Quantum Chem. **13**, 697 (1978).

[10] C. Kollmar, J. Chem. Phys. **125**, 084108 (2006).

[11] A. E. DePrince III and D. A. Mazziotti, Phys. Rev. A **76**, 042501 (2007).

[12] A. E. DePrince III and D. A. Mazziotti, J. Chem. Phys. B **112**, 16158 (2008).

[13] A. E. DePrince III, E. Kamarchik, and D. A. Mazziotti, J. Chem. Phys. **128**, 234103 (2008).

[14] A. E. DePrince III and D. A. Mazziotti, J. Chem. Phys. **130**, 164109 (2009).

[15] C. A. Schwerdtfeger, A. E. DePrince III, and D. A. Mazziotti, J. Chem. Phys. **134**, 174102 (2011).

[16] C. A. Schwerdtfeger and D. A. Mazziotti, J. Phys. Chem. A **115**, 12011 (2011).

[17] A. M. Sand, C. S. Schwerdtfeger, and D. A. Mazziotti, J. Chem. Phys. **136**, 034112 (2012).

[18] R. D. Bach, A. L. Owensby, C. Gonzalez, H. B. Schlegel, and J. J. W. McDouall, J. Am. Chem. Soc. **113**, 6001 (1991).

[19] O. Bain and P. A. Giguere, Can. J. Chem **33**, 527 (1955).

[20] J. A. Pople, K. Raghavachari, M. J. Frisch, S. J. Binkley, and P. v. R. Schleyer, J. Am. Chem. Soc. **105**, 6389 (1983).

[21] C. Meredith, T. P. Hamilton, and H. F. Schaefer III, J. Phys. Chem. **96**, 9250 (1992).

[22] H. H. Huang, Y. Xie, and H. F. Schaefer III, J. Phys. Chem. **100**, 6076 (1996).

[23] Y. Ge, K. Olsen, R. I. Kaiser, and J. D. Head, *Astrochemistry: From Laboratory Studies to Astronomical Observations* (American Institute of Physics, New York, 2006).

[24] R. Sayos, C. Oliva, and M. Gonzales, **113**, 6736 (2000).

[25] A. J. Kirby, J. E. Davies, T. A. S. Brandao, P. F. da Silva, W. R. Rocha, and F. Nome, J. Am. Chem. Soc. **128**, 12374 (2006).

[26] A. J. Kirby, J. E. Davies, D. J. Fox, D. R. W. Hodgson, A. E. Goeta, M. F. Lima, J. P. Priebe, and F. N. J. A. Santaballa, Chem Commun. **46**, 1302 (2010).

[27] C. Trindle and D. D. Shillady, J. Am. Chem. Soc. **95**, 703 (1973).

[28] J. F. Olsen and J. M. Howell, J. Fluorine Chem. **10**, 197 (1977).

[29] B. T. Hart, Aust. J. Chem. **29**, 231 (1976).

[30] H. Wallmeier and W. Kutzelnigg, J. Am. Chem. Soc. **101**, 2804 (1979).

[31] L. Radom, J. S. Binkley, and J. A. Pople, Aust. J. Chem. **30**, 699 (1977).

[32] F. Grein and L. J. Lawlor, Theor. Chem. Acc. **63**, 161 (1983).

[33] J. A. Pople, K. Raghavachari, M. J. Frisch, J. S. Binkley, and P. v. R. Schleyer, J. Am. Chem. Soc. **105**, 6389 (1983).

[34] S. H. Mousavipour, F. Pirhadi, and A. HabibAgahi, J. Phys. Chem. A **113**, 12961 (2009).

[35] Q. Wang, C. Wei, L. M. Perez, W. J. Rogers, M. B. Hall, and M. S. Mannan, J. Phys. Chem. A **114**, 9262 (2010).

[36] M. Bronstrup, D. Schrder, I. Kretzschmar, C. A. Schalley, and H. Schwarz, Eur. J. Inorg. Chem. **10**, 1529 (1998).

[37] M. Y. A. I. Gonzalez, O. Mo, Int. J. Mass Spectrom. **179/180**, 77 (1998).

[38] G. D. Purvis and R. J. Bartlett, J. Chem. Phys. **76**, 1910 (1982).

[39] P. Piecuch, S. A. Kucharski, K. Kowalski, and M. Musial, Comp. Phys. Commun. **149**, 71 (2002).

[40] K. Kowalski and P. Piecuch, J. Chem. Phys. **113**, 18 (2000).

[41] K. Kowalski and P. Piecuch, J. Chem. Phys. **113**, 5644 (2000).

[42] T. H. Dunning, Jr., J. Chem. Phys. **90**, 1007 (1989).

[43] M. W. Schmidt, K. K. Baldridge, J. A. Boatz, S. T. Elbert, M. S. Gordon, J. H. Jensen, S. Koseki, N. Matsunaga, K. A. Nguyen, S. J. Su, et al., J. Comput. Chem. **14**, 1347 (1993).

[44] A. K. Wilson and T. H. Dunning, Jr., J. Chem. Phys. **106**, 8718 (1997).

[45] W. Klopper and T. Helgaker, Theor. Chem. Acc. **99**, 265 (1998).

[46] D. A. Mazziotti, J. Chem. Phys. **126**, 184101 (2007).

[47] E. F. Valeev, W. D. Allen, R. Hernandez, C. D. Scherrill, and H. F. Schaefer, J. Chem. Phys. **118**, 8594 (1994).

[48] A. Halkier, T. Helgaker, P. Jorgensen, W. Klopper, H. Koch, J. Olsen, and A. K. Wilson, Chem. Phys. Letters **286**, 243 (1998).

[49] M. Wloch, J. R. Gour, K. Kowalski, and P. Piecuch, JCP **122**, 214107 (2005).

CHAPTER 4

RELATIVE ENERGIES AND GEOMETRIES OF THE *CIS*- AND *TRANS*-HO_3 RADICALS FROM THE PARAMETRIC 2-ELECTRON DENSITY MATRIX METHOD

This chapter contains parts of an article that was originally published in the *Journal of Physical Chemistry A*. Reprinted with permission from [E. P. Hoy, C. A. Schwerdtfeger, and D. A. Mazziotti, *J. Phys. Chem. A*, **117(8)**, 1817 (2013)].

4.1 Introduction

In 1952 at a conference in Chalk River A. John Coleman recognized that the ground-state energy and properties of an N-electron atom or molecule could in principle be computed as a linear functional of the 2-electron reduced density matrix (2-RDM) rather than the N-electron wave function [1]. This observation was the beginning of a new field in electronic structure—namely, reduced-density-matrix mechanics [2, 3]—in which the 2-RDM rather than the many-electron wave function is the basic computational variable.

Direct calculation of the 2-RDM requires that it be constrained by a set of conditions to derive from the integration of an N-electron density matrix. These constraints, called N-representability conditions by Coleman in 1963 [4], are necessary to ensure that the 2-RDM represents a realistic N-electron system [5–8]. Three general approaches for the direct calculation of the 2-RDM include: (i) the minimization of the energy with the 2-RDM constrained *explicitly* by N-representability conditions, which leads to a problem in semidefinite programming [9–13], (ii) the minimization of the energy with the 2-RDM parameterized (or constrained *implicitly*) by N-representability conditions [3, 14–18], and (iii) the calculation of the 2-RDM from the solution of the contracted Schrödinger equation (or its anti-Hermitian part) with cumulant-based reconstruction of the higher RDMs [3, 19–23]. In this paper we

focus on the second category of methods, the parametric 2-RDM methods, and their application to a problem representative of computing small energy differences in chemistry, the relative electronic energies of the HO_3 radical's two isomers.

Weinhold and Wilson [24, 25] developed one of the earliest parametric 2-RDM methods. They parameterized the 2-RDM as a functional of the parameters of the configuration interaction doubles (CID) wave function with the aim of developing a more general parametrization beyond a specific wave-function ansatz. More recently, Kollmar [26] and Mazziotti [14, 15] extended the work of Weinhold and Wilson to obtain 2-RDM parameterizations that are size extensive generalizations of the CID parametrization. The derivation of the Mazziotti parametrization is detailed in Chapter 2. Mazziotti's family of parameterizations can be shown to be a significant generalization of the traditional coupled electron-pair methods. While the traditional CEPA methods are based solely on perturbative arguments, the parametric 2-RDM methods have parameterizations that consider the N-representability of the 2-RDM. Here we employ the parametric 2-RDM method with the M parametrization, which we denote as the 2-RDM(M) method [3, 14, 15]. The 2-RDM(M) method has an accuracy approaching that of coupled cluster with single, double, and triple excitations, especially in the presence of some multi-reference correlation, at a computational cost that is less than coupled cluster with single-double excitations. Applications have been made to several closed-shell molecular systems [3, 14–18] including the calculation of (i) the small barrier separating oxywater from hydrogen peroxide [16], (ii) the relative energies of the *cis-cis* and *cis-trans* isomers of carbonic acid, and (iii) the rotational barrier separating *cis* and *trans* diazene [17]. Recently the 2-RDM(M) method has been extended to open-shell systems [27], which often require a multi-configurational reference to obtain chemically accurate energies and barriers [28]. In this chapter we apply the open-shell version of the 2-RDM(M) method to the isomers of the HO_3 radical.

The hydridotrioxygen molecule (HO_3) has been the subject of many experimental and computational studies due to its potential importance in atmospheric, combustion, and or-

ganic/biochemical oxidation processes [29–32]. In recent years the molecule's potential role as a reservoir for atmospheric OH has been particularly well examined [33–40]. HO_3 was first observed experimentally by Cacace *et al.* in 1999 using neutralization-reionization mass spectrometry [41]. The following year Nelander *et al.* reported its presence in Ar and H_2O ice matrices based on infrared spectroscopy results [42, 43]. The rotational spectrum of HO_3 was measured by Suma *et al.* in 2005 using Fourier-transform microwave spectroscopy. Based on the experimental rotational constants and theoretical dipole moment calculations, Suma *et al.* determined that the *trans* isomer of HO_3 was the source of this rotational spectrum. Subsequent experiments observed the fundamental HOO bend around 1250 cm^{-1} by irradiating $H_2^{18}O + O_2$ ice mixtures [44, 45]. The amount of energy required to dissociate $HO_3(\ X^2A'')$ to $OH(\ ^2\Pi_i)$+$O_2(\ ^3\Sigma_g^-)$ was established to have an experimental upper limit between 5.31 to 6.12 kcal/mol by a series of studies in 2007 and 2008 [33–36] and was given a value of 2.97 ± 0.07 kcal/mol (barrierless) by Le Picard *et al.* based on kinetic studies [37, 38]. Additionally, Lester and co-workers confirmed that the *trans* isomer is the primary contributor to the HO_3 rotational spectrum and suggested that *cis*-HO_3 likely appears in the spectrum as broad, unstructured peak [30, 33–36].

The HO_3 molecule has also received significant theoretical attention due to its potential importance in atmospheric processes and the notable difficulties in reconciling theoretical and experimental results [29, 31, 32, 39, 40, 46–53, 53–73]. In this study we investigate two of these issues: matching the theoretical to the experimental geometric parameters for the *trans*-HO_3 state (especially the unusually long central oxygen-oxygen bond) [32, 74] and determining whether the *cis*- or *trans*-HO_3 isomer is more favorable energetically [31, 35, 36, 39, 48, 73, 74]. Some disagreement exists as to the importance of multi-reference correlation and/or higher-order excitations to the HO_3 problem [31, 32, 39, 73]. The parametric 2-RDM(M) method's results for the *cis*- and *trans*-HO_3 states are compared to those from single-reference coupled cluster methods as well as previous experimental and theoretical results [36, 73, 74] in order to better understand the role of correlation in the energies and

geometries of the HO_3 states.

4.2 Applications

4.2.1 Computational Methods

We examined two isomers of the HO_3 radical and their transition state: *cis*- HO_3, *trans*-HO_3, and their isomerization transition state, using the open-shell versions of 2-RDM(M), coupled cluster with single and double excitations [CCSD] [75, 76], completely renormalized coupled cluster exploiting left eigenstates [CR-CCSD(T)L or CR-CCL] [75, 76], and coupled cluster with single and double excitations plus perturbative triple excitations [CCSD(T)] [77–82]. The CCSD and CR-CCL calculations were performed with the GAMESS electronic structure package [83], and the CCSD(T) results were computed using Gaussian 09 [84]. The open-shell parametric 2-RDM calculations were performed using a GAMESS implementation of the method discussed in Refs. [3, 15, 16, 27]. Using the numerical finite-difference optimization in GAMESS for the CCSD, CR-CCL, and 2-RDM(M) methods, we optimized the geometries of each molecule to a tolerance of 10^{-7} Hartrees/Å in the cc-pVTZ and aug-cc-pVTZ basis sets and then calculated single-point energies at these minimum-energy geometries in the cc-pVQZ and aug-cc-pVQZ basis sets. The core orbital of each oxygen was frozen for both the optimization and single-point calculations. The energy differences involving the two isomers and their transition state were calculated in the cc-pVQZ and aug-cc-pVQZ basis sets both with and without the addition of harmonic zero-point vibrational energies. The harmonic zero-point energies were calculated in the cc-pVDZ basis set by numerical finite differences using the GAMESS electronic structure package for CCSD, CR-CCL, and 2-RDM(M) and the Gaussian 09 package for CCSD(T) [83, 84].

Table 4.1: The natural-orbital occupation numbers as calculated by the 2-RDM(M) method in the cc-pVQZ and aug-cc-pVQZ basis sets are presented.

	Natural-orbital occupation numbers					
	HONO-1		HONO		LUNO	
Molecule	cc-pVQZ	aug-cc-pVQZ	cc-pVQZ	aug-cc-pVQZ	cc-pVQZ	aug-cc-pVQZ
trans	0.9485	0.9410	0.4992	0.4954	0.0585	0.0674
cis	0.9521	0.9449	0.4990	0.4966	0.0538	0.0612
TS	0.9486	0.9401	0.5012	0.4996	0.0542	0.0645

4.2.2 Results

We calculated the natural-orbital occupation numbers for each isomer and their transition state using the 2-RDM(M) method in the cc-pVQZ and aug-cc-pVQZ basis sets. The results of these calculations can be found in Table 4.1. The deviations of the second highest occupied natural-orbital (HONO-1) occupation number from 1.0, the highest occupied natural-orbital (HONO) occupation number from 0.5, and the lowest unoccupied natural-orbital (LUNO) occupation number from 0.0 indicate increasing multi-reference character. Both the HONO-1 and LUNO numbers show that *cis*-HO_3, *trans*-HO_3, and their transition state have a small but noticeable amount of multi-reference character. The *trans* isomer is the most multi-referenced with the transition state having slightly less multi-reference character. In previous studies of ammonia oxide and oxywater by Hoy *et al.* and Schwerdtfeger *et al.*, small differences in multi-reference character were found to alter the relative energy differences between isomers noticeably, especially when the energy differences were small [16, 18]. The energies from all of the methods including coupled cluster are not invariant to orbital rotations between the occupied and virtual orbitals. Because the natural occupation numbers are not too far from 0 and 1, energy variations from changes in the reference determinant are likely not large. The parametric 2-RDM method also has a slight invariance with respect to rotations between occupied orbitals and between virtual orbitals. Calculations of this latter invariance, to be published elsewhere, show that typically it also has a small effect on the energy.

Table 4.2: The total electronic energies before harmonic zero-point vibrational energies *plus* 225 Hartrees are given for the cc-pVQZ and aug-cc-pVQZ basis sets.

		Total electronic energy +225 (H)			
Molecule	Basis Set	CCSD	2-RDM(M)	CR-CCL	CCSD(T)
trans-HO_3	cc-pVQZ	-0.802560	-0.837671	-0.838718	-0.839630
cis-HO_3		-0.803949	-0.837227	-0.839737	-0.840244
TS		-0.802261	-0.834424	-0.837823	-0.838569
trans-HO_3	aug-cc-pVQZ	-0.810248	-0.850797	-0.845735	-0.848349
cis-HO_3		-0.811341	-0.850146	-0.846471	-0.848597
TS		-0.810000	-0.847562	-0.844740	-0.847217

Table 4.2 contains the total electronic energies before the addition of harmonic zero-point vibrational energies (harmonic ZPEs) for each of the states studied in the cc-pVQZ and aug-cc-pVQZ basis sets. In the cc-pVQZ basis set the parametric 2-RDM(M) method recovers an amount of correlation energy between CCSD and CCSD(T), which is consistent with the results from previous studies of closed-shell molecules [16–18, 85]. In the aug-cc-pVQZ basis set the parametric 2-RDM(M) method yields correlation energies that are lower than those from CCSD(T) by 0-0.0024 H. Previous calculations with the 2-RDM method indicate that it recovers more correlation energy than CCSD(T) only when there are significant contributions from multi-reference effects [17]. In conjunction with the natural-orbital occupation numbers, this finding suggests that the 2-RDM(M) method is capturing additional multi-reference correlation beyond that from the coupled cluster methods.

The energy differences between the HO_3 isomers before and after the addition of harmonic zero-point vibrational energies are given in Tables 4.3 and 4.4 respectively. Considering the uncorrected results first, we see that the 2-RDM(M) method predicts that the *trans*-HO_3 isomer is lower in energy than the *cis* isomer in the cc-pVQZ basis set by 0.28 kcal/mol. The addition of augmented functions to the basis set lowers the *trans* further relative to the *cis* and thereby increases the predicted energy gap between the two isomers to 0.41 kcal/mol. With the addition of harmonic zero-point vibrational energies (Table 4.4), the 2-RDM(M) *predicts a trans-cis energy difference of -1.71 kcal/mol in the cc-pVQZ basis set*

Table 4.3: The energy differences between states before the addition of harmonic zero-point energies are presented for cc-pVQZ and aug-cc-pVQZ basis sets. For comparison, MRCI(Q) cc-pVQZ and aug-cc-pVQZ *trans-cis* energy differences calculated by Varandas in 2012 are provided [73].

		$\Delta E_{\text{X-Y}}$(kcal/mol)				
X-Y	Basis Set	CCSD	2-RDM(M)	CR-CCL	CCSD(T)	MRCI(Q)
trans-cis	cc-pVQZ	0.87	-0.28	0.64	0.39	-0.05
TS-*trans*		0.19	2.04	0.56	0.65	
trans-cis	aug-cc-pVQZ	0.69	-0.41	0.46	0.16	-0.22
TS-*trans*		0.16	2.03	0.62	0.71	

Table 4.4: The energy barriers after the inclusion of harmonic zero-point vibrational energies for cc-pVQZ and aug-cc-pVQZ basis sets are reported in this table.

		$\Delta E_{\text{X-Y}}$(kcal/mol)			
X-Y	Basis Set	CCSD	2-RDM(M)	CR-CCL	CCSD(T)
trans-cis	cc-pVQZ	0.61	-1.71	0.39	0.02
TS-*trans*		-0.04	2.04	0.55	0.11
trans-cis	aug-cc-pVQZ	0.42	-1.84	0.21	-0.21
TS-*trans*		-0.07	2.04	0.61	0.17

and -1.84 kcal/mol in the aug-cc-pVQZ basis set due to *cis* state having a harmonic zero-point vibrational energy which is 1.43 kcal/mol larger than the *trans* harmonic zero-point vibrational energy. The addition of harmonic zero-point vibrational energies or augmented functions does not noticeably change the energy difference between the transition state and the *trans* isomer for the 2-RDM(M) method which remains at ∼2.04 kcal/mol for all the cases studied.

Without including harmonic zero-point vibrational energies (Table 4.3), all of the coupled cluster methods predict that the *cis*-HO_3 isomer is lower in energy than the *trans*-HO_3 isomer. Among the coupled cluster methods, the energetic favorability of the *cis* isomer is largest for the CCSD method which predicts a 0.87 kcal/mol difference in favor of the *cis* isomer in the cc-pVQZ basis set and smallest for the CCSD(T) method which predicts a 0.39 kcal/mol difference in favor of the *cis* isomer. Similarly to the 2-RDM(M) method, the *trans* state is lowered in energy relative to the cis state by the addition of augmented functions to the basis set resulting in a smaller *trans-cis* gap for all three coupled cluster methods. In the aug-cc-pVQZ basis set, the CCSD method predicts a *trans-cis* gap of 0.69 kcal/mol while the CCSD(T) method predicts a difference of 0.16 kcal/mol in favor of the *cis* isomer. Additionally, the couple cluster methods all predict that the *trans* state is less than 1 kcal/mol lower than the transition state before the addition of harmonic zero-point vibrational energies.

Once harmonic zero-point vibrational energies are included, as shown in Table 4.4, the CCSD and CR-CCL methods in the aug-cc-pVQZ basis set predict that *cis*-HO_3 remains lower than *trans*-HO_3 by 0.42 and 0.21 kcal/mol, respectively. Of the coupled cluster methods, only the CCSD(T) method predicts that the relative ordering of the *cis* and *trans* states changes once harmonic zero-point vibrational energies are included. The CCSD(T) method predicts that the *trans* isomer is 0.02 kcal/mol higher than the *cis* isomer in the cc-pVQZ basis set but that the *trans* isomer is 0.21 kcal/mol lower than the *cis* isomer in the aug-cc-pVQZ basis. With the addition of harmonic zero-point energies to the CCSD

Table 4.5: The harmonic frequencies calculated in the cc-pVDZ basis set for each molecule and method are provided in the table below. Experimental results from Derro *et al.* for the *trans* isomer are provided for comparison[36].

		Harmonic Frequencies (cm^{-1})				
Molecule	Basis Set	CCSD	2-RDM(M)	CR-CC(T)	CCSD(T)	Exp
trans-HO_3	ω_1	106.67	72.66	145.55	120.92	122
	ω_2	466.75	136.75	316.33	179.96	144
	ω_3	681.05	449.47	562.53	475.62	482
	ω_4	1233.95	979.20	1178.43	1055.72	998
	ω_5	1369.38	1425.01	1360.24	1455.06	
	ω_6	3774.56	3727.83	3737.22	3722.39	3528
Transition State	ω_2	483.83	111.52	345.60	63.73	
	ω_3	695.15	480.72	627.59	462.60	
	ω_4	1217.50	1015.18	1243.47	973.89	
	ω_5	1296.31	1353.19	1336.75	1421.32	
	ω_6	3778.68	3843.99	3738.20	3710.66	
cis-HO_3	ω_1	230.79	352.46	220.71	206.00	
	ω_2	494.19	414.63	362.15	242.77	
	ω_3	723.56	779.94	623.80	569.41	
	ω_4	1220.48	1167.89	1217.89	1213.71	
	ω_5	1423.75	1452.61	1361.33	1346.41	
	ω_6	3722.78	3630.43	3690.99	3686.54	

methods energy results, the CCSD method predicts in both the cc- pVQZ and aug-cc-pVQZ basis sets that the *trans* isomer is higher in energy than the transition state by less than 0.1 kcal/mol. The CCSD(T) method predicts that the addition of harmonic zero-point energies lowers of the transition state to ∼0.2 kcal/mol above the *trans* state. The addition of harmonic zero-point vibrational energies to our total electronic energies does not noticeably change this energy difference in the CR-CCL method. Comparison of Tables 4.3 and 4.4 shows that the addition of the harmonic zero-point energies stabilizes the *trans* relative to the *cis* for all of the methods. The 2-RDM(M) method manifests the largest stabilization of ≈1.4 kcal/mol, which is approximately 1 kcal/mol greater than that found in CCSD(T). The origin of this stabilization can be seen in the harmonic vibrational frequencies in Table 4.5. While the 2-RDM(M)'s predicted frequencies for *cis* are close to those from CCSD, the predicted frequencies for *trans* are close to those from CCSD(T). This subtle difference between the frequencies for *cis* and *trans* is enough to account for the increased stabilization from 2-RDM(M).

The parametric 2-RDM(M) method predicts that the *trans* isomer is more stable than the *cis* isomer both before and after harmonic zero-point vibrational energies are added while CCSD(T) only favors the *trans* in the aug-cc-pVQZ basis set after harmonic zero-point vibrational energies are added. Figure 4.1 graphically compares the relative energies with harmonic zero-point energies included from the 2-RDM(M), CCSD, and CCSD(T) methods in the (a) cc-pVQZ and (b) aug-cc-pVQZ basis sets. When we compare these results to the multi-reference configuration (MRCI) results of Suma *et al.* and Varandas *et al.*, we see some interesting parallels between the predictions of the MRCI and 2-RDM(M) method [31, 48, 73, 74]. Suma *et al.* optimized the HO_3 using the multi-reference single and double excitation configuration interaction method with the Davidson correction (MRCI+Q) in the aug-cc-pVTZ basis set, which predicted an energetic favoring of the *trans* isomer by 0.266 kcal/mol and an isomerization barrier of 0.921 kcal/mol. In a 2012 paper Varandas, using the MRCI and MRCI+Q methods in multiple correlation-consistent basis sets with and

Table 4.6: The oxygen bond lengths calculated in the aug-cc-pVTZ basis set are reported. The total correlation energy recovered in the aug-cc-pVQZ basis set for each molecule is given in the rows marked CE (correlation energy) below the relevant parameters. The experimental values for the *trans*-HO_3 b_{oo1} bond length are 1.225* Å [74] and 1.235 Å [32] while the values for the b_{oo2} bond length are 1.688 Å [74] and 1.648 Å [32]. *Fixed at the MRCI+Q value in order to estimate the other geometric parameters.

		Geometries(Å or °)			
Molecule	Parameter	CCSD	2-RDM(M)	CR-CCL	CCSD(T)
trans-HO_3	b_{oo1}	1.2489	1.2446	1.2387	1.2304
	b_{oo2}	1.4917	1.6187	1.5595	1.6050
	CE	-0.7718	-0.8297	-0.8156	-0.8248
cis-HO_3	b_{oo1}	1.2611	1.2652	1.2576	1.2520
	b_{oo2}	1.4667	1.5740	1.5129	1.5403
	CE	-0.7725	-0.8252	-0.8126	-0.8176
TS	b_{oo1}	1.2558	1.2527	1.2505	1.2416
	b_{oo2}	1.4863	1.6173	1.5448	1.5875
	d_{oooh}	124.04	84.76	90.28	80.44
	CE	-0.7700	-0.8262	-0.8120	-0.8210

without extrapolation to the basis-set limit, predicts the *trans*-*cis* differences between 0.1 to 0.6 kcal/mol in favor of the *trans* isomer. The MCRI(Q) results from the Varandas paper in the cc-pVQZ and aug-cc-VQZ basis sets are given in Table 4.3 for comparison. Overall, we find that the 2-RDM(M)'s predicted results are closer to those predicted by multi-reference calculations than those from single-reference CCSD, especially in the energetic stability of the *trans* isomer relative to the *cis* isomer and the height of the barrier to isomerization ($\approx$ 2 kcal/mol).

Table 4.6 contains the oxygen bond lengths for each of the two isomers and their transition states calculated in the aug-cc-pVTZ basis set. We focus on the oxygen bond lengths here since they are typically underestimated by theoretical methods relative to experiment [32, 74]. For completeness, the full set of geometries for both the optimizations and the harmonic zero-point vibrational energy calculations are available in the supplemental information of the published paper. Comparing the 2-RDM(M) results to CCSD results for the *trans*-HO_3 state, we find that the parametric 2-RDM(M) method predicts a geometry with longer

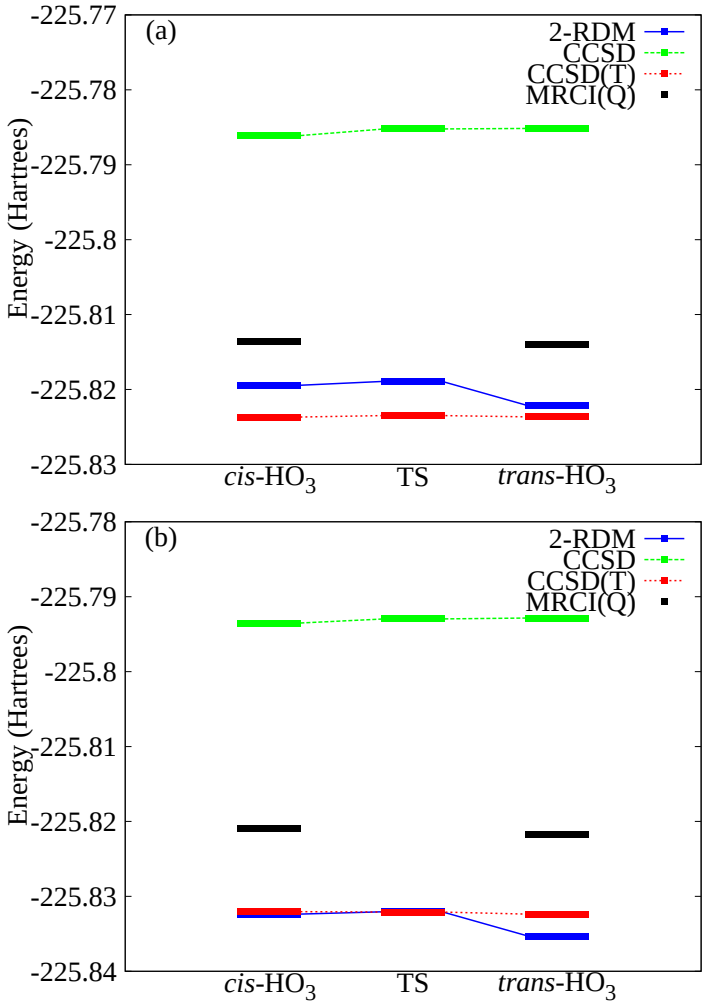

Figure 4.1: Relative energies of the two HO_3 isomers and their transition state from the 2-RDM(M), CCSD, and CCSD(T) methods are shown for the (a) cc-pVQZ and (b) aug-cc-pVQZ basis sets. **MRCI(Q)** calculations in the cc-pVQZ (a) and aug-cc-pVQZ (b) basis sets including harmonic vibrational zero-point energies extrapolated to the basis set limit from Ref. [73].

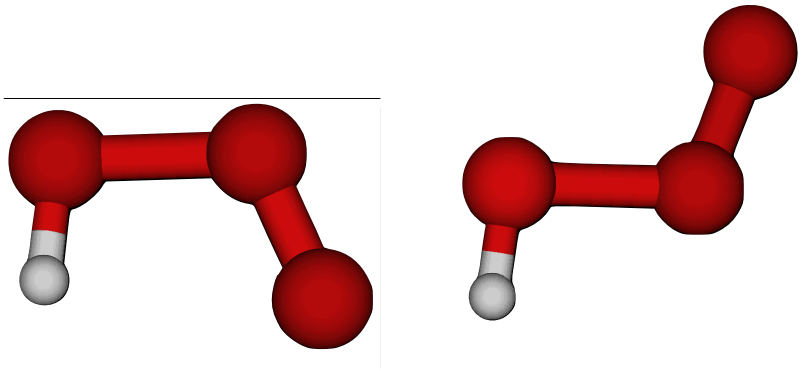

Figure 4.2: Figures show the (a) *cis*- and (b) *trans*-HO_3 geometries as calculated by the 2-RDM(M) method in the aug-cc-pVTZ basis set.

oxygen-oxygen bonds than CCSD in both basis sets. Compared to the experimental results of McCarthy *et al.* ($b_{oo1} = 1.235$ and $b_{oo2} = 1.684$), 2-RDM(M) gives a longer bond length, 1.2446 Å , for the b_{oo1} bond and a shorter one, 1.6187 Å , for the b_{oo2} at the aug-cc-pVTZ level. Both the CCSD and CR-CCL methods predict much shorter bond lengths for the b_{oo2} bond than the 2-RDM(M) method. The best coupled cluster method in terms of matching the experimental geometries, CCSD(T), predicts a b_{oo1} bond length of 1.2304 in the aug-cc-pVQZ basis set; however, the b_{oo2} bond length predicted by CCSD(T) is shorter (1.6050) than the one predicted by the 2-RDM(M) method and farther from the experimental value. Looking at the trends in the coupled cluster methods, we can see that in moving from CCSD to CCSD(T) the b_{oo1} bond length decreases while the b_{oo2} bond length increases. Although not shown in Table 4.6, the 2-RDM(M) method displays a similar behaviour when augmented functions are added to the basis set. Taken together these results suggest that increasing the dynamic correlation energy recovered shortens the b_{oo1} bond and lengthens the b_{oo2} bond while the addition of multi-reference correlation lengthens both bonds. To help explain and support these results, we consider the correlation energy recovery of the 2-RDM(M) method as compared to the coupled cluster methods.

For the HO_3 isomers we find that the 2-RDM(M) method recovers 101-103% of the

correlation energy added to CCSD by CR-CC(L) at the cc-pVQZ level. At the aug-cc-pVQZ level, this increases to 130-132%. These results are indicative of multi-reference character as the 2-RDM(M) method only recovered more correlation energy than CR-CC or CCSD(T) in the presence of multi-reference correlation such as seen in the transition state of diazene studied by Sand, Schwerdtfeger, and Mazziotti in 2012 [17]. Both natural-orbital occupation numbers and the total energy recovered suggest that multi-reference correlation plays a non-trivial role in describing the energetics of this system in line with some previous HO_3 studies [31, 48, 73]. The longer oxygen-oxygen bonds of the HO_3 isomers, as predicted by 2-RDM(M), are a likely consequence of the multi-reference correlation. A similar effect is caused by the addition of perturbative triples to CCSD [CCSD(T)]. Therefore, it is likely that a high level of both dynamic and multi-reference correlation is need to describe the geometry of this system.

4.3 Discussion and Conclusions

In this study we employed the parametric 2-RDM(M) method and several coupled cluster methods to study the HO_3 molecular system in the cc-pVQZ and aug-cc-pVQZ basis sets. The study represents the first application of the parametric 2-RDM(M) method to an open-shell system of significant chemical interest. The two key features examined were (i) the relative orderings of the *cis* and *trans* isomers of HO_3 and (ii) the experimental geometries of *trans*-HO_3. Experimental results suggest that the *trans*-HO_3 isomer is the lower in energy than the *cis*-state and possesses a long central oxygen-oxygen bond that is difficult for theoretical methods to match [30, 32–36, 74]. The 2-RDM(M) method predicted that the *trans*-HO_3 isomer is lower in energy than the *cis*-HO_3 isomer by between 1.71 to 1.81 kcal/mol once harmonic zero-point vibrational energies are added and between 0.28 to 0.41 kcal/mol *without including the zero-point energies*. The CCSD and CR-CCL methods both predict that *cis*-HO_3 is lower in energy than *trans*-HO_3. Of the coupled cluster methods, only the CCSD(T) method in the aug-cc-pVQZ basis set predicted that the trans

isomer is lower in energy by 0.21 kcal/mol once harmonic zero-point vibrational energies are included.

A key difference between the CCSD(T) and 2-RDM(M) results points to the ability of the 2-RDM(M) method, as seen in Ref. [17], to capture some electron correlation which is traditionally as multi-reference correlation. Without including harmonic zero-point vibrational energies in the results, only the 2-RDM(M) method predicts that *trans*-HO_3 is electronically favored over the *cis* isomer. Based on the natural-orbital occupation numbers and correlation energy recovered, we find that the difference is based, at least in part, on the degree of multi-reference correlation captured by the 2-RDM(M) method. This conclusion is consistent with previous studies on the topic which suggest that multi-reference correlation is necessary to describe this system [31, 40, 45, 48, 52, 63, 65, 73, 74, 86]. Most notably, we find that the CCSD method, the least multi-referenced of the coupled cluster methods employed, showed the largest energetic favoring of the *cis*-isomer before and after harmonic zero-point vibrational energies are added while the 2-RDM(M), which is capable of describing multi-referenced systems, predicted the largest energy difference in favor of *trans*-HO_3.

After considering the geometry results, we found that the parametric 2-RDM(M) method predicted longer oxygen-oxygen bonds overall than predicted by the coupled cluster methods. In the aug-cc-pVTZ basis set the 2-RDM(M) method predicted a central oxygen-oxygen bond length (b_{oo2}) for *trans*-HO_3 of 1.6187 Å compared to the 1.4917 Å bond length predicted by CCSD and the 1.6050 Å bond length predicted by CCSD(T). Compared to the coupled clusters results, the 2-RDM(M) result was closer to but still shorter than the experimental bond length of 1.684/1.688 Å [32, 74]. In the same basis set the second oxygen-oxygen bond (b_{oo1}) was predicted by the 2-RDM(M) method to be 1.2446 Å long. The addition of augmented functions notably improved the geometry results which depend heavily on correlation energy recovery. Other multi-referenced methods from previous studies, particularly MRCI and MRCI(Q) results extrapolated to the basis-set limit, have been able to match the experimental central oxygen-oxygen bond length even more closely than 2-RDM(M)

[31, 52, 73, 74]. Considering this along with the lengthening of the central bond and shortening of the b_{oo1} bond with basis set size, we speculate that a 2-RDM(M) optimization in the aug-cc-pVQZ or larger basis set would potentially yield further improvements to the geometries and hence, should be considered for future studies of this system.

With the extension of the parametric 2-RDM(M) method to open-shell systems, we have a method that is capable of treating a large variety of systems with a high degree of accuracy [3, 14–18, 85]. With a computational cost equivalent to configuration interaction with single and double excitations (CISD) and less than that of CCSD, the 2-RDM(M) method is capable of approaching the accuracy of coupled cluster with full triple excitations in single-reference cases as well as being able to treat some multi-reference cases. In this study, we found that the 2-RDM(M) method predicts that *trans*-HO_3 is lower in energy than *cis*-HO_3 in both the cc-pVQZ and aug-cc-pVQZ basis sets in line with experimental results; furthermore, it improves on the predicted oxygen-oxygen bond lengths predicted by CCSD relative to experimental results. Both the energetic and geometric predictions are consistent with previous results from multi-reference methods. Even though the parametric 2-RDM method is a single-reference theory, the present results in addition to earlier calculations [14–17] demonstrate its ability to capture multi-reference correlation effects. The open-shell 2-RDM(M) method, which performs similarly to its closed-shell counterpart, is applicable to a wide range of moderately correlated open-shell chemical systems.

4.4 References

[1] A. J. Coleman and V. I. Yukalov, *Reduced Density Matrices: Coulson's Challenge* (Springer, New York, 2000).

[2] D. A. Mazziotti, ed., *Two-Electron Reduced-Density-Matrix Mechanics*, vol. 134 of *Advances in Chemical Physics* (Wiley, New York, 2007).

[3] D. A. Mazziotti, Chem. Rev. **112**, 244 (2012).

[4] A. J. Coleman, Rev. Mod. Phys. **35**, 668 (1963).

[5] C. Garrod and J. Percus, J. Math. Phys. **5**, 1756 (1964).

[6] J. E. Harriman, Phys. Rev. A **17**, 1257 (1978).

[7] R. M. Erdahl, Int. J. Quantum Chem. **13**, 697 (1978).

[8] D. A. Mazziotti, Phys. Rev. Lett. **108**, 263002 (2012).

[9] Z. Zhao, B. J. Braams, H. Fukuda, M. L. Overton, and J. K. Percus, J. Chem. Phys. **120**, 2095 (2004).

[10] E. Cancés, G. Stoltz, and M. Lewin, J. Chem. Phys. **125**, 064101 (2006).

[11] D. A. Mazziotti, Phys. Rev. Lett. **93**, 213001 (2004).

[12] D. A. Mazziotti, Phys. Rev. Lett. **106**, 083001 (2011).

[13] B. Verstichel, H. van Aggelen, D. Van Neck, P. W. Ayers, and P. Bultinck, Phys. Rev. A **80**, 032508 (2009).

[14] D. A. Mazziotti, Phys. Rev. Lett. **101**, 253002 (2008).

[15] D. A. Mazziotti, Phys. Rev. A **81**, 062515 (2010).

[16] C. A. Schwerdtfeger, A. E. DePrince III, and D. A. Mazziotti, J. Chem. Phys. **134**, 174102 (2011).

[17] A. M. Sand, C. S. Schwerdtfeger, and D. A. Mazziotti, J. Chem. Phys. **136**, 034112 (2012).

[18] E. P. Hoy, C. S. Schwerdtfeger, and D. A. Mazziotti, Mol. Phys. **107**, 765 (2012).

[19] F. Colmenero and C. Valdemoro, Phys. Rev. A **47**, 979 (1993).

[20] H. Nakatsuji and K. Yasuda, Phys. Rev. Lett. **76**, 1039 (1996).

[21] D. A. Mazziotti, Phys. Rev. A **57**, 4219 (1998).

[22] D. A. Mazziotti, Phys. Rev. Lett. **97**, 143002 (2006).

[23] D. A. Mazziotti, Phys. Rev. A **76**, 052502 (2007).

[24] F. Weinhold and E. B. Wilson, J. Chem. Phys. **46**, 2752 (1967).

[25] F. Weinhold and E. B. Wilson, J. Chem. Phys. **47**, 2298 (1967).

[26] C. Kollmar, J. Chem. Phys. **125**, 084108 (2006).

[27] C. A. Schwerdtfeger and D. A. Mazziotti, J. Chem. Phys. **137** (2012).

[28] T. Bally and W. T. Borden, *Calculations on Open-Shell Molecules: A Beginner's Guide* (John Wiley and Sons Inc, New York, 2007), pp. 1–97.

[29] M. Speranza, Inorg. Chem. **35**, 6140 (1996).

[30] C. Murray, E. L. Derro, T. D. Sechler, and M. I. Lester, Acc. Chem. Res. **42**, 419 (2009).

[31] A. J. C. Varandas, Phys. Chem. Chem. Phys. **13**, 9796 (2011).

[32] M. C. McCarthy, V. Lattanzi, D. Kokkin, O. M. ,Jr., and J. F. Stanton, J. Chem. Phys. **136**, 034303 (2012).

[33] C. Murray, E. L. Derro, T. D. Sechler, and M. I. Lester, **111**, 4727 (2007).

[34] E. L. Derro, C. Murray, T. D. Sechler, and M. I. Lester, J. Phys. Chem. A **111**, 11592 (2007).

[35] E. L. Derro, T. D. Sechler, C. Murray, and M. I. Lester, J. Phys. Chem. A **112**, 9269 (2008).

[36] E. L. Derro, T. D. Sechler, C. Murray, and M. I. Lester, J. Chem. Phys. **128**, 244313 (2008).

[37] S. D. L. Picard, M. Tizniti, A. Canosa, I. R. Sims, and I. W. M. Smith, Science **328**, 1258 (2010).

[38] M. Tizniti, S. D. L. Picard, A. Canosa, I. R. Sims, and I. W. M. Smith, Phys. Chem. Chem. Phys. **12**, 12702 (2010).

[39] M. E. Varner, M. E. Harding, J. Vazquez, J. Gauss, and J. Stanton, J. Phys. Chem. A **113**, 11238 (2009).

[40] J. M. Anglada, S. Olivella, and A. Sole, J. Chem. Theory Comput. **6**, 2743 (2010).

[41] F. Cacace, G. de Petris, F. Pepi, and A. Troiani, Science **285**, 81 (1999).

[42] B. Nelander, A. Engdahl, and T. Svensson, Chem. Phys. Letters **332**, 403 (2000).

[43] B. Nelander, A. Engdahl, and T. Svensson, Science **3339**, 295 (2001).

[44] P. D. Cooper, M. H. Moore, and R. L. Hudson, J. Phys. Chem. A **110**, 7985 (2006).

[45] W. Zheng, D. Jewitt, and R. I. Kaiser, Phys. Chem. Chem. Phys. **9**, 2556 (2007).

[46] M. E. Varner, M. E. Harding, J. Gauss, and J. F. Stanton, Chem. Phys. **346**, 53 (2008).

[47] A. J. C. Varandas, Phys. Chem. Chem. Phys. **13**, 15619 (2011).

[48] J. M. Beames, M. I. Lester, C. Murray, M. E. Varner, and J. F. Stanton, J. Chem. Phys. **134**, 044304 (2011).

[49] A. J. C. Varandas and H. G. Yu, Mol. Phys. **91**, 301 (1997).

[50] M. Speranza, J. Phys. Chem. **102**, 7535 (1998).

[51] P. A. Denis, M. Kieninger, O. N. Ventura, R. E. Cachau, and G. H. F. Diercksen, Chem. Phys. Letters **365**, 440 (2002).

[52] B. J. Braams and H.-G. Yu, Phys. Chem. Chem. Phys. **10**, 3150 (2008).

[53] P. A. Denis and F. R. Ornellas, J. Phys. Chem. A **113**, 499 (2009).

[54] D. J. Grant, D. A. Dixon, J. S. Francisco, D. Feller, and K. A. Peterson, J. Phys. Chem. A **113**, 11343 (2009).

[55] M. Dupuis, G. Fitzgerald, B. Hammond, W. A. Lester Jr., and H. F. Schaefer III, J. Chem. Phys. **84**, 2691 (1996).

[56] R. J. Blint and M. D. Newton, J. Chem. Phys. **59**, 6220 (1973).

[57] K. B. Mathisen and P. E. M. Siegbahn, Chem. Phys. **90**, 225 (1984).

[58] W. M. F. Fabian, J. Kalcher, and R. Janoschek, Theor. Chem. Acc. **114**, 182 (2005).

[59] H. G. Yu and A. J. C. Varandas, Chem. Phys. Letters **334**, 173 (2001).

[60] P. A. Denis, M. Kieninger, O. N. Ventura, R. E. Cachau, and G. H. F. Diercksen, Chem. Phys. Letters **377**, 483 (2002).

[61] A. Mansergas and J. M. Anglada, Comp. Phys. Commun. **7**, 1488 (2006).

[62] S. Chalmet and M. F. Ruiz-Lopez, Phys. Chem. Chem. Phys. **7**, 463 (2006).

[63] A. Mansergas, J. M. Anglada, S. Olivella, M. F. Ruiz-Lopez, and M. Martins-Costa, Phys. Chem. Chem. Phys. **9**, 5865 (2007).

[64] L. P. Viegas, A. Branco, and A. J. C. Varandas, J. Chem. Theory Comput. **6**, 2751 (2010).

[65] O. Setokuchi, M. Sato, and S. Matuzawa, J. Phys. Chem. A **104**, 3204 (2000).

[66] A. Karton, S. Parthiban, and J. M. L. Martin, J. Phys. Chem. A **113**, 4802 (2009).

[67] M. A. Vincent and I. H. Hillier, J. Phys. Chem. **99**, 3109 (1995).

[68] P. A. Denis and F. R. Ornellas, Chem. Phys. Letters **464**, 150 (2008).

[69] J. Cerkovnik, E. Erzen, J. Koller, and B. Plesnicar, J. Am. Chem. Soc. **124**, 404 (2002).

[70] T. P. W. Jungkamp and J. H. Steinfeld, Chem. Phys. Letters **257**, 15 (1996).

[71] Z. F. Xu and M. C. Lin, Chem. Phys. Letters **440**, 12 (2007).

[72] S. Chalment and M. F. Ruiz-Lopez, J. Chem. Phys. **124**, 194502 (2006).

[73] A. J. C. Varandas, J. Chem. Theory Comput. **8**, 428 (2012).

[74] K. Suma, Y. Sumiyoshi, and Y. Endo, Science **308**, 1885 (2005).

[75] P. Piecuch and M. Wloch, J. Chem. Phys. **123**, 224105 (2005).

[76] M. Wloch, J. R. Gour, and P. Piecuch, J. Phys. Chem. A **111**, 11359 (2007).

[77] J. Cizek, *Advances in Chemical Physics*, vol. 14 (Wiley Interscience, New York, 1969).

[78] G. D. Purvis and R. J. Bartlett, J. Chem. Phys. **76**, 1910 (1982).

[79] G. E. Scuseria, C. L. Janssen, and H. F. Schaefer III, J. Chem. Phys. **89**, 7382 (1988).

[80] G. E. Scuseria and H. F. Schaefer III, J. Chem. Phys. **90**, 3700 (1989).

[81] J. D. Watts, J. Gauss, and R. J. Bartlett, J. Chem. Phys. **98**, 8718 (1993).

[82] J. A. Pople, M. Head-Gordon, and K. Raghavachari, J. Chem. Phys. **87**, 5968 (1987).

[83] M. W. Schmidt, K. K. Baldridge, J. A. Boatz, S. T. Elbert, M. S. Gordon, J. H. Jensen, S. Koseki, N. Matsunaga, K. A. Nguyen, S. J. Su, et al., J. Comput. Chem. **14**, 1347 (1993).

[84] M. J. Frisch, G. W. Trucks, H. B. Schlegel, G. E. Scuseria, M. A. Robb, J. R. Cheeseman, G. Scalmani, V. Barone, B. Mennucci, G. A. Petersson, et al., *Gaussian 09 Revision A.1*, gaussian Inc. Wallingford CT 2009.

[85] C. A. Schwerdtfeger and D. A. Mazziotti, J. Phys. Chem. A **115**, 12011 (2011).

[86] D. G. Semesko and S. L. Khursan, J. Phys. Chem. A **82**, 1439 (2008).

CHAPTER 5

ENERGIES AND STRUCTURES IN BIRADICAL CHEMISTRY FROM THE PARAMETRIC TWO-ELECTRON REDUCED-DENSITY MATRIX METHOD: APPLICATIONS TO THE BENZENE AND CYCLOBUTADIENE BIRADICALS

This chapter contains parts of an article that was originally published in *Physical Chemistry Chemical Physics*. Reprinted with permission from [A. L. McManus, E. P. Hoy and D. A. Mazziotti, *Phys. Chem. Chem. Phys.*, **17**, 12521 (2015)].

5.1 Introduction

The general class of organic biradicals has motivated a multitude of experimental and theoretical studies [1–16]. These species have been identified as intermediates in many relevant organic reactions, including photochemical processes [6–8], the Bergman cyclization reaction [9–12], and a number of cycloaddition reactions [13–16]. Meanwhile, the electronic structure of biradicals makes them challenging for theoretical studies.

A species is classified as a *biradical* if it contains two degenerate molecular orbitals on separate atomic centers and two electrons with which to fill them [17–19]. These species are distinguished from the more general class of *diradicals*, which contain two unpaired electrons that may or may not be localized on separate atomic centers [20]. Biradical systems in which the unpaired electrons do not interact significantly have been referred to as *biradicaloids* [21].

The pair of singly occupied degenerate orbitals in biradical systems generates multi-reference correlation, in which two or more determinants contribute significantly to the wavefunction at the zeroith order of perturbation theory. The description of highly multi-referenced systems is difficult for *single-reference methods*, methods in which a single

determinant is employed in the lowest order of the perturbation theory. The parametric two-electron reduced-density matrix (p2-RDM) method [22–24] is a single-reference method that has recently been shown to perform well on some forms of multi-reference correlation, including the treatment of diradical chemistry [25, 26] (for further details, see below). Recently, further efforts have been undertaken to better describe multi-reference electron correlation using single-reference methods [27, 28].

Two specific classes of organic biradicals, the benzene and the cyclobutadiene biradicals, are investigated in this work. The benzynes represent a more widely studied class of organic biradicals, and *p*-benzyne has been of particular interest due to its identification as an intermediate in the Bergman cyclization reaction, the process by which enediyne anti-tumor agents are observed to cleave DNA [2, 9–12]. The relative energies of *o*-, *m*-, and *p*-benzyne have been determined experimentally and investigated with a variety of theoretical methods, but theoretical results have so far proven difficult to reconcile with experiment. [1, 3, 5, 29, 30] Relative energy predictions within experimental error have so far been obtained only by performing configuration interaction (CI) singlepoint calculations at geometries optimized with multi-reference methods, as seen in Nicolaide's and Wierschke's studies [29, 30]. The second class of organic biradicals, those derived from cyclobutadiene, have not been studied extensively, owing to the instability of cyclobutadiene relative to other cyclic polyenes [31, 32]. The cyclobutadiene biradicals thus represent a class of organic biradicals that are of interest from a theoretical standpoint, particularly for the potential comparison of their electronic structure to that of the benzynes.

In this work, we use the p2-RDM method [22–24] to investigate two classes of biradicals, the benzene and the cyclobutadiene biradicals, in terms of their molecular energies, equilibrium geometries, and natural-orbital occupations. The p2-RDM method scales in floating-point operations as $\kappa\, N^2(r-N)^4$, where r is the rank of the one-electron basis set, N is the number of electrons, and κ is a constant prefactor, here equal to that of configuration-interaction with single and double excitations. The p2-RDM method has been previously

applied to similar systems that cannot be well-described by single-reference methods, including the prediction of the transition state energy between the *cis*- and *trans*- isomers of diazene [25], the determination of the relative stability of the cage and prism isomers of the water hexamer [33], and the prediction of the energies of the diradical isomers of olympicene [26]. In each of these cases, the p2-RDM method was seen to return energies and molecular structures comparable to those obtained from multi-reference methods.

We compare the p2-RDM method's predictions with experimentally-determined relative energies of the benzynes and with predictions obtained from wavefunction-based methods. In the extrapolated basis set limit, the p2-RDM method predicts relative energy values nearly consistent with experiment, giving a level of accuracy that improves upon traditional single-reference wavefunction methods.

5.2 Applications

5.2.1 Methodology

Geometry optimizations were performed on the cyclobutadiene biradicals and the benzynes using the parametric 2-RDM method [p2-RDM] [23–25, 34] and select coupled cluster methods: coupled cluster with single and double excitations [CCSD] [35, 36], coupled cluster with a triples correction [CCSD(T)] [36], and completely renormalized coupled cluster [CR-CC] [37]. For the *cis*- and *trans*-cyclobutadiene biradicals, multi-configurational self-consistent field [MCSCF] optimizations were also performed using an active space of (5,5) [38, 39]. All optimizations utilized the correlation-consistent valence polarized double-ζ basis set (cc-pVDZ) [40].

For the benzynes, singlepoint calculations using the larger basis set of correlation-consistent valence polarized triple-ζ (cc-pVTZ) were also performed, and Hartree-Fock energies were obtained using the correlation-consistent valence polarized quadruple-ζ (cc-pVQZ) basis set [40]. Correlation energies were obtained using the cc-pVDZ and cc-pVTZ basis sets

with all methods. A three-point complete basis set (CBS) extrapolation of the Hartree-Fock energy was then implemented by the formula $E^X_{RHF} = E^{CBS}_{RHF} + \beta\, X^{-3}$, using values from the cc-pVDZ, cc-pVTZ, and cc-pVQZ basis sets. The extrapolation of the correlation energy was first performed for all methods according to the less precise two-point formula $E^X_{corr} = E^{CBS}_{corr} + \beta \exp(-\alpha\, X)$, using values from the cc-pVDZ and cc-pVTZ basis sets. For the p2-RDM method, the calculation of the correlation energy was also performed according to the three-point formula, using the value obtained with the cc-pVQZ basis set as the third point.

Geometric optimizations with the p2-RDM method were performed through a combination of finite-differentials that approximate the gradient as well as derivative-free methods. Both the coupled-cluster and MCSCF calculations were performed with the GAMESS electronic structure package [41], while p2-RDM calculations were performed using the implementation in Ref. 24. We were unable to obtain an equilibrium CCSD(T) geometry for *p*-benzyne. Subsequent *p*-benzyne energy values for CCSD(T) are therefore calculated at the CR-CC equilibrium geometry.

Natural-orbital occupation numbers were calculated at the CCSD and p2-RDM equilibrium geometries of the benzynes and the cyclobutadiene biradicals [42]. For the benzynes, MCSCF(5,5) natural-orbital occupation numbers were calculated at the optimized p2-RDM geometries, while for the cyclobutadiene biradicals, MCSCF(5,5) natural-orbital occupation numbers were taken from the fully-optimized MCSCF(5,5) geometries. The natural-orbitals of the benzynes from the p2-RDM method were visualized for the N^{th} and $(N+1)^{\text{th}}$ natural-orbitals. Visualizations of natural-orbitals were obtained using MacMolPlt [43].

5.2.2 Results

The p2-RDM method is applied to two distinct families of organic biradicals, the cyclobutadiene biradicals and the benzynes, with respect to their molecular energies, equilibrium geometries, and natural-orbital occupations. These results are compared to those of wavefunction-

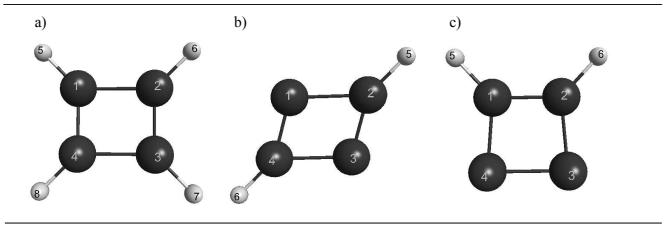

Figure 5.1: Molecules (a) cyclobutadiene, (b) the *cis*-cyclobutadiene biradical, and (c) the *trans*-cyclobutadiene biradical are shown at the p2-RDM/cc-pVDZ optimized geometries.

based methods and, in the case of the benzynes, to experimental results.

Cyclobutadiene and its Biradicals

Molecular geometries for the optimized cyclobutadiene and its *cis*- and *trans*-biradicals are presented in Table 5.1, with labeled atoms corresponding to the scheme in Figure 5.1. Because geometries did not vary substantially by method, we present only the values predicted by the p2-RDM and the CCSD methods. The optimized cyclobutadiene geometry was found to be rectangular, with the $C_{(1)}C_{(2)}$ and $C_{(2)}C_{(3)}$ bonds measuring 1.582 and 1.365 Å in the p2-RDM prediction, consistent with previous theoretical studies. [44, 45] In the *trans*-biradical, which resembles a parallelogram, the radical separation is predicted by the CCSD and the p2-RDM methods to be 1.759 and 1.763 Å, respectively. In the *cis*-biradical, which resembles a trapezoid, the radical separation is predicted to be 1.614 and 1.626 Å, respectively. The p2-RDM method in general predicts longer bond lengths, with the difference being more more substantial in the biradicals than in cyclobutadiene.

The energy values at the equilibrium geometries are presented in Table 5.2. For both cyclobutadiene and its biradicals, the CCSD(T) method recovers the greatest amount of correlation energy and thus predicts the lowest absolute energy of the four methods tested. The p2-RDM method's predictions of correlation and absolute energy compare to those of the CR-CC method in the case of the *cis*- and *trans*-biradicals. For cyclobutadiene, the species displaying the greatest amount of correlation energy, the p2-RDM method's predictions

Table 5.1: Geometric parameters (angstroms and degrees) of p2-RDM and CCSD optimized cyclobutadiene and its *cis*- and *trans*-biradicals. All optimizations performed with the cc-pVDZ basis set.

		Bond Lengths (Å) and Angles (°)	
Molecule	Parameter	CCSD	p2-RDM
cyclobutadiene	$C_{(1)}C_{(2)}$	1.582	1.582
	$C_{(2)}C_{(3)}$	1.355	1.365
	$C_{(1)}H_{(5)}$	1.093	1.093
	$\theta(C_{(1)}, C_{(2)}, C_{(3)})$	90.0	90.0
	$\theta(C_{(1)}, C_{(2)}, H_{(6)})$	135.1	135.1
cis-biradical	$C_{(1)}C_{(2)}$	1.385	1.387
	$C_{(2)}C_{(3)}$	1.493	1.497
	$C_{(3)}C_{(4)}$	1.614	1.626
	$C_{(1)}H_{(5)}$	1.105	1.107
	$\theta(C_{(1)}, C_{(2)}, C_{(3)})$	85.6	85.5
	$\theta(C_{(2)}, C_{(3)}, C_{(4)})$	94.4	94.6
	$\theta(C_{(1)}, C_{(2)}, H_{(6)})$	132.4	132.7
trans-biradical	$C_{(1)}C_{(2)}$	1.592	1.585
	$C_{(2)}C_{(3)}$	1.300	1.320
	$C_{(1)}C_{(3)}$	1.759	1.763
	$C_{(2)}H_{(5)}$	1.078	1.083
	$\theta(C_{(1)}, C_{(2)}, C_{(3)})$	74.2	74.1
	$\theta(C_{(2)}, C_{(3)}, C_{(4)})$	105.8	105.9
	$\theta(C_{(1)}, C_{(2)}, H_{(5)})$	135.2	135.8

Table 5.2: Comparison of absolute energy values of cyclobutadiene and its *cis*- and *trans*-biradicals optimized with the p2-RDM method and coupled-cluster methods. All optimizations were performed with the cc-pVDZ basis set. Absolute and correlation energy values are reported in Hartrees.

		Energy	
	Method	Total	Correlation
cis-biradical	CCSD	-152.8452	-0.4969
	CR-CC	-152.8624	-0.5149
	p2-RDM	-152.8646	-0.5169
	CCSD(T)	-152.8691	-0.5220
trans-biradical	CCSD	-152.9320	-0.5348
	CR-CC	-152.9533	-0.5579
	p2-RDM	-152.9554	-0.5576
	CCSD(T)	-152.9629	-0.5694
cyclobutadiene	CCSD	-154.2177	-0.5644
	CR-CC	-154.2175	-0.5837
	p2-RDM	-154.2396	-0.5865
	CCSD(T)	-154.2431	-0.5920

compare to those of the CCSD(T) method.

The relative energies of cyclobutadiene and its biradicals are presented in Table 5.3. The energy ordering of the three molecules is seen to be consistent across all four methods, with cyclobutadiene on the order of 180 and 240 kcal/mol lower in energy than the *trans*- and *cis*-biradical, respectively. The predicted cyclobutadiene/*cis*-biradical relative energy values vary less than 1.00 kcal/mol among methods, while the predicted relative energies of cyclobutadiene and its *trans*-biradical vary less than 4 kcal/mol. The p2-RDM method consistently predicts relative energy values lower than the CCSD predictions but higher than the CR-CC predictions.

The natural-orbital occupation numbers of cyclobutadiene and its biradicals are presented in Table 5.4. If N represents the highest occupied natural-orbital, then multi-reference character is demonstrated by the deviation of the occupation numbers of N and $(N+1)$ from 1 and 0, respectively. For cyclobutadiene as well as the *trans*-biradical, the p2-RDM method predicts occupation numbers that more closely resemble those obtained from the

Table 5.3: Relative energies of cyclobutadiene and its *cis*- and *trans*-biradicals calculated with the p2-RDM, CCSD, CR-CC, and CCSD(T) methods. All calculations are performed with a basis set of cc-pVDZ. Relative energies of the biradical species are calculated as the difference between the energy of cyclobutadiene and the energy of the biradical plus two hydrogen atoms at a large distance from one another.

	Relative Energy (kcal/mol)		
Method	cyclobutadiene	*trans*-	*cis*-
CCSD	0.00	183.85	238.34
CR-CC	0.00	181.79	238.76
p2-RDM	0.00	182.98	238.96
CCSD(T)	0.00	180.45	239.31

Table 5.4: Natural-orbital occupation numbers of cyclobutadiene and its *cis*- and *trans*-biradicals calculated with the p2-RDM, CCSD, and MCSCF(5,5) methods. All calculations utilized a cc-pVDZ basis set.

	Natural-Orbital Occupation Numbers					
	N			$(N+1)$		
Molecule	CCSD	MCSCF(5,5)	p2-RDM	CCSD	MCSCF(5,5)	p2-RDM
cyclobutadiene	0.941	0.924	0.906	0.050	0.076	0.083
trans-biradical	0.953	0.943	0.940	0.042	0.061	0.054
cis-biradical	0.959	0.903	0.946	0.032	0.104	0.045

MCSCF calculations. The p2-RDM and MCSCF N^{th} natural-orbital occupations are 0.906 and 0.924 for cyclobutadiene, and 0.940 and 0.943 for the *trans*-biradical. For the *cis*-biradical, however, the p2-RDM occupations more closely resemble those obtained from the CCSD calculations. The natural-orbital occupation numbers indicate a small degree of variation in multi-reference character between the three species investigated. None of the methods employed predict any of the three species to be highly multi-referenced, meaning all three species possess biradical character.

The Benzynes

Molecular geometries for the equilibrium geometries of *o*-, *m*-, and *p*-benzyne are presented in Table 5.5, with labeled atoms corresponding to the scheme in Figure 5.2. In contrast to the optimized cyclobutadiene biradical geometries, the benzyne geometries vary appreciably between methods. In general, the CCSD(T) method predicts the longest bond lengths. The p2-RDM method predicts bond lengths that are shorter than but comparable to those predicted by the CCSD(T) method. The shortest bond lengths of the four optimized geometries are predicted by the CCSD method, and the CR-CC results typically lie between those of the CCSD and p2-RDM methods.

In the optimized *o*- and *m*-benzyne geometries, the distance between the radical centers is seen to decrease relative to the distance of the carbon atoms in the parent benzene. This effect is most obvious in the *m*-benzyne case, in which the angle $\theta(C_{(1)}, C_{(2)}, C_{(3)})$ measures 71.6°, 95.6°, 100.1°, and 100.1° for the CCSD, CR-CC, CCSD(T), and p2-RDM methods, respectively. These angle values correspond to a radical center separation distance of 1.596, 2.045, 2.132, and 2.128 Å, meaning the CCSD method predicts a radical center separation distance of approximately the length of a carbon-carbon single bond. A similar but less pronounced effect is seen in the *o*-benzyne case, in which the distance between the radical centers is predicted to be 1.267, 1.273, 1.280, and 1.277 Å by the CCSD, CR-CC, CCSD(T), and p2-RDM methods, respectively.

Unlike *o*- and *m*-benzyne, *p*-benzyne is predicted to show increased radical center separation as well as increased $C_{(2)}C_{(3)}$ bond lengths relative to the parent benzene. This lengthening effect is most dramatic in the CR-CC and CCSD optimizations, which predict radical center separations of 2.746 and 2.750 Å and $C_{(2)}C_{(3)}$ bond lengths of 1.460 and 1.455 Å, respectively, compared to the p2-RDM predictions of 2.699 and 1.421 Å.

The predicted energies associated with the equilibrium benzyne geometries are presented in Table 5.6. The recovery of electron correlation energy is seen to increase as ortho < meta < para, indicating that multi-reference character in turn increases along that sequence. For

Table 5.5: Geometric parameters (angstroms and degrees) of *o*-, *m*-, and *p*-benzyne are presented for four different methods: p2-RDM, CCSD(T), CR-CC, and CCSD. Optimizations were performed with the cc-pVDZ basis set.

		Bond Lengths (Å) and Angles (°)			
Molecule	Parameter	CCSD	CR-CC	CCSD(T)	p2-RDM
o-benzyne	$C_{(1)}C_{(2)}$	1.267	1.273	1.280	1.277
	$C_{(2)}C_{(3)}$	1.402	1.404	1.406	1.404
	$C_{(3)}C_{(4)}$	1.415	1.418	1.422	1.421
	$C_{(4)}C_{(5)}$	1.422	1.423	1.424	1.422
	$\theta(C_{(1)}, C_{(2)}, C_{(3)})$	126.7	126.6	126.5	126.1
	$\theta(C_{(2)}, C_{(3)}, C_{(4)})$	110.7	110.9	111.0	111.5
	$\theta(C_{(3)}, C_{(4)}, C_{(5)})$	122.5	122.5	122.5	122.3
m-benzyne	$C_{(1)}C_{(2)}$	1.365	1.380	1.390	1.388
	$C_{(1)}C_{(3)}$	1.596	2.045	2.132	2.128
	$C_{(3)}C_{(4)}$	1.395	1.390	1.394	1.392
	$C_{(4)}C_{(5)}$	1.421	1.413	1.416	1.415
	$\theta(C_{(1)}, C_{(2)}, C_{(3)})$	71.6	95.6	100.1	100.1
	$\theta(C_{(2)}, C_{(3)}, C_{(4)})$	160.0	138.8	135.1	135.2
	$\theta(C_{(3)}, C_{(4)}, C_{(5)})$	108.3	116.6	117.6	117.4
	$\theta(C_{(4)}, C_{(5)}, C_{(6)})$	111.8	113.5	114.5	118.4
p-benzyne	$C_{(1)}C_{(2)}$	1.370	1.377	——	1.400
	$C_{(2)}C_{(3)}$	1.460	1.455	——	1.421
	$\theta(C_{(1)}, C_{(2)}, C_{(3)})$	118.0	118.1	——	117.1
	$\theta(C_{(3)}, C_{(4)}, C_{(5)})$	124.0	123.9	——	125.8

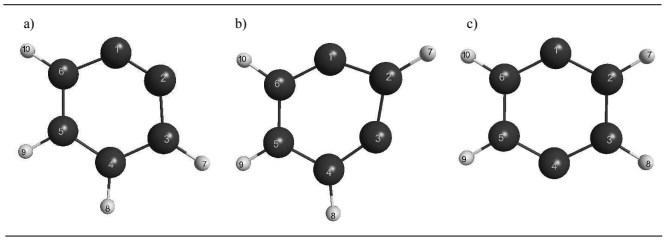

Figure 5.2: Molecules (a) *o*-benzyne, (b) *m*-benzyne, and (c) *p*-benzyne are shown at the p2-RDM/cc-pVDZ optimized geometries.

Table 5.6: Comparison of absolute energy values of the benzynes optimized with the p2-RDM method and coupled-cluster methods, using the cc-pVDZ and the cc-pVTZ basis sets. The calculated complete basis set extrapolation is also presented. Hartree-Fock and correlation energy values are reported in Hartrees.

		Energy					
		cc-pVDZ		cc-pVTZ		CBS	
Molecule	Method	HF	Corr.	HF	Corr.	HF	Corr.
para	CCSD	-229.4013	-0.8703	-229.4559	-1.0095	-229.4751	-1.0681
	CR-CC	-229.4000	-0.9117	-229.4542	-1.0617	-229.4734	-1.1248
	p2-RDM	-229.3986	-0.9451	-229.4529	-1.0951	-229.4721	-1.1583
	CCSD(T)[1]	-229.4013	-0.9731	-229.4521	-1.0971	-229.4718	-1.1493
meta	CCSD	-229.3886	-0.8062	-229.4432	-0.9509	-229.4622	-1.0117
	CR-CC	-229.3619	-0.8623	-229.4158	-1.0152	-229.4349	-1.0797
	p2-RDM	-229.3553	-0.8725	-229.4062	-1.0251	-229.4256	-1.0894
	CCSD(T)	-229.3545	-0.8888	-229.4076	-1.0470	-229.4267	-1.1136
ortho	CCSD	-229.2848	-0.8174	-229.3382	-0.9603	-229.3576	-1.0204
	CR-CC	-229.2826	-0.8471	-229.3352	-1.0006	-229.3547	-1.0653
	p2-RDM	-229.2678	-0.8525	-229.3202	-1.0045	-229.3398	-1.0685
	CCSD(T)	-229.2826	-0.8649	-229.3352	-1.0238	-229.3547	-1.0906

the ortho- and meta-benzynes, the p2-RDM method's correlation energy predictions agree with those of the CR-CC method. For the para case, the p2-RDM prediction agrees most closely with that of the CCSD(T) method.

The natural-orbital occupation numbers are presented for the benzynes in Table 5.7, with natural-orbital visualizations presented in Figure 5.3. Both *o*- and *m*-benzyne exhibit a low degree of multi-reference correlation according to all three methods, indicating their biradicaloid character. The p2-RDM method predicts the N^{th} orbital occupation numbers of *o*- and *m*-benzyne to be 0.909 and 0.865, respectively. These values are comparable to those obtained from the MCSCF method: 0.913 for *o*-benzyne and 0.864 for *m*-benzyne. The electron density of the N^{th} and $(N+1)^{\text{th}}$ natural-orbitals of *o*- and *m*-benzyne reveal bonding and antibonding orbitals, respectively, which supports a primarily single-determinant description of their chemistry.

Unlike *o*- and *m*-benzyne, *p*-benzyne is shown to be highly multi-referenced according

Table 5.7: Natural orbital occupation numbers of benzene and its biradicals calculated with a cc-pVDZ basis set.

	Natural-Orbital Occupation Numbers					
	N			$(N+1)$		
Molecule	CCSD	MCSCF$(5,5)^{a}$	p2-RDM	CCSD	MCSCF$(5,5)^{a}$	p2-RDM
Benzene	0.957	0.968	0.946	0.035	0.032	0.046
o-benzyne	0.937	0.913	0.909	0.060	0.090	0.089
m-benzyne	0.956	0.864	0.865	0.036	0.137	0.128
p-benzyne	0.848	0.621	0.543	0.150	0.381	0.454

to the p2-RDM and MCSCF descriptions. The N^{th} natural-orbital occupation number of *p*-benzyne is predicted to be 0.621 and 0.543 by the MCSCF and the p2-RDM methods, respectively. The N^{th} and $(N+1)^{\text{th}}$ natural-orbital densities of *p*-benzyne also indicate a high degree of multi-reference character, with the N^{th} orbital taking the form of an antibonding orbital and the $(N+1)^{\text{th}}$ orbital resembling a bonding orbital. Notably, the p2-RDM natural orbitals closely resemble the MCSCF natural orbitals obtained by Wierschke *et al.* [30]

Table 5.8 shows the predicted relative energies of the benzynes calculated with a variety of methods and levels of theory. All methods tested predict an energy ordering of ortho < meta < para, a result consistent with preexisting theoretical results as well as with experimental determinations [1, 3–5, 29].

These may be compared to Wenthold *et al.*'s experimental relative energy values [5]. Taking into account the experimental error of ±3.1 kcal/mol, all methods and basis sets tested predict an ortho/meta energy splitting consistent with the experimentally-determined values. The ortho/para energy splitting poses a greater challenge; the only calculated result consistent with experimental data, 33.2 kcal/mol, is predicted by the CR-CC method with a basis set of cc-pVDZ. The CCSD method consistently overestimates the energy splitting, and its accuracy decreases with increasing basis-set size. While the CR-CC results are accurate for a smaller basis set, they too increasingly overestimate the ortho/para energy splitting as basis set size increases, predicting an ortho/para energy difference 7.6 kcal/mol above the exper-

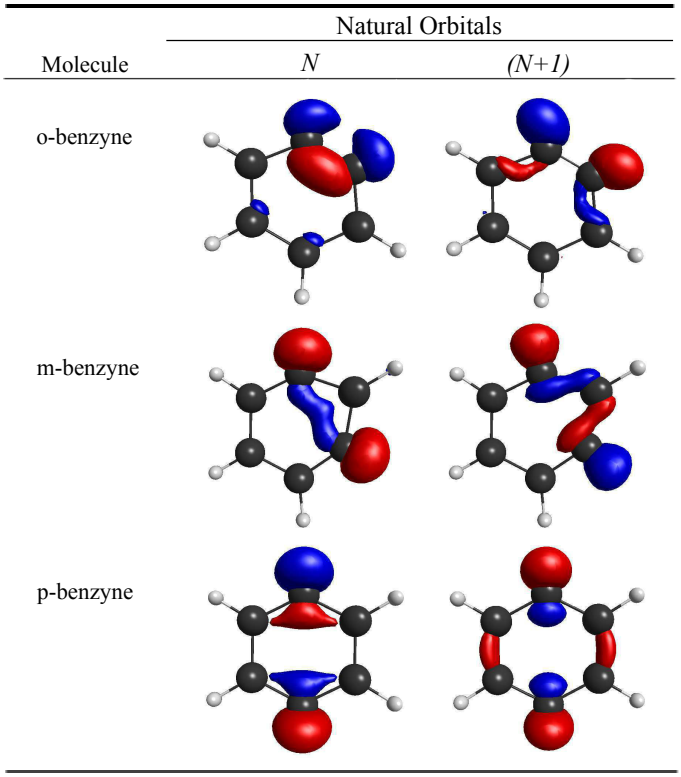

Figure 5.3: Visualizations of the N^{th} and $(N+1)^{\text{th}}$ natural-orbitals of *o*-, *m*-, and *p*-benzyne are shown at the p2-RDM/cc-pVDZ optimized geometries.

Table 5.8: Comparison of calculated relative energies of the benzynes with values from theory and experiment. Values for the cc-pVDZ basis set are calculated at fully optimized geometries, while cc-pVTZ values represent singlepoints calculated at cc-pVDZ geometries. Relative energy values for the complete basis set (CBS) extrapolation are reported. Unless otherwise noted, CBS extrapolations for the Hartree-Fock energy were performed according to the three-point cc-pVDZ/cc-pVTZ/cc-pVQZ formula, while CBS extrapolations for correlation energy were carried out according to the two-point cc-pVDZ/cc-pVTZ formula. All energies are reported relative to *o*-benzyne in kcal/mol.

	Relative Energy (kcal/mol)					
	cc-pVDZ		cc-pVTZ		CBS	
Method	m-benzyne	p-benzyne	m-benzyne	p-benzyne	m-benzyne	p-benzyne
CCSD	15.0	39.8	13.8	42.9	13.6	43.8
CR-CC	14.4	33.2	15.0	36.4	15.2	37.2
CCSD(T)[2]	12.4	16.5	13.4	27.4	13.9	36.6
p2-RDM	14.7	24.0	16.4	26.4	16.1/16.5[3]	26.7/27.5[b]
CCSD(T)[4]	14.6	27.2				
CASPT2[c]	10.1	21.7				
Expt.[5]					15.3±3.1	31.2±3.1

imental value in the complete basis set. Given the notable difference between Debbert's [1] DFT/BPW91-optimized CCSD(T) results and the CCSD(T) results presented in this work, the CCSD(T) predictions must be regarded as sensitive to geometry and therefore less reliable. However, the CCSD(T) results presented here indicate that the CCSD(T) method in the complete basis set predicts a fairly accurate ortho/para energy splitting of 5.4 kcal/mol above the experimental value. Similar to the CCSD(T) method, the p2-RDM method shows an improvement with increased basis set size, predicting an ortho/para energy splitting of 26.7 kcal/mol in the complete basis set, a value 4.5 kcal/mol below the experimental value, or within 1.4 kcal/mol of the experimental range. Furthermore, when the p2-RDM correlation energy is calculated according to the three-point extrapolation formula, the p2-RDM method predicts an ortho/para energy splitting of 27.5 kcal/mol in the complete basis set limit. This prediction is 3.7 kcal/mol below the observed value and nearly consistent with experiment.

5.3 Discussion and Conclusion

The molecules investigated in this work are primarily biradicals whose electronic structure by definition has the potential to display multi-reference (strong) electron correlation and thus deviate from the Hartree-Fock description. The correlation energy present could potentially be recovered by multi-reference methods. However, only one biradical species investigated in this work, *p*-benzyne, was found to require a multi-reference description for the identification of its equilibrium geometry. Single-reference descriptions were found to be adequate for all species that displayed biradicaloid character; that is, the cyclobutadiene biradicals and *o*- and *m*-benzyne. The visualization of the p2-RDM method's predicted natural orbitals identifies the reason for this fundamental difference between *p*-benzyne and its isomers: while the N^{th} natural orbitals of *o*- and *m*-benzyne feature sharing of electron density and therefore favor a single-reference description, the extent of radical separation in *p*-benzyne prohibits any lowering in energy from the sharing of electron density, thus giving the multi-reference description the energetic advantage.

The variation in degree of multi-reference character among biradical isomers has implications for the congruence of the 2-RDM method's predictions with other theoretical predictions and experimental values. When the level of multi-reference electron correlation is low or moderate, as it is for *o*- and *m*-benzyne and both cyclobutadiene biradicals, the p2-RDM energies are comparable to those from the CR-CC method. In the *p*-benzyne case, however, in which the level of multi-reference electron correlation is substantial enough to require a multi-reference treatment, the p2-RDM method predicts an electronic energy that is 11-12 kcal/mol below the CR-CC prediction. This lowering of the *p*-benzyne electronic energy in turn allows the p2-RDM method in the extrapolated basis-set limit to predict relative energies within 3.7 kcal/mol of experimental values [5].

The accuracy of the p2-RDM method's relative-energy predictions compares to that of the CCSD(T) method. Debbert's CCSD(T) calculations underestimate the ortho/para energy difference by 0.9 kcal/mol [1], a prediction very similar to that obtained by the p2-RDM

method. The CCSD(T) results obtained in this work compare to those obtained from the p2-RDM method in terms of magnitude of error but not in their sign, with the CCSD(T) method overestimating the ortho/para energy difference by 2.3 kcal/mol. Full configuration interaction (CI) and correlation-consistent configuration interaction (CCCI) calculations performed by Nicolaides [29] and Wierschke [30] accurately predict experimental relative energy values, thus potentially improving upon the p2-RDM predictions, but these methods confer additional computational cost that may not be transferrable to larger biradical systems. In describing the electronic energies of the benzynes, the p2-RDM method yields results that agree with traditional single-reference wavefunction methods in the cases of *o*- and *m*-benzyne and yet agree with multi-reference methods in the case of *p*-benzyne, where multi-reference electron correlation becomes important. This resiliency in the description of electron correlation allows the p2-RDM method to be nearly consistent with experimental results.

Accurate treatment of biradical chemistry requires the ability to describe systems that feature varying degrees of multi-reference electron correlation. Building upon recent applications to biradical molecular systems, we demonstrate that the p2-RDM method is a potentially useful means by which to study a variety of biradical systems, including those with a lesser degree of multi-reference correlation. Biradical chemistry is important to a range of problems in chemistry, physics, and molecular biology, and the treatment of biradical systems with the p2-RDM method has a broad range of potential applications.

5.4 References

[1] S. L. Debbert and C. J. Cramer, Int. J. Mass Spectrom. **201**, 1 (2000).

[2] T. D. Crawford, J. Chem. Phys. **114**, 10638 (2001).

[3] R. Lindh, T. J. Lee, A. Bernhardsson, B. J. Persson, and G. Karlstrom, J. Am. Chem. Soc. **117**, 7186 (1995).

[4] E. Kraka and D. Cremer, J. Am. Chem. Soc. **116**, 4929 (1994).

[5] P. G. Wenthold, R. R. Squires, and W. C. Lineberger, J. Am. Chem. Soc. **120**, 5279 (1998).

[6] W. Tumas, D. R. Wheeler, and R. H. Grubbs, J. Am. Chem. Soc. **109**, 6182 (1987).

[7] M. C. Sajimon, D. Ramaiah, K. G. Thomas, and M. V. George, **66**, 3182 (2001).

[8] R. Bos, S. A. Tonkin, G. R. Hanson, C. M. Hindson, K. F. Lim, and N. W. Barnett, J. Am. Chem. Soc. **131**, 2770 (2009).

[9] K. C. Nicolaou, Y. Ogawa, G. Zuccarello, E. J. Schweiger, and T. Kumazawa, J. Am. Chem. Soc. **110**, 4866 (1988).

[10] E. Kraka and D. Cremer, J. Am. Chem. Soc. **122**, 8245 (2000).

[11] D. B. Borders and T. W. Doyle, eds., *Enediyne Antibiotics as Antitumor Agents* (Marcel Dekker, New York, 1995).

[12] M. Krupicka, W. Sander, and D. Marx, J. Chem. Phys. Lett. **5**, 905 (2014).

[13] P. D. Bartlett and R. C. Wheland, J. Am. Chem. Soc. **94**, 2145 (1972).

[14] K. Cheng and P. J. Wagner, J. Am. Chem. Soc. **116**, 7945 (1994).

[15] C. E. Dixon, D. W. Hughes, and K. M. Baines, J. Am. Chem. Soc. **120**, 11049 (1998).

[16] K. K. Milnes, M. C. Jennings, and K. M. Baines, J. Am. Chem. Soc. **128**, 2491 (2006).

[17] N. J. Turro, J. Climate **46**, 2 (1968).

[18] M. J. S. Dewar and C. Jie, J. Am. Chem. Soc. **109**, 5893 (1987).

[19] N. C. Yang and A. J. Castro, J. Am. Chem. Soc. **82**, 6208 (1960).

[20] V. N. Staroverov and E. R. Davidson, J. Am. Chem. Soc. **122**, 186 (2000).

[21] M. J. S. Dewar and E. F. Healy, Chem. Phys. Letters **141**, 521 (1987).

[22] D. A. Mazziotti, Phys. Rev. Lett. **101**, 253002 (2008).

[23] D. A. Mazziotti, Phys. Rev. A **81**, 062515 (2010).

[24] D. A. Mazziotti, Chem. Rev. **112**, 244 (2012).

[25] A. M. Sand, C. A. Schwerdtfeger, and D. A. Mazziotti, J. Chem. Phys. **136**, 034112 (2012).

[26] A. J. Valentine and D. A. Mazziotti, J. Phys. Chem. A **117**, 9746 (2013).

[27] J. J. Phillips and D. Zgid, J. Chem. Phys. **140**, 241101 (2014).

[28] G. E. Scuseria, C. A. Jimenez-Hoyos, T. M. Henderson, K. Samanta, and J. K. Ellis, J. Chem. Phys. **135**, 124108 (2011).

[29] A. Nicolaides and W. T. Borden, J. Am. Chem. Soc. **115**, 11951 (1993).

[30] S. G. Wierschke, J. J. Nash, and R. R. Squires, J. Am. Chem. Soc. **115**, 11958 (1993).

[31] L. Watts, J. D. Fitzpatrick, and R. Pettit, J. Am. Chem. Soc. **87**, 3253 (1965).

[32] M. P. Cava and M. J. Mitchell, *Cyclobutadiene and Related Compounds*, vol. Organic Chemistry: A Series of Monographs (Academic Press, New York, 1967).

[33] J. J. Foley IV and D. A. Mazziotti, J. Phys. Chem. A **117**, 6712 (2013).

[34] C. A. Schwerdtfeger, A. E. DePrince III, and D. A. Mazziotti, J. Chem. Phys. **134**, 174102 (2011).

[35] G. D. Purvis and R. J. Bartlett, J. Chem. Phys. **76**, 1910 (1982).

[36] P. Piecuch, S. A. Kucharski, K. Kowalski, and M. Musial, Comp. Phys. Commun. **149**, 71 (2002).

[37] P. Piecuch and M. Wloch, J. Chem. Phys. **123**, 224105 (2005).

[38] K. Ruedenberg and K. R. Sundberg, *MCSCF Studies of Chemical Reactions I. Natural Reaction Orbitals and Localized Reaction Orbitals*, vol. Quantum Science: Methods and Structure (Plenum Press, New York, 1976).

[39] J. Olsen, D. L. Yeager, and P. Jorgensen, eds., *Optimization and Characterization of a Multiconfigurational Self-Consistent Field (MCSCF) State*, vol. Advances in Chemical Physics, Vol. 54 (Wiley, New York, 1983).

[40] T. H. Dunning, Jr., J. Chem. Phys. **90**, 1007 (1989).

[41] M. W. Schmidt, K. K. Baldridge, J. A. Boatz, S. T. Elbert, M. S. Gordon, J. H. Jensen, S. Koseki, N. Matsunaga, K. A. Nguyen, S. J. Su, et al., J. Comput. Chem. **14**, 1347 (1993).

[42] D. Doehnert and J. Koutecky, J. Am. Chem. Soc. **102**, 1789 (1980).

[43] B. M. Bode and M. S. Gorden, J. Mol. Graphics. Mod. **16**, 133 (1998).

[44] Y. Li and K. N. Houk, J. Am. Chem. Soc. **118**, 880 (1996).

[45] P. B. Karadakov, J. Chem. Phys. **112**, 7303 (2008).

CHAPTER 6

COMPARISON OF LOW-RANK TENSOR EXPANSIONS FOR THE ACCELERATION OF QUANTUM COMPUTATIONS

6.1 Introduction

The high computational scaling of *ab initio* quantum mechanical methods is an important outstanding problem and the subject of numerous recent studies [1–12]. Popular *ab initio* methods such as coupled cluster with single and double excitations (CCSD) require at least r^6 floating point operations per energy calculation where r is the total number of basis functions [13]. While this scaling is acceptable for small- to medium-sized molecular systems, larger systems such as those found in biology, solid-state chemistry, or polymer chemistry are often beyond the reach of these methods. Reducing their scaling would open many new problems to quantum chemical treatment.

In 2012, two new techniques for reducing the scaling of quantum methods by factorizing the two-electron amplitudes were introduced. The low-rank spectral expansion method developed by Schwerdtfeger and Mazziotti [10] decomposes the 2-excitation amplitudes using the three forms of the 2-electron reduced density matrix (2-RDM): the 2-particle(^2D), 2-hole(^2Q), and particle-hole (^2G) matrices [14–18]. This method was shown to reduce the theoretical scaling of the parametric 2-RDM method from $\mathrm{O}(r^6)$ to $\mathrm{O}((r_D^2 + r_Q^2 + r_G^2)r^4)$ where r_D, r_Q, and r_G, much less than r, are the ranks of 2-particle, 2-hole, and particle-hole decompositions in the expansion. Additionally, the spectral expansion can be applied to any method which employs two-electron excitations such as configuration interaction with single and double excitations (CISD) and CCSD. The tensor hypercontraction method which

was originally developed to reduce the size of the electron repulsion integral tensor [6] was extended to the two-electron amplitudes by Hohenstein, Parrish, Sherrill, and Martinez [8]. This factorization has been applied to multiple quantum methods including the MP2, MP4, CISD, CCSD, and CC2 methods [6–9, 11].

While both approaches have been independently shown to be effective methods for decomposing the 2-excitation amplitudes, a direct comparison between the two methods has not yet been published. In this paper, we compare the two factorizations by applying them to the parametric 2-RDM method with the Mazziotti (M) functional or p2-RDM [19–21]. The p2-RDM method, which was developed to expand and improve on the functional originally developed by Kollmar in 2006 [22], has been utilized to study small energy differences including the energy barrier between oxywater and hydrogen peroxide [23, 24], the relative populations of *cis* and *trans* carbonic acid at 210 K [25], the diradical barrier to rotation of *cis* and *trans* diazene [26], the energies of the *cis* and *trans* HOOO radical [27], and the relative energies of olympicene and its isomers [28]. It is one of the fastest 2-RDM methods currently available with equivalent computational scaling to that of CISD, $O(r^6)$. To assess the accuracy and efficiency of these two factorizations, we present the correlation energies recovered of several inorganic molecules and the potential energy curves of HF and OH^+. We also examine the scaling of the factorizations with system size by calculating the correlation energy recoveries for a series of alkane chains, the dissociation of ethane to methyl radicals, and the size consistency of non-interacting helium atoms.

6.2 Theory

6.2.1 Low-Rank Spectral Expansion

The two-electron excitation amplitudes (${}^2T_{ij}^{ab}$) can be decomposed into three spectral expansions based on the three forms of the 2-RDM, the 2-particle (${}^2D$), the 2-hole (${}^2Q$), and

the particle-hole (${}^2G$) matrices, as detailed in 2012 by Schwerdtfeger and Mazziotti [10]:

$$ {}^2T_{ij}^{ab} = \sum_{u=1}^{N(N-1)/2} \langle\Psi|\hat{a}_a^\dagger \hat{a}_b^\dagger|\eta_u\rangle\langle\eta_u|\hat{a}_j \hat{a}_i|\Psi_0\rangle, \tag{6.1} $$

$$ {}^2T_{ij}^{ab} = \sum_{u=1}^{H(H-1)/2} \langle\Psi|\hat{a}_i \hat{a}_j|\chi_u\rangle\langle\chi_u|\hat{a}_b^\dagger \hat{a}_a^\dagger|\Psi_0\rangle, \tag{6.2} $$

$$ {}^2T_{ij}^{ab} = \sum_{u=1}^{NH} \langle\Psi|\hat{a}_a^\dagger \hat{a}_i|\xi_u\rangle\langle\xi_u|\hat{a}_b^\dagger \hat{a}_j|\Psi_0\rangle, \tag{6.3} $$

where (η_u), (χ_u), and (ξ_u) are $(N-2)$-, $(N+2)$-, and N-electron wavefunctions, N and H are the number of particles and holes, i and j are occupied orbitals, and a and b are unoccupied orbitals. These equations can be rewritten in tensor notation and combined to obtain a single expansion with significantly improved convergence,

$$ {}^2T_{ij}^{ab} = \sum_{u=1}^{r_D} R_u^{ab}\, S_{ij}^u + \sum_{u=1}^{r_Q} V_u^{ij}\, W_{ab}^u + \sum_{u=1}^{r_G} X_u^{ai}\, Y_{bj}^u. \tag{6.4} $$

By restricting r_D, r_Q, and r_G to be less than their theoretical maximums of $N(N-1)/2$, $H(H-1)/2$, and NH respectively, we generate a lower-rank approximation to the full ${}^2T_{ij}^{ab}$ amplitudes. For details on restricting ${}^2T_{ij}^{ab}$ to be antisymmetric, refer to Ref. [10].

6.2.2 THC Factorization

The tensor hypercontraction (THC) method was originally developed by Hohnstein, Parrish, and Martinez in 2012 to reduce the scaling of the 2-electron integral tensor [6]. While this is sufficient for lowering the scaling of perturbation theory methods such as MP2 and MP3, for methods such as CISD and CCSD this was not sufficient to reduce the overall scaling of the methods below O(N^5) due to the presence of the 2-electron excitation amplitudes. As shown in a later paper, the tensor hypercontraction approximation can be applied to the 2-excitation amplitudes as well [8].

For this study, we decompose the 2-excitation amplitudes by defining a set of auxiliary basis X, for each molecular orbital, giving us the following form for the amplitudes

$$ {}^2T_{ij}^{ab} = \sum_{p}^{f} \sum_{q}^{f} X_{ap}\, X_{bq}\, Z_{pq}\, X_{ip}\, X_{jq}. \tag{6.5} $$

We treat X and Z as arbitrary matrices of dimensions rxf and fxf, respectively where both X and Z are determined variationally to minimize the energy. To ensure that the overall method remains antisymmetric, the tensor hypercontraction decomposition can be rewritten in terms of α and β spin orbitals. While the $\alpha\beta$ coefficients are the same as those of Eq. (6.5), the $\alpha\alpha$ and $\beta\beta$ coefficients assume the following form

$$ \begin{aligned} {}^2T_{ij}^{ab} = \sum_{p}^{f} \sum_{q}^{f} & [\, X_{ap}(\alpha)\, X_{bq}(\alpha) - \, X_{bp}(\alpha)\, X_{aq}(\alpha)] \\ & \times Z_{pq}(\alpha\alpha) [\, X_{ip}(\alpha)\, X_{jq}(\alpha) - \, X_{jp}(\alpha)\, X_{iq}(\alpha)] \end{aligned} \tag{6.6} $$

to maintain antisymmetry with an arbitrary Z matrix.

6.2.3 Theoretical Scaling

Decomposing the ${}^2T$ coefficients using either the low-rank spectral expansion or tensor hypercontraction method allows for a reduction in theoretical scaling compared to the full-rank method. The p2-RDM method employing the spectral expansion factorization scales as $(r_D^2 + r_Q^2 + r_G^2)r^4$ in floating-point operations [10]. Small values of r_D, r_Q, r_G of either 1 or 2 are typically sufficient to obtain $\approx 99\%$ of the correlation energy for 10 electron systems in any basis set. Hence, the ranks r_D, r_Q, r_G are generally much less than r. According to calculations in Ref. [10] and Section 6.3, the ranks r_D, r_Q, and r_G must increase linearly with the system size to maintain the size extensivity of the p2-RDM method. Hence, in the asymptotic limit of r the method scales in floating-point operations as $\mathrm{O}(r^6)$ with a small prefactor. As discussed in the Conclusions, however, the scaling of both the spectral expan-

sion method can be further improved through tensor decomposition of the Hamiltonian, i.e. through density fitting [29, 30] or Cholesky decomposition [31–34].

By using similar procedure to Ref. [10], we can determine the reduction in theoretical scaling that occurs when one decomposes the 2-RDM ${}^2T$ coefficients using the tensor hypercontraction method. For the tensor hypercontraction version of the 2-RDM method, the term with the highest cost in terms of floating-point operations scales as $O(fr^4)$ where f is the number of auxiliary functions, which results in fourth-order scaling when the size of the auxiliary basis set is fixed. As with the spectral expansions, the results in Section 6.3 show that the number f of auxiliary functions must be increased linearly with system size to maintain the size extensivity of the p2-RDM method. Because the floating-point operations scale linearly with f, in the asymptotic limit of r the method scales as $\mathrm{O}(r^5)$. As shown in Ref. [12], however, tensor hypercontraction of the 2-excitation amplitudes can be combined with a tensor hypercontraction of the Hamiltonian to achieve an $\mathrm{O}(r^4)$ p2-RDM method.

Asymptotically, storage of the 2-excitation tensors in the spectral expansion method scales as $\mathrm{O}(r^3)$ while storage of the 2-excitation tensors in the tensor hypercontraction scales as $\mathrm{O}(r^2)$. For both the spectral expansion and tensor hypercontraction method, the number of iterations to minimize the energy is larger than it is for the conventional p2-RDM without tensor factorization because the tensor factorizations introduce additional nonlinearity into the optimization. However, the spectral expansion method requires significantly fewer iterations than tensor hypercontraction (see Table 6.2), which results in a lower constant prefactor.

6.3 Applications

6.3.1 Computational Methods

All calculations in this paper were performed using a modified implementation of the parametric 2-RDM method in Ref. [23]. The results given are for the cc-pVDZ basis set with

lowest core orbitals frozen unless otherwise stated. Energy minimizations are performed with a limited-memory quasi-Newton method (L-BFGS) [35]. The derivatives for the low-rank spectral expansion and tensor hypercontraction methods were obtained using the chain rule. As a result, we do not present computational timings as the full-rank derivatives must still be calculated to obtain the low-rank derivatives in the current implementation.

6.3.2 Results

Table 6.1 contains the correlation energies from the factorization calculations given as a percentage of the full-rank correlation energy (or correlation energy recovery) for both the spectral expansion and tensor hypercontraction p2-RDM calculations. We can see that both approximations recover a significant percentage of the correlation energy of the full-rank method even at low values of $r_D/r_Q/r_G$ and f. The two factorizations achieve a correlation energy recovery above 90% at $r_D/r_Q/r_G = 1/1/1$ for the spectral expansion method and 10 auxiliary functions for the tensor hypercontraction method. However, the spectral expansion achieves $> 99\%$ recovery at $r_D/r_Q/r_G = 2/2/2$ while the tensor hypercontraction requires 40 auxiliary functions to achieve the same level of accuracy for all three molecules. This is also shown by Fig. 6.1 which displays the convergence of both factorizations to the full-rank method with increasing numbers of their respective ranks (or auxiliary functions).

The number of L-BFGS iterations required to obtain the results in Table 6.1 are reported in Table 6.2. Tensor elements in both methods were initialized by random guesses. For the spectral expansion factorization, the calculations converged within at most 900 iterations, and four of the calculations converged in less than 200 iterations. As the value of $r_D/r_Q/r_G$ goes from 1/1/1 to 4/4/4, the number of L-BFGS iterations required generally decreased except for the H_2O and CO^+ calculations at 2/2/2 where an increase in the number of iterations was observed. Tensor hypercontraction required over 1000 iterations for the calculations to converge and in two cases it only converged after the tolerance controlling convergence was lowered from 10^{-6} to 10^{-5} a.u. The latter problem was observed frequently for the tensor

Table 6.1: The percentage of the full-rank correlation recovered by the low-rank spectral expansion and tensor hypercontraction methods is reported for three simple molecules for the cc-pVTZ basis set.

		$r_D/r_Q/r_G$				
Molecule	Full correlation energy (a.u.)	1/0/1	1/1/1	2/2/2	3/3/3	4/4/4
H_2O	-0.27404	78.8	93.9	99.9	100.0	100.0
CO^+	-0.38767	80.3	91.6	99.3	100.0	100.0
N_2	-0.38372	87.1	97.4	100.0	100.0	100.0
		Number of auxiliary functions (f)				
Molecule	Full correlation energy (a.u.)	5	10	20	30	40
H_2O	-0.27404	77.8	92.5	97.8	98.7	99.0
CO^+	-0.38767	76.0	90.3	97.3	98.4	99.2
N_2	-0.38372	86.2	95.0	98.2	99.4	99.8

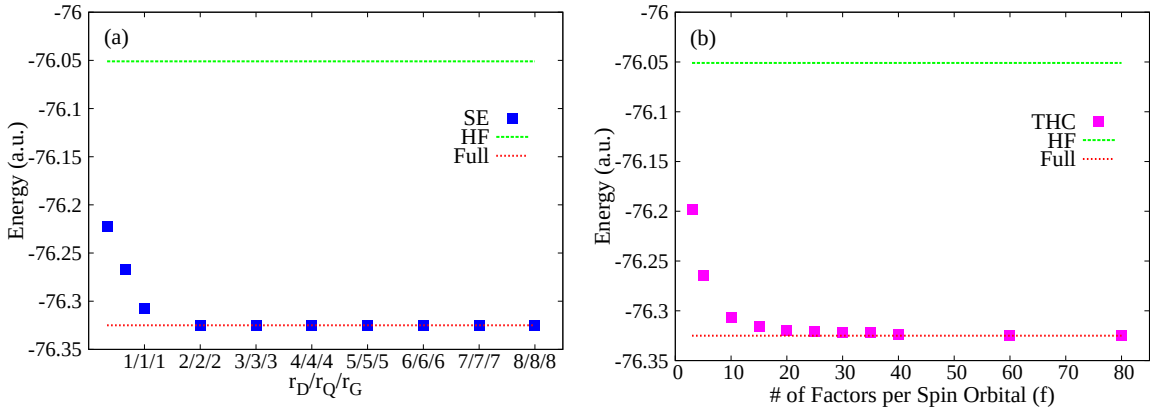

Figure 6.1: Part (a) shows the convergence of the spectral expansion methods to the full-rank result for water in the cc-pVTZ basis set. Part (b) shows the same results for the tensor hypercontraction method.

Table 6.2: The numbers of L-BFGS iterations required to obtain the results in Table 6.1 are presented in the table below. The values were converged to a tolerance of 10^{-6} a.u. The values marked with a * only converged after the tolerance was lowered to 10^{-5} a.u. For comparison the numbers of L-BFGS iterations required by the full-rank p2-RDM method are 26, 56, and 46 for H_2O, CO^+, and N_2, respectively.

	$r_D/r_Q/r_G$				
Molecule	1/0/1	1/1/1	2/2/2	3/3/3	4/4/4
H_2O	188	472	684	200	183
CO^+	166	456	894	341	233
N_2	193	555	529	310	278
	Number of auxiliary functions (f)				
Molecule	5	10	20	30	40
H_2O	2585	2367	2136	1960	1911
CO^+	1909	2254	2565	1875	2664
N_2	1513	1241*	1202*	2243	1563

hypercontraction calculations at low numbers of auxiliary functions, but it generally was resolved when a sufficient number of functions was used. The spectral expansion did not exhibit this behavior, and hence, it could be converged to the same tolerance as the full-rank calculation for all values of $r_D/r_Q/r_G$.

Table 6.3 contains the lowest eigenvalues for the ${}^2D$, ${}^2Q$, and ${}^2G$ matrices of OH^+ calculated by the p2-RDM method with tensor hypercontraction. In order to satisfy the 2-positivity conditions for N-representability, the eigenvalues of the ${}^2D$, ${}^2Q$, and ${}^2G$ matrices must be nonnegative. [15–18] The magnitude of the largest negative eigenvalues, therefore, provides a measure of the deviation of a 2-RDM from N-representability. The difference between the full-rank and tensor hypercontraction results is very small with both displaying a deviation from zero on the order of 10^{-4} near the equilibrium geometry and 10^{-3} at stretched geometries. Similar results for OH^+ from the p2-RDM method with low-rank spectral expansion were reported in Ref. [10].

Calculated potential energy curves for the OH^+ molecule are presented in Fig. 6.2. As shown in Ref. [10], the 1/1/1 spectral expansion is sufficient to reproduce the shape of the potential from the full-rank spectral expansion with a maximum error of only 3.7 mH. The

Table 6.3: The lowest eigenvalues for the two-particle (${}^2D$), two-hole (${}^2Q$), and particle-hole (${}^2G$) matrices for the triplet state of OH+ as calculated by the tensor hypercontraction method are displayed in the table below.

		Lowest eigenvalues			
Bond length (Å)	Matrix	3	5	10	Full[10]
1.3	${}^2D$	-2.1e-4	-2.6e-4	-3.6e-4	-3.7e-4
	${}^2Q$	-1.4e-4	-1.0e-4	-1.1e-4	-9.8e-5
	${}^2G$	-2.8e-4	-3.3e-4	-3.9e-4	-3.9e-4
2.3	${}^2D$	-3.3e-3	-6.0e-3	-4.4e-3	-4.4e-3
	${}^2Q$	-1.7e-3	-2.8e-3	-5.7e-4	-5.3e-4
	${}^2G$	-5.9e-3	-8.5e-3	-6.5e-3	-6.5e-3

difference between the minimum and maximum errors or the non-parallelity error (NPE) is only 3.6 mH. Tensor hypercontraction predicts similar results when 10 auxiliary functions ($f = 10$) are used with a maximum error of 2.5 mH and an NPE of 1.7 mH. At 3 functions, considerable variance in the potential curve is noticeable leading to a maximum error of 58 mH and an NPE of 34 mH. These errors decline to 12 and 8.2 mH respectively when one uses the 5 auxiliary functions for the calculation. The unevenness in the potential energy curve, however, does not disappear completely until 10 auxiliary functions are used. The spectral expansion does not exhibit this behavior even for ranks less than 1/1/1 [10].

Figure 6.3 displays the calculated potential energy curves for the HF molecule. We find that the p2-RDM method with the 2/2/2 rank gives a maximum error of 2.3 mH and an NPE of 0.21 mH relative to the full-rank method. The calculated results for the 1/1/1 rank unexpectedly drop in energy when the bond length exceeds 2.3 Å; similar behavior is also observed with tensor hypercontraction when either 3 and 5 auxiliary functions is employed. With 5 functions, the largest energy error and NPE were 27 and 23 mH, respectively. Because tensor hypercontraction did not converge beyond 2.2 Å with $f = 10$, it is not known whether the drop in energy disappears as f increases.

The percentage of correlation energy recovered for a series of alkane chains in both C_s and C_{2v} symmetries from both the low-rank spectral expansion and tensor hypercontraction

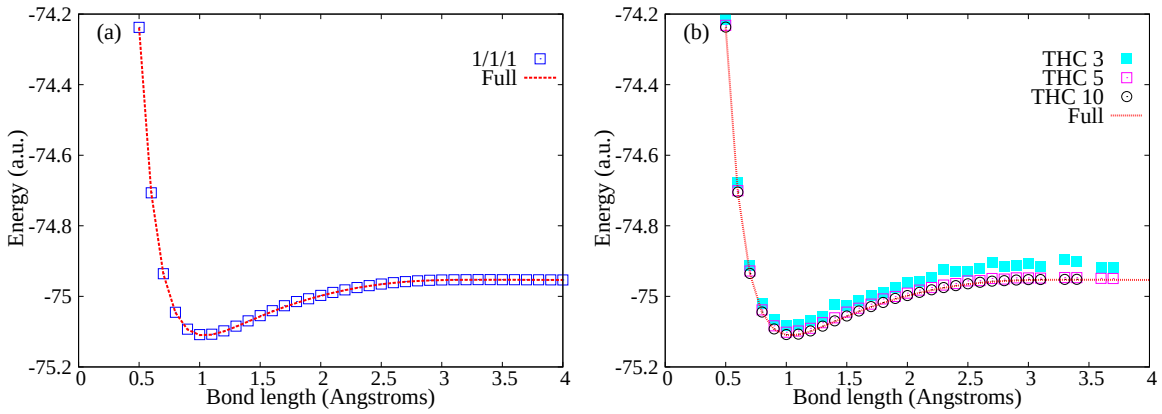

Figure 6.2: OH+ dissociation curve in the cc-pVDZ basis set from the p2-RDM method with the (a) spectral expansion and (b) tensor hypercontraction methods. Results are compared to those from the full-rank p2-RDM method.

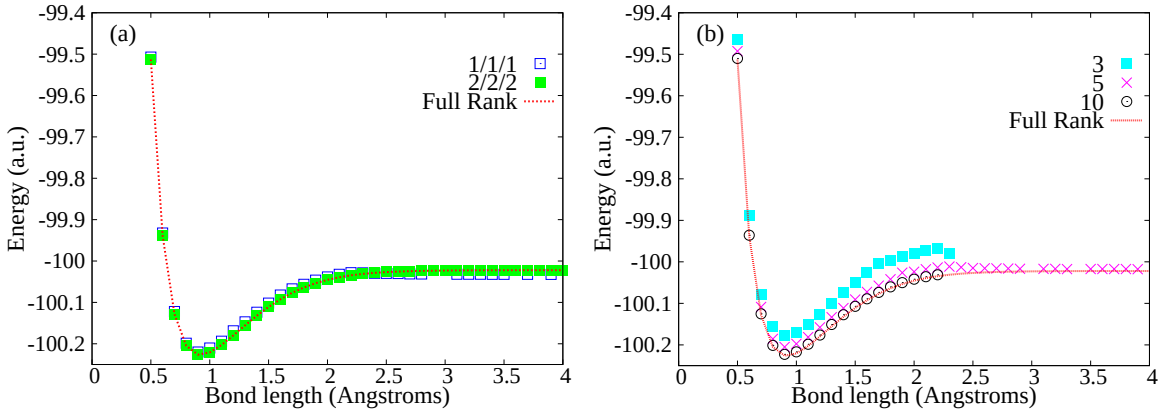

Figure 6.3: HF dissociation curve in the cc-pVDZ basis set from the p2-RDM method with the (a) spectral expansion and (b) tensor hypercontraction methods. Results are compared to those from the full-rank p2-RDM method.

Table 6.4: We report the correlation energy recovered from both tensor methods as compared to the energy recovered from the full-rank p2-RDM for a series of alkanes using both C_s and C_{2v} symmetry.

	% of full correlation energy					
	C_s				C_{2v}	
$r_D/r_Q/r_G$	CH_4	C_2H_6	C_3H_8	C_4H_{10}	CH_4	C_3H_8
1/1/1	80.1	62.4	49.4	39.3	96.0	70.4
2/2/2		83.7	72.6	63.4		89.6
3/3/3			84.0	76.4		95.5
4/4/4				83.9		
# of functions (f)	CH_4	C_2H_6	C_3H_8	C_4H_{10}	CH_4	C_3H_8
10	86.2	62.8	44.3	34.6	94.23	70.0
20		86.8	71.5	53.9		91.5
30			87.1	77.5		97.4
40				87.8		

is reported in Table 6.4. When ${}^2T$ is factorized using either the low-rank spectral expansion or tensor hypercontraction methods, the number of factor matrices must be increased with system size to recover a similar percentage of the correlation energy. Using higher point-group symmetry, we find, increases the amount of correlation energy recovered at a given rank. For example, the correlation energy recovered increases by 10-20% and 10-30% for the low-rank spectral expansion and tensor hypercontraction, respectively, when the point-group symmetry is increased from C_s to C_{2v}. The improvement occurs because at higher symmetry each symmetry block of ${}^2T$ is given its own tensor expansion while at lower symmetry the tensor expansion must generate the symmetry block structure of ${}^2T$, which requires a larger expansion.

Table 6.5 contains the reaction energies from the two factorizations required to break an ethane molecule into two methyl radicals. As was shown by Schwerdtfeger and Mazziotti previously [10] the factorizations must be scaled with system size to obtain size consistent results. If both the ethane molecule and smaller methyl radical are treated using the same low rank, the dissociation energy is lower than dissociation energy calculated from the full-rank method by 20-60 kcal/mol. By using twice the rank for the ethane calculation compared

Table 6.5: The calculated reaction energies for the dissociation of ethane to two methyl radicals using the cc-pVDZ basis set are presented. The upper set of calculations in the table use the same tensor rank (auxiliary functions) for both the ethane and methyl molecules while the lower set of calculations use twice the tensor rank (auxiliary functions) for the ethane calculation compared to the methyl calculation.

SE			THC		
CH_4	C_2H_6	RE (kcal/mol)	CH_4	C_2H_6	RE (kcal/mol)
1/1/1	1/1/1	44.5	5	5	43.3
2/2/2	2/2/2	69.0	10	10	42.4
3/3/3	3/3/3	84.7	15	15	63.6
1/1/1	2/2/2	91.2	5	10	94.1
2/2/2	4/4/4	96.0	10	20	94.4
3/3/3	6/6/6	100.1	15	30	100.0
Full		102.1	Full		102.1

to the methyl calculation, however, the dissociation energies can be brought between 2-8 kcal/mol of the full-rank value.

A comparison of the energy of two helium atoms separated by 200 Å with the energy of two individual helium atoms is displayed in Table 6.6. If a method is size consistent, the two values will be the same. The full-rank p2-RDM method has been shown previously to be size consistent for its helium dissociation [36]. For low values of $r_D/r_Q/r_G$ and auxiliary functions, the two factorizations predict a 1-3 mH difference between the separated helium dimer and individual helium atoms. As with the alkane series and ethane reaction-energy calculations, this difference diminishes as the rank increases, dropping to 10^{-7} by 1/1/1 for the spectral expansion method and by $f = 20$ for the tensor hypercontraction method.

6.4 Discussion and Conclusions

Two promising new methods, low-rank spectral expansion and tensor hypercontraction, for factorizing the 2-electron excitation amplitudes were examined to evaluate their potential for use in future low-rank *ab initio* quantum chemistry methods. The ideal factorization would lower the scaling of an energy calculation without imposing additional costs or sacri-

Table 6.6: The total energy of a helium dimer with a bond length of 200 Å is compared to the energy of two individual helium atoms. Calculations are presented from the p2-RDM method with the spectral expansion (top) and tensor hypercontraction (bottom) factorizations. Both factorizations become size consistent as the ranks of the expansions increase.

	$r_D/r_Q/r_G$				
	1/0/0	1/0/1	1/1/1	2/2/2	Full
He x 2	-5.763890	-5.763890	-5.775190	-5.775190	-5.775190
He_2(200 Å)	-5.742755	-5.769520	-5.775190	-5.775189	-5.775190
He_2 - He x 2	3.24345e-2	5.66983e-3	1.18025e-7	4.33509e-7	1.32217e-9
	Number of auxiliary functions (f)				
	3	5	10	20	Full
He x 2	-5.775189	-5.775189	-5.775189	-5.775189	-5.775190
He_2(200 Å)	-5.763844	-5.775187	-5.775177	-5.775178	-5.775190
He_2 - He x 2	1.13452e-2	2.17419e-6	3.12588e-6	6.73077e-7	1.32217e-9

ficing the computational advantages of the original method. To test the energy recovery of each factorization compared to the full-rank p2-RDM method, we studied several inorganic molecules as well as the potential energy curves of HF and OH^+.

For the inorganic molecules we found that the energy recovery of both methods exceeds 90% at 1/1/1 for the low-rank spectral expansion method and 10 auxiliary functions for the tensor hypercontraction method. Both tensor methods showed a very minor increase in N-representability error compared to the full-rank method. In comparison to tensor hypercontraction, the spectral expansion method required fewer iterations in the unconstrained optimization to converge the ground-state energy.

An important property of the p2-RDM method, employed in many of its chemical applications [23–26, 26, 28] is its ability to capture significant multi-reference correlation effects at transition states and stretched geometries that are typically difficult to treat by single-reference methods. As seen for the spectral expansion method in an earlier paper [10], the p2-RDM method continues to capture multi-reference correlation with both spectral expansion and tensor hypercontraction. In this paper the potential energy curves of both singlet HF and triplet OH^+ were computed. For both molecules the full-rank p2-RDM method

yielded more accurate curves than CCSD, especially in the dissociation region. The combination of the p2-RDM method with the tensor methods to achieve rank reduction did not impede its accuracy. For small ranks (or auxiliary functions), less than or equal to ten, the low-rank 2-RDM methods converged to the energy curves from the full-rank method. Some convergence problems for tensor hypercontraction appeared in the form of non-smooth potential energy surfaces in the dissociation region of HF. Although the spectral expansion did not exhibit these problems, it did display a drop in energy for the HF dissociation around 2.3 Å which was also noted for tensor hypercontraction at $f = 3$ and $f = 5$.

Both size extensivity and size consistency of the low-rank p2-RDM methods were explored through calculations on a series of alkanes, the dissociation of ethane to methyl radicals, and infinitely separated helium atoms. A method is *size extensive* if and only if its energy scales linearly with system size; a method is *size consistent* if and only if the energy of two infinitely separated monomers is equal to the sum of the monomer energies. Unlike CISD, the p2-RDM method is derived to yield size extensive and size consistent energies. In this paper we found that the p2-RDM method in combination with spectral expansion or tensor hypercontraction maintains the size extensivity and size consistency of the full-rank p2-RDM if the rank of the tensor expansion increases with system size. For the alkanes, for example, the percentage of the full-rank correlation energy recovered by low-rank methods remained constant if and only if the rank (or the number of auxiliary functions) increased linearly with the length of the chain. Similarly, the dissociation of ethane into two methyl radicals required that the rank of the tensor decomposition of ethane be twice the decomposition of a single methyl radical. Finally, the size consistency of two helium atoms at nearly infinite separation was restored in either the tensor methods when the rank of the tensor expansion was sufficiently large.

The tensor decomposition of the two-electron excitation amplitudes in the p2-RDM generates a formally $O(r^4)$ method if and only if the rank (or the number of auxiliary functions) of the tensor expansion remains constant with respect to system size as measured by r.

Hence, to achieve a size extensive $O(r^4)$ method with either the spectral expansion or tensor hypercontraction methods, further cost reduction is required. One approach is to employ a tensor decomposition for the electron repulsion integrals within the molecular Hamiltonian. The decomposition can be achieved in a variety of ways including density fitting [29, 30], Cholesky factorization [31–34], and tensor hypercontraction [6–9]. Recently, a size extensive $O(r^4)$ p2-RDM method has been developed by using tensor hypercontraction for both the two-electron excitations and the two-electron molecular integrals (see Ref. [12] for further details).

The reduction of the size of the 2-electron excitation tensor is important to reducing the computational scaling of *ab initio* quantum chemical methods and allowing them to treat large chemical systems which can be studied currently only by methods such as density functional theory [37]. We found that both low-rank spectral expansion and tensor hypercontraction are effective methods to factorize the 2-excitation amplitudes into lower-rank tensors while recovering the majority of the correlation energy of a full-rank method. Both factorizations lower the theoretical cost of the p2-RDM method while preserving its computational and energetic properties, and its ability to capture multi-reference correlation effects [10]. While the two factorizations produced similar correlation energy recoveries, the spectral expansion factorization proved to be the more computationally efficient and stable method, in practice requiring less time and fewer iterations to converge to a predicted result. In the limit of infinite system size, however, the tensor hypercontraction of $O(r^5)$ should be more efficient than the spectral expansion of $O(r^6)$. In light of the present results, both tensor methods provide valuable starting points for the development of fast, low-cost p2-RDM methods with $O(r^4)$ scaling and more generally improved low-rank *ab initio* methods.

6.5 References

[1] T. Kinoshita, O. Hino, and R. J. Bartlett, J. Chem. Phys. **119**, 7756 (2003).

[2] G. J. O. Beran and M. Head-Gordon, J. Chem. Phys. **121**, 78 (2004).

[3] F. Bell, D. S. Lambrecht, and M. Head-Gordon, Mol. Phys. **108**, 2759 (2010).

[4] J. Yang, Y. Kurashige, F. R. Manby, and G. K. L. Chan, J. Chem. Phys. **134**, 044123 (2011).

[5] U. Benedikt, A. A. Auer, M. Espig, and W. Hackbusch, J. Chem. Phys. **134**, 054118 (2011).

[6] E. G. Hohenstein, R. M. Parrish, and T. J. Martinez, J. Chem. Phys. **137**, 044103 (2012).

[7] R. M. Parrish, E. G. Hohenstein, T. J. Martinez, and C. D. Sherill, J. Chem. Phys. **137**, 224106 (2012).

[8] E. G. Hohenstein, R. M. Parrish, C. D. Sherrill, and T. J. Martinez, J. Chem. Phys. **137**, 221101 (2012).

[9] E. G. Hohenstein, R. M. Parrish, C. D. Sherrill, and T. J. Martinez, J. Chem. Phys. **138**, 12411 (2013).

[10] C. A. Schwerdtfeger and D. A. Mazziotti, J. Chem. Phys. **137**, 244103 (2012).

[11] N. Shenvi, H. V. Aggelen, and W. Yang, arXiv **1209.2935** (2012).

[12] N. Shenvi, H. V. Aggelen, Y. Yang, W. Yang, C. Schwerdtfeger, and D. Mazziotti, J. Chem. Phys. **139**, 054110 (2013).

[13] R. Bartlett and M. Musial, Rev. Mod. Phys. **79**, 291 (2007).

[14] A. J. Coleman and V. I. Yukalov, *Reduced Density Matrices: Coulson's Challenge* (Springer, New York, 2000).

[15] D. A. Mazziotti, ed., *Two-Electron Reduced-Density-Matrix Mechanics*, vol. 134 of *Advances in Chemical Physics* (Wiley, New York, 2007).

[16] R. M. Erdahl, Int. J. Quantum Chem. **13**, 697 (1978).

[17] M. V. Mihailovic and M. Rosina, **A237**, 221 (1975).

[18] C. Garrod and J. Percus, J. Math. Phys. **5**, 1756 (1964).

[19] D. A. Mazziotti, Phys. Rev. Lett. **101**, 253002 (2008).

[20] D. A. Mazziotti, Phys. Rev. A **81**, 062515 (2010).

[21] D. A. Mazziotti, Chem. Rev. **112**, 244 (2012).

[22] C. Kollmar, J. Chem. Phys. **125**, 084108 (2006).

[23] C. A. Schwerdtfeger, A. E. DePrince III, and D. A. Mazziotti, J. Chem. Phys. **134**, 174102 (2011).

[24] E. P. Hoy, C. S. Schwerdtfeger, and D. A. Mazziotti, Mol. Phys. **107**, 765 (2012).

[25] C. A. Schwerdtfeger and D. A. Mazziotti, J. Phys. Chem. A **115**, 12011 (2011).

[26] A. M. Sand, C. S. Schwerdtfeger, and D. A. Mazziotti, J. Chem. Phys. **136**, 034112 (2012).

[27] E. P. Hoy, C. S. Schwerdtfeger, and D. A. Mazziotti, J. Phys. Chem. A **117**, 1817 (2013).

[28] A. J. S. Valentine and D. A. Mazziotti, J. Phys. Chem. A **117** (????).

[29] W. Feyerseisen, G. Fitzgerald, and A. Komoricki, Chem. Phys. Letters **208**, 359 (1903).

[30] F. Weigend and M. Haser, Theor. Chem. Acc. **97**, 331 (1997).

[31] N. H. F. Beebe and J. Linderberg, Int. J. Quantum Chem. **12**, 683 (1977).

[32] S. Wilson, **58**, 71 (1990).

[33] H. Koch, A. S. D. Meras, and T. B. Pedersen, J. Chem. Phys. **118**, 9481 (2003).

[34] F. Aquilante, L. Gagliardi, T. B. Pedersen, and R. Lindh, J. Chem. Phys. **130**, 154107 (2009).

[35] J. Nocedal and S. J. Wright, *Numerical Optimization* (Springer, New York, 2006).

[36] A. Sand and D. A. Mazziotti, J. Chem. Phys. **138**, 244102 (2013).

[37] R. G. Parr and W. Yang, *Density Functional Theory* (Oxford University Press, Oxford, 1994).

CHAPTER 7

POSITIVE SEMIDEFINITE TENSOR FACTORIZATIONS OF THE TWO-ELECTRON INTEGRAL MATRIX FOR LOW-SCALING *AB INITIO* ELECTRONIC STRUCTURE

7.1 Introduction

When seeking to describe the electronic properties of large organic and biological molecular systems, chemists often employ computationally inexpensive electronic structure methods such as the Hartree-Fock and density functional theories. These two methods have computational scalings of r^3, where r is the total number of basis functions. The key limitation of these methods is their incomplete description of electron correlation with Hartree-Fock not treating any electron correlation and density functional theory not being able to describe multi-reference (static) correlation. Higher accuracy, correlated electronic structure methods such as *ab initio* wavefunction or reduced density matrix (2-RDM) methods generally require at least r^6 floating-point operations for an energy calculation. In order to treat electron correlation in larger systems properly, decreasing the scaling of correlated *ab initio* methods toward the r^3 scaling of Hartree-Fock and density functional theories is desirable, particularly if the resulting method is able to capture static correlation.

One technique to reduce the scaling of wavefunction and density matrix methods toward r^3 is tensor factorization [1–4]. Typically, the fourth-order tensors such as the two-electron repulsion integral matrix and the two-electron excitation tensor are divided into lower-order tensors. This allows for the use of fast partial summation of the lower order tensors in lieu of more expensive calculations using the original tensors. The effectiveness of this approach,

however, depends heavily on the choice of the electronic structure methods and the factorizations. Ideally, we want to start with an *ab initio* method that is computationally efficient (scaling of r^6) and capable of recovering a significant portion of the correlation energy including static correlation. One technique that fulfils both criterion is the parametric 2-electron reduced density matrix (p2-RDM) method [5–15]. Reducing the scaling of this method toward r^3 can be accomplished by factorizing the 2-electron integral matrix and/or the 2-electron excitation tensor. In 2012 Schwerdtfeger and Mazziotti factorized the p2-RDM 2-electron excitation tensor using a spectral expansion method based on the 2-positivity conditions found in RDM theory [16]. This approach generates an $O(r^4)$ non-size-extensive p2-RDM method or an $O(r^5)$ size-extensive method. A method is *size extensive* if the error in the computed energy scales linearly with system size. In 2013 Shenvi *et al.* developed a fourth-order size-extensive p2-RDM method using the tensor hypercontraction factorization [4, 17–22]. We have previously compared these two approaches in terms of their ability to factorize the 2-electron excitation tensors of the p2-RDM method in Ref. [23]. When applied to the electron repulsion integral matrix, however, tensor hypercontraction and similar decompositions [1–3, 24] do not rigorously preserve the positive semidefiniteness of the integral matrix. In this paper we consider a general family of positive semidefinite factorizations of the electron repulsion integral matrix.

The Cholesky factorization is the simplest factorization whose factors maintain the positive semidefinite character of the original matrix. This factorization eliminates eigenvalues that are zero or nearly zero from the integral matrix to reduce the size of the tensor that must be stored, which is especially useful for large basis sets [25]. The method has recently received renewed interest both as a generator of auxiliary basis sets for the density-fitting method and as a low-rank method in its own right [26–39]. While the Cholesky factorization is both numerically stable and readily computed, it alone is not sufficient to reduce the overall computational scaling of correlated electronic structure theories, such as the p2-RDM method, toward that of the Hartree-Fock method and density functional theory. This lim-

itation is due to an insufficient decoupling of orbital indices in the performance of partial summations with the Cholesky factors. In order to achieve scaling reduction toward r^3, it is necessary that all of the original tensor indices are situated on separate tensor factors as in tensor hypercontraction. All currently available factorizations with such flexibility, however, do not maintain the positive semidefinite character of the original integral matrix. It is desirable to have a positive semidefinite factorization like the Cholesky factorization that also allows for efficient partial summation like tensor hypercontraction.

In this paper we consider a family of positive semidefinite (PSD) factorizations that generalize the Cholesky factorization. Specifically, we focus on a factorization that places each of the original tensor indices on separate tensor factors. The resulting factorization has nearly the same partial summation flexibility as methods like tensor hypercontraction while preserving the positive semidefiniteness of the Cholesky factorization. To illustrate the factorization, we examine several small molecules including H_2O, CO, N_2, HF, and OH and a series of 8 linear alkane chains using a modified p2-RDM method capable of decomposing the 2-electron integrals by both the Cholesky and the more general positive semidefinite factorizations.

7.2 Theory

In section 7.2.1 we discuss the Cholesky factorization of the electron repulsion integral matrix. In section 7.2.2 we theoretically develop the generalized family of positive semidefinite (PSD) factorizations of the electron repulsion integral matrix.

7.2.1 Cholesky Factorizations

Any $n \times n$ positive semidefinite matrix A can be written as

$$A = C\,C^{\dagger}, \tag{7.1}$$

where C is a general $n \times n$ matrix. For the symmetric, positive-semidefinite two-electron integral matrix

$$^2V_{kl}^{ij} = \int dr_1 \int dr_2 \sigma_i(r_1)\sigma_k(r_{1'})\, r_{12}^{-1} \sigma_j(r_2)\sigma_l(r_{2'}), \tag{7.2}$$

we can perform the above factorization. Importantly, because the elements of $^2V_{jl}^{ik}$ decay exponentially with the separation between r_1 and r_1' (or r_2 and r_2'), the number of non-negligible eigenvalues scales linearly with r. Therefore,

$$^2V_{ik}^{jl} \approx \sum_{M=1}^{\kappa r} C_M^{ik}\, C_{jl}^M, \tag{7.3}$$

where κ is a small nonnegative integer. If we choose the C matrices to be lower triangular matrices L, we have the Cholesky factorization

$$^2V_{ij}^{kl} \approx \sum_{M=1}^{\kappa r} L_M^{ik}\, L_{jl}^M. \tag{7.4}$$

The Cholesky factorization corresponds to density fitting [36, 40–48] of the integrals in an atomic basis, the Cholesky basis, with both one- and two-atom centered basis functions [28, 36]. The full Cholesky factorization with $\kappa = r$ is formally exact for positive semidefinite matrices but is usually calculated using a pivoting algorithm where κ is determined by an accuracy threshold [49], which reduces computational storage particularly for larger basis sets [25, 30]. Given an accuracy threshold of 10^{-4}, we can expect to generate a basis set of Cholesky tensors roughly 3-5 times the size of the molecular one, reducing the number of integrals that must be stored from r^4 to 3-5 r^3 [36].

The Cholesky tensors in this paper were computed using a modified version of the pivoted Cholesky factorization from Ref. [50]. The primary modification to the algorithm is the replacement of the accuracy threshold with a fixed stopping point based on the dimension of the Cholesky tensor basis set. This approach was chosen in order to standardize the size of

the Cholesky basis at κ times the size r of the molecular basis set (κr) where κ is typically in the range $3-5$ to ensure accurate reproduction of molecular energies and properties at both equilibrium and non-equilibrium geometries.

7.2.2 Positive Semidefinite Factorizations

While performing the Cholesky factorization on the 2-electron integrals can decrease the integral matrix storage requirements for an electronic structure method, it alone is not necessarily sufficient to reduce the overall computational scaling of the method. To reduce the computational scaling, we may need to further decompose the 2-electron integral matrix to separate the molecular indices. Hence, we consider a family of positive semidefinite (PSD) factorizations that factor the 2-electron integral matrix to keep the approximation to the two-electron integral matrix positive semidefinite. The family can be formally characterized as the set of factorizations that parameterize the factor C_M^{ik} in Eq. (7.3). By construction, each factorization in the set is expressible in the form $CC^\dagger$ and hence, is positive semidefinite. In this paper we focus specifically on the factorization from the following parametrization of C_M^{ik} in Eq. (7.3):

$$C_M^{ik} \approx \sum_{p=1}^{K} \sum_{q=p-w}^{p+w} R_p^i \, R_q^k \, B_M^{pq}. \tag{7.5}$$

where B is a banded kernel matrix. The factorization indices p and q are connected to each other by a half-bandwidth w, which means that for each index p, the range of the index q is defined to be $p \pm w$. The bandwidth is related to the half-bandwidth by $2w+1$. The maximum value K for the index p should scale linearly with the number of orbitals; it can be set to the number M of Cholesky vectors. If $w = r$, where r is the rank of the orbital basis set, the PSD factorization is a generalization of the Cholesky factorization in which B is not restricted to be a lower triangular matrix. If $w = 0$, then $p = q$ and the PSD factorization is a single-index factorization similar to factorizations like CANDECOMP/PARAFAC and tensor hypercontraction (THC) [4]. Important features of the PSD factorization in Eq. 7.5

are: (1) its rigorous preservation of the positive semidefiniteness of the two-electron integral matrix due to the preservation of the overall form and symmetry of the Cholesky factorization e.g. ${}^2V = CC^\dagger$, (2) its ability through its half-bandwidth w to interpolate between Cholesky and THC-like factorizations, and (3) its applicability to other 3-index decompositions such as the density-fitting and spectral expansion factorizations.

7.3 Applications

7.3.1 Computational Methods

The p2-RDM calculations in this study were preformed using a modified version of the implementation in Ref. [8]. First, the two-electron integrals were first decomposed using the modified low-rank pivoted Cholesky algorithm by Harbrecht, Peters, and Schneider [50]. Second, the Cholesky tensors were decomposed by minimizing the sum of the squares of the residuals in Eq. (7.5) with a limited-memory quasi-Newton's method (L-BFGS) with an optimality tolerance of 0.001 a.u.. Third, for testing purposes in this paper the full two-electron integral matrix was rebuilt from the PSD tensors and employed in calculations with the p2-RDM method. In all calculations the number of Cholesky basis functions is fixed at $5r$, that is $\kappa = 5$, to ensure accurate reproduction of the potential energy surface. All calculations were performed without using symmetry or freezing core orbitals.

7.3.2 Results

Table 7.1 shows the percentage of the correlation energy recovered by the Cholesky and PSD factorizations for H_2O, CO, and N_2 in the cc-pVTZ basis set. The Cholesky factorization gives a consistent recovery of approximately 99.98% for each molecule. The PSD correlation energy recoveries are also approximately 100% for all half-bandwidths studied. Increasing the half-bandwidth w brings the correlation recoveries of the PSD factorizations closer to those of the Cholesky factorizations. The PSD factorization performed particularly well for

Table 7.1: The percentage of the p2-RDM correlation energy recovered is reported for three PSD factorizations and the Cholesky factorization for three molecules in the cc-pVTZ basis set. The numbers M and K of Cholesky and PSD factors, respectively, are fixed at $5r$ for all factorizations, but the half-bandwidth w of the PSD factorizations varies from 0 to 4.

		Percent Correlation Recovery				
		PSD Factorization				Cholesky
Molecule	Full corr. energy (a.u.)	$w = 0$	$w = 1$	$w = 2$	$w = 4$	Factorization
H_2O	-0.28737	99.91	99.98	99.98	99.97	99.97
CO	-0.41525	100.02	99.94	99.97	100.00	99.98
N_2	-0.41007	100.11	100.23	100.08	99.99	99.98

H_2O where it reproduced the Cholesky's correlation recovery with a bandwidth of only ± 1.

A similar pattern can be seen in Table 7.2 which contains the percentage of the correlation energy recovered for a series of linear alkane chains. As in Table 7.1, the PSD recoveries move toward the Cholesky result as the bandwidth increases. For $w = 0$ and $w = 1$, the percentage of correlation energy recovered by the PSD factorizations slowly increases with system size, but for $w = 4$ this increase disappears with the percentage of correlation energy recovered being fairly constant at approximately 100.2% for all cases but methane. This result suggests that a small, fixed half-bandwidth w of approximately 4 is needed to maintain the size extensivity of the Cholesky factorization.

The errors in total energy per carbon atom from the p2-RDM method are compared for the Cholesky and PSD factorizations of the two-electron integrals for several alkane chains in Table 7.3. The errors are reported relative to the total energy from the p2-RDM method without approximation to the two-electron integrals. If the two-electron integral factorizations are size extensive, then these errors should be relatively constant as the number of carbon atoms increases. This is true for the Cholesky factorization which gives a total energy error of approximately 0.0014 a.u. for 6 of the 8 calculations. As observed in the correlation energy recoveries, the PSD for $w = 4$ yields energies per carbon atom that are very similar to those of the Cholesky factorization. If no width is used, the errors are noticeably larger than those of the Cholesky factorization, particularly for the larger chains.

Table 7.2: The percentage of the correlation energy recovered is reported for several PSD factorizations and the Cholesky factorization for a series of eight linear alkane chains in the cc-pVDZ basis set. The numbers M and K of Cholesky and PSD factors, respectively, are fixed at $5r$ for all factorizations, but the half-bandwidth w of the PSD factorizations varies from 0 to 4.

	Percentage of Correlation Energy			
	PSD Factorization			Cholesky
Molecule	$w = 0$	$w = 1$	$w = 4$	Factorization
CH_4	100.0	99.8	99.9	99.8
C_2H_6	100.3	100.0	100.2	99.9
C_3H_8	100.5	100.1	100.1	99.8
C_4H_{10}	100.8	100.4	100.3	99.8
C_5H_{12}	101.3	100.6	100.2	99.8
C_6H_{14}	101.7	100.8	100.2	99.8
C_7H_{16}	101.6	101.8	100.3	99.8
C_8H_{18}	101.8	100.8	100.2	99.7

However, the results suggest that for all PSD factorizations, even when $w = 0$, the error per carbon becomes fairly constant after butane, indicating size extensivity.

For the alkane chains table 7.4 reports the mean and max unsigned errors of the elements of the two-electron integral matrices from each factorization approximation. The mean unsigned error is the sum of the absolute values of the differences of the approximate and exact two-electron integrals normalized by the number of integrals. The max unsigned error is the largest absolute difference between the integrals. Both the mean and max error, which are largest when $w = 0$, decrease toward their Cholesky values as w increases. For all factorizations the max error is relatively constant as the system size increases while the mean error decreases with system size. These results as well as the reported errors per carbon atom indicate that the factorizations are size extensive.

Table 7.5 reports the total integral storage costs of each factorization for each alkane chain. The storage requirements for the 2-electron integrals using a traditional storage with 8-fold symmetry grows from ∼1 megabyte (MB) for methane to ∼1.6 gigabytes (GB) for octane. The Cholesky factorizations reduces the storage costs by an order of magnitude,

Table 7.3: The errors in total energy per carbon atom from the p2-RDM method are compared for the Cholesky and PSD factorizations of the two-electron integrals for several alkane chains. The numbers M and K of Cholesky and PSD factors, respectively, are fixed at $5r$ for all factorizations, but the half-bandwidth w of the PSD factorizations varies from 0 to 4. For all PSD factorizations, even when $w = 0$, the error per carbon becomes fairly constant after butane, indicating size extensivity.

	Error (a.u.)			
	PSD Factorization			Cholesky
Molecule	$w = 0$	$w = 1$	$w = 4$	Factorization
CH_4	$+5.7e$-4	$-3.5e$-3	$-1.3e$-3	$-2.3e$-3
C_2H_6	$+2.5e$-2	$-1.5e$-2	$-2.9e$-3	$+1.5e$-3
C_3H_8	$+5.5e$-2	$+2.4e$-3	$+2.0e$-3	$+1.5e$-3
C_4H_{10}	$+8.2e$-2	$+6.1e$-3	$+1.5e$-3	$+1.4e$-3
C_5H_{12}	$+1.0e$-1	$-7.8e$-3	$-1.9e$-3	$+1.2e$-3
C_6H_{14}	$+1.2e$-1	$-5.1e$-4	$-1.6e$-3	$+6.9e$-4
C_7H_{16}	$+1.3e$-1	$-6.3e$-3	$+6.8e$-4	$+1.5e$-3
C_8H_{18}	$+1.3e$-1	$-9.6e$-3	$-1.8e$-3	$+1.4e$-3

Table 7.4: The mean unsigned and max unsigned errors of the two-electron integrals from the Cholesky and PSD factorizations are reported for the alkane chains. The numbers M and K of Cholesky and PSD factors, respectively, are fixed at $5r$ for all factorizations, and the half-bandwidth w of the PSD factorizations varies from 0 to 4.

	Mean Error				Max Error			
	PSD Factorization			Cholesky	PSD Factorization			Cholesky
Molec.	$w = 0$	$w = 1$	$w = 4$	Factorization	$w = 0$	$w = 1$	$w = 4$	Factorization
CH_4	$4.8e$-4	$4.2e$-4	$4.0e$-5	$3.1e$-5	$2.4e$-3	$1.6e$-3	$4.2e$-4	$4.0e$-4
C_2H_6	$2.1e$-4	$2.0e$-4	$1.3e$-4	$3.3e$-5	$1.8e$-3	$9.2e$-4	$6.9e$-4	$3.3e$-4
C_3H_8	$1.4e$-4	$1.3e$-4	$9.2e$-5	$2.0e$-5	$1.5e$-3	$9.9e$-3	$4.9e$-4	$2.5e$-4
C_4H_{10}	$9.6e$-5	$8.5e$-5	$6.2e$-5	$2.8e$-5	$1.7e$-4	$1.3e$-4	$4.8e$-4	$2.1e$-4
C_5H_{12}	$7.3e$-5	$6.8e$-5	$4.6e$-5	$2.2e$-5	$1.9e$-3	$1.2e$-4	$3.5e$-4	$1.8e$-4
C_6H_{14}	$5.3e$-5	$4.7e$-5	$3.3e$-5	$1.1e$-5	$1.5e$-3	$6.2e$-4	$3.1e$-4	$1.6e$-4
C_7H_{16}	$4.5e$-5	$4.5e$-5	$3.0e$-5	$1.5e$-5	$1.7e$-3	$7.3e$-4	$3.4e$-4	$1.3e$-4
C_8H_{18}	$3.8e$-5	$3.1e$-5	$2.5e$-5	$1.3e$-5	$1.7e$-3	$6.3e$-4	$3.5e$-4	$1.3e$-4

Table 7.5: The total integral storage costs of the full integrals with 8-fold symmetry, the Cholesky factorization, and two PSD factorizations are presented for all eight alkanes from Table 7.2. Memory usage is reported in megabytes (MB).

		Memory Usage (MB)			
Molecule	Orbitals	8-fold Integrals	Cholesky	PSD($w = 1$)	PSD($w = 4$)
CH_4	34	1.34	0.79	0.18	0.46
C_2H_6	58	11.32	3.90	0.54	1.35
C_3H_8	82	45.21	11.03	1.08	2.69
C_4H_{10}	106	126.25	23.82	1.80	4.49
C_5H_{12}	130	285.61	43.94	2.70	6.76
C_6H_{14}	154	562.45	73.05	3.79	9.49
C_7H_{16}	178	1003.88	112.80	5.07	12.67
C_8H_{18}	202	1664.97	164.85	6.53	16.32

requiring ∼0.16 GB for the octane calculation. The PSD factorization with a half-bandwidth of 4 reduces the storage costs by another order of magnitude, requiring only ∼0.016 GB of storage space for the octane calculation. Using a half-bandwidth of one further reduces the cost by about 50%. Since the PSD storage costs have roughly an r^2 scaling for a fixed half-bandwidth compared to the r^3 and r^4 storage costs scaling of Cholesky and unfactorized integrals, their advantage in memory storage will only grow with system size particularly if we can generate the PSD factors directly without forming the 2-electron integrals.

The eigenvalues of a positive semidefinite matrix should be by definition non-negative. To demonstrate that the PSD factorizations are positive semidefinite, we report in Figure 7.1 the eigenvalues of methane's two-electron integral matrix computed with (a) no factorization, (b) the Cholesky factorization, and (c) the PSD(w=4) factorizations. Zero eigenvalues are not reported. The plots show that the errors in the eigenvalues for the two factorizations are small. Furthermore, the errors are almost entirely a result of the original Cholesky factorization with the PSD factorization very closely reproducing the Cholesky eigenvalues especially for the larger bandwidths. The PSD(w=0) and (w=1) eigenvalues, albeit not shown, are very similar to those of the PSD(w=4) factorization. None of the factorizations has negative eigenvalues and therefore, each factorization is positive semidefinite as expected.

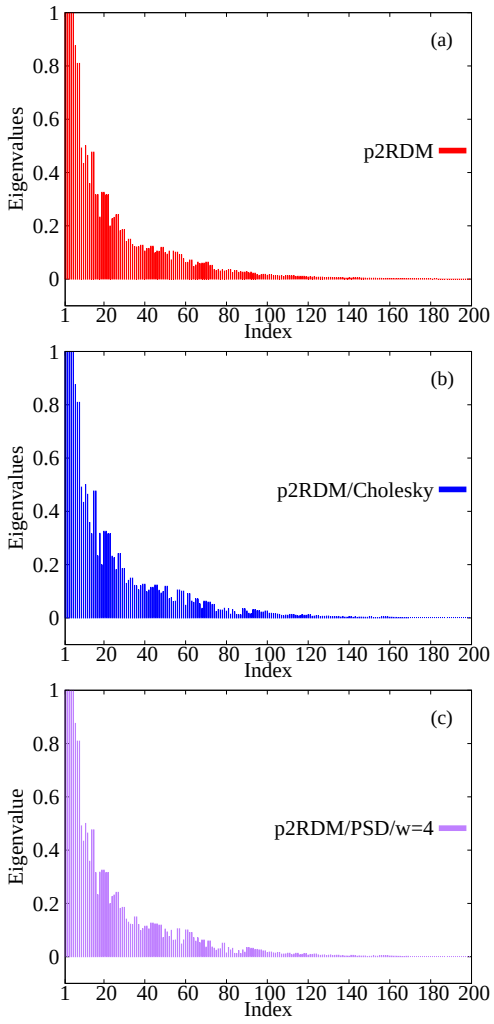

Figure 7.1: The non-zero eigenvalues of the two-electron integral matrix of methane are shown with the integrals generated with (a) no factorization (b) the Cholesky factorization, and (c) the PSD factorization at the half-bandwidth $w = 4$. The first 4 eigenvalues, which have a magnitude larger than 1, as well as the zero eigenvalues are not shown to make the non-zero eigenvalues more visible. The first four eigenvalues also show good agreement between the three methods.

Table 7.6: The number of iterations required to compute the PSD factorization from the Cholesky factorization is shown for the alkane chain calculations. While fluctuations in the number of iterations are present, particularly for butane and pentane, the number of iterations does not grow appreciably with system size beyond butane.

	Number of Iterations		
	PSD Factorization		
Molecule	$w = 0$	$w = 1$	$w = 4$
CH_4	1261	2274	202
C_2H_6	1650	3055	2329
C_3H_8	2168	3399	4014
C_4H_{10}	5034	7469	12267
C_5H_{12}	6140	28366	19950
C_6H_{14}	5587	10492	3130
C_7H_{16}	6071	5213	13672
C_8H_{18}	8087	11935	10462

For the PSD factorization to be $O(r^4)$ the number of iterations to compute the PSD factorization from the Cholesky factorization must not increase with r. Table 7.6 shows the number of iterations required by the quasi-Newton's method for the alkane chain calculations. While fluctuations in the number of iterations are present, particularly for butane and pentane, the number of iterations does not grow appreciably with system size beyond butane.

Figure 7.2 compare the potential energy curves of hydrogen fluoride and the hydroxyl radical ion from the p2-RDM method with and without PSD two-electron integral factorizations. For both cases, the curves from the PSD factorizations with either $w = 1$ or $w = 4$ show good agreement with the curve from the p2-RDM method without integral factorization. As long as a sufficiently large Cholesky factorization (i.e. $\kappa = 5r$) is employed to seed the PSD factorization, the PSD factorization is capable of reproducing the dissociation curve without integral approximation at very small bandwidths. Practically, the selection of a nonzero half-bandwidth, which generalizes factorizations like THC, is important to ensure good convergence of the optimization.

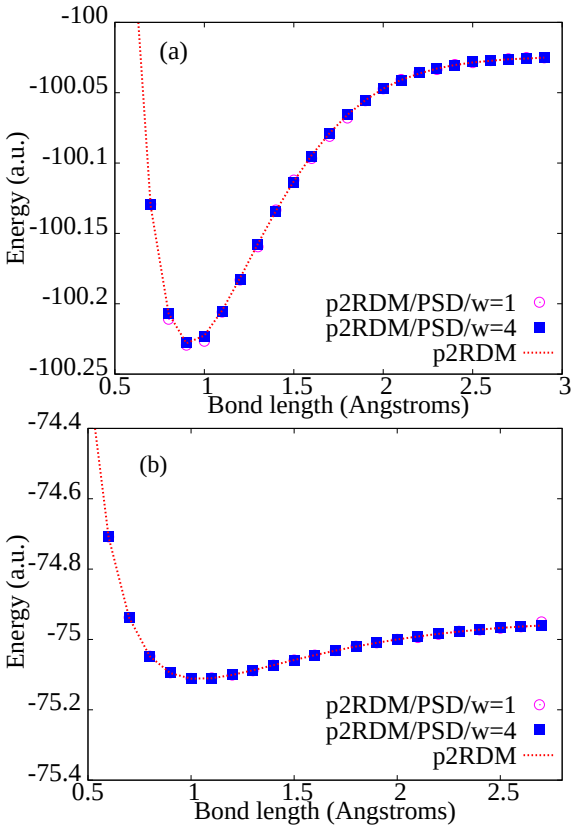

Figure 7.2: The potential energy curves of (a) hydrogen fluoride HF and (b) hydroxyl radical OH^+ from the p2-RDM method with and without PSD two-electron integral factorizations are compared. The curve from the PSD factorization with either $w = 1$ or $w = 4$ shows good agreement with the curve from the p2-RDM method without integral factorization. The basis set is cc-pVDZ.

7.4 Discussion and Conclusions

The positive semidefinite factorization (PSD) of the Cholesky factors provides a size extensive, efficient, and positive semidefinite alternative to traditional factorizations such as CANDECOMP/PARAFAC and tensor hypercontraction. The PSD factorization generates a new family of factorizations with similar partial summation characteristics to tensor hypercontraction for low bandwidths while maintaining the positive semidefinite character and size consistency of the Cholesky factorization. In this study, we investigated the efficacy of this family of decompositions for the two-electron repulsion integral matrices of inorganic molecules and alkane chains.

With a small, fixed half-bandwidth $w = 4$ the PSD factorization maintains the accuracy of the energies from the parent Cholesky factorization with $\kappa = 5r$. While the storage of the Cholesky factorization scales as $O(r^3)$ where r is the rank of the one-electron basis set, the storage of the PSD factorization with small integer w scales as $O(r^2)$. Furthermore, the PSD factorization improves the computational scaling of floating-point operations within *ab initio* electronic structure relative to the Cholesky factorization. For example, while the molecular two-electron integral transformation with the Cholesky factorization scales like $O(r^5)$, the molecular two-electron integral transformation with the PSD factorization scales as $O(r^4)$. The alkane chain results demonstrate that neither the energy errors nor the computational effort required to derive the PSD factors scale with the system size. Importantly, as shown in the dissociation curves of HF and OH^+, the PSD factorization retains the ability of the p2-RDM method to capture electronic correlation including multi-reference correlation. For future applications to geometry optimization and molecular dynamics, analytic nuclear gradients of the PSD factorization can be obtained from modest extensions of the gradients developed for the Cholesky factorization [25, 27].

The present results with the PSD family of factorizations suggest that a new electronic structure method could be developed based on a current r^6 method such as p2-RDM using the positive semidefinite factorization to reduce computational scaling toward the r^3

computational scaling of Hartree-Fock and density functional theory. If both the integral matrix and the 2-electron excitation tensors are factorized and efficient partial summation is employed, this approach has to potential to create a p2-RDM method with $O(r^4)$ scaling, an ideal combination of traits for addressing highly correlated systems that are too large for current *ab initio* methods, particularly those with multi-reference character.

7.5 References

[1] A. Cicohocki, R. Zdunek, A. H. Phan, and S. Amari, *Nonnegative Matrix and Tensor Factorizations: Applications to Exploratory Multi-way Data Analysis and Blind Source Separation* (Wiley, New York, 2009).

[2] T. Kinoshita, O. Hino, and R. J. Bartlett, J. Chem. Phys. **119**, 7756 (2003).

[3] F. Bell, D. S. Lambrecht, and M. Head-Gordon, Molecular Physics **108**, 2759 (2010).

[4] E. G. Hohenstein, R. M. Parrish, and T. J. Martinez, J. Chem. Phys. **137**, 044103 (2012).

[5] D. A. Mazziotti, Phys. Rev. Lett. **101**, 253002 (2008).

[6] D. A. Mazziotti, Phys. Rev. A **81**, 062515 (2010).

[7] C. A. Schwerdtfeger and D. A. Mazziotti, J. Phys. Chem. A **115**, 12011 (2011).

[8] C. A. Schwerdtfeger and D. A. Mazziotti, J. Chem. Phys. **137** (2012).

[9] D. A. Mazziotti, Chem. Rev. **112**, 244 (2012).

[10] A. M. Sand, C. S. Schwerdtfeger, and D. A. Mazziotti, J. Chem. Phys. **136**, 034112 (2012).

[11] E. P. Hoy, C. S. Schwerdtfeger, and D. A. Mazziotti, Mol. Phys. **107**, 765 (2012).

[12] E. P. Hoy, C. S. Schwerdtfeger, and D. A. Mazziotti, J. Phys. Chem. A **117**, 1817 (2013).

[13] A. M. Sand and D. A. Mazziotti, Comp. Theor. Chem. **1003**, 44 (2013).

[14] A. M. Sand and D. A. Mazziotti, J. Chem. Phys. **138**, 244102 (2013).

[15] L. W. Bertels and D. A. Mazziotti, J. Chem. Phys. **141**, 044305 (2014), URL http://scitation.aip.org/content/aip/journal/jcp/141/4/10.1063/1.4890117.

[16] C. A. Schwerdtfeger and D. A. Mazziotti, J. Chem. Phys. **137**, 244103 (2012).

[17] R. M. Parrish, E. G. Hohenstein, T. J. Martinez, and C. D. Sherill, J. Chem. Phys. **137**, 224106 (2012).

[18] E. G. Hohenstein, R. M. Parrish, C. D. Sherrill, and T. J. Martinez, J. Chem. Phys. **137**, 221101 (2012).

[19] E. G. Hohenstein, R. M. Parrish, C. D. Sherrill, and T. J. Martinez, J. Chem. Phys. **138**, 12411 (2013).

[20] N. Shenvi, H. V. Aggelen, Y. Yang, W. Yang, C. Schwerdtfeger, and D. Mazziotti, J. Chem. Phys. **139**, 054110 (2013).

[21] E. G. Hohenstein, S. I. L. Kokkila, R. M. Parrish, and T. J. Martnez, The Journal of Physical Chemistry B **117**, 12972 (2013).

[22] R. M. Parrish, D. C. Sherrill, E. G. Hohenstein, S. I. L. Kokkila, and T. J. Martnez, The Journal of Chemical Physics **140**, 181102 (2014), URL http://scitation.aip.org/content/aip/journal/jcp/140/18/10.1063/1.4876016.

[23] E. P. Hoy, N. Shenvi, and D. A. Mazziotti, J. Phys. Chem. **139**, 034105 (2013).

[24] G. J. O. Beran and M. Head-Gordon, J. Chem. Phys. **121**, 78 (2004).

[25] D. W. ONeal and J. Simons, Int. J. Quantum Chem. **36**, 673 (1989).

[26] I. Roeggen and E. Wisloff-Nilseen, Chem. Phys. Letters **132**, 154 (1986).

[27] F. Aquilante, R. Lindh, and T. B. Pedersen, J. Chem. Phys. **129**, 034106 (2008).

[28] T. B. Pedersen, F. Aquilante, and R. Lindh, Theor. Chem. Acc. **124**, 1 (2009).

[29] F. Aquilante, L. Gagliardi, T. B. Pedersen, and R. Lindh, J. Chem. Phys. **130**, 154107 (2009).

[30] H. Koch, A. S. de Meras, and T. B. Pedersen, J. Phys. Chem. **118**, 9481 (2003).

[31] L. Boman, H. Koch, and A. S. de Meras, J. Phys. Chem. **129**, 134107 (2008).

[32] I. Roeggen and T. Johansen, J. Chem. Phys. **128**, 194107 (2008).

[33] F. Weigend, M. Kattannek, and R. Ahlrichs, J. Phys. Chem. **130**, 164106 (2009).

[34] E. G. Hohenstein and C. D. Sherrill, J. Chem. Phys. **132**, 184111 (2010).

[35] T. S. Chwee and E. A. Carter, J. Chem. Phys. **132**, 074104 (2010).

[36] S. Reine, T. Helgaker, and R. Lindh, WIREs Comput. Mol. Sci. **2**, 290 (2012).

[37] E. Epifanovsky, D. Zuev, X. Feng, K. Khistyaev, Y. Shao, and A. I. Krylov, J. Chem. Phys. **139**, 134105 (2013).

[38] A. E. DePrince and C. D. Sherrill, J. Chem. Theory Comput. **9**, 26872696 (2013).

[39] A. E. DePrince, M. R. Kennedy, B. G. Sumpter, and C. D. Sherrill, Mol. Phys. **112**, 1 (2014).

[40] J. L. Whitten, J. Chem. Phys. **58**, 4496 (1973).

[41] B. I. Dunlap, J. W. D. Connolly, and J. R. Sabin, Int. J. Quantum Chem. **12(S11)**, 81 (1977).

[42] B. I. Dunlap, J. W. D. Connolly, and J. R. Sabin, J. Chem. Phys. **71**, 3396 (1979).

[43] M. Feyereisen, G. Fitzgerald, and A. Komornicki, Chem. Phys. Letters **201**, 359 (1993).

[44] O. Vahtras, J. Almlof, and M. Feyereisen, Chem. Phys. Letters **213**, 514 (1993).

[45] A. P. Rendell and T. J. Lee, J. Chem. Phys. **101**, 400 (1994).

[46] F. Weigend, Phys. Chem. Chem. Phys. **4**, 4285 (2002).

[47] A. Sodt, J. E. Subotnik, and M. Head-Gordon, J. Chem. Phys. **125**, 194109 (2006).

[48] H. J. Werner, F. R. Manby, and P. J. Knowles, J. Chem. Phys. **118**, 8149 (2003).

[49] K. Brandhorst and M. Head-Gordon, Journal of Chemical Theory and Computation **7**, 351 (2011).

[50] H. Harbrecht, M. Peters, and R. Schneider, App. Num. Math. **63**, 428 (2012).